

Characteristics Improvement of Quantum Dot Semiconductor Optical Amplifier for
Access Network



A Dissertation Submitted in Partial Fulfillment of the Requirements
for the Degree of Doctor of Philosophy in Electrical Engineering

Department of Electrical Engineering

FACULTY OF ENGINEERING

Chulalongkorn University

Academic Year 2020

Copyright of Chulalongkorn University

การปรับปรุงคุณลักษณะเฉพาะของตัวขยายแสงแบบสารกึ่งตัวนำชนิดควอนตัมดอทเพื่อใช้ใน
โครงข่ายเข้าถึงข้อมูล



วิทยานิพนธ์นี้เป็นส่วนหนึ่งของการศึกษาตามหลักสูตรปริญญาวิศวกรรมศาสตรดุษฎีบัณฑิต
สาขาวิชาวิศวกรรมไฟฟ้า ภาควิชาวิศวกรรมไฟฟ้า
คณะวิศวกรรมศาสตร์ จุฬาลงกรณ์มหาวิทยาลัย
ปีการศึกษา 2563
ลิขสิทธิ์ของจุฬาลงกรณ์มหาวิทยาลัย

Thesis Title Characteristics Improvement of Quantum
Dot Semiconductor Optical Amplifier for Access Network
By Miss Budsara Boriboon
Field of Study Electrical Engineering
Thesis Advisor Associate Professor Dr. Duang-rudee Worasuchep

Accepted by the FACULTY OF ENGINEERING, Chulalongkorn University in Partial
Fulfillment of the Requirement for the Doctor of Philosophy

..... Dean of the FACULTY OF
ENGINEERING
(Professor Dr. SUPOT TEACHAVORASINSKUN)

DISSERTATION COMMITTEE

..... Chairman
(Assistant Professor Dr. Tuptim Angkaew)

..... Thesis Advisor
(Associate Professor Dr. Duang-rudee Worasuchep)

..... Examiner
(Professor Dr. Songphol Kanjanachuchai)

..... Examiner
(Assistant Professor Dr. Chanin Wissawinthon)

..... External Examiner
(Associate Professor Dr. Ukrit Mankong)

บุษรา บริบูรณ์ : การปรับปรุงคุณลักษณะเฉพาะของตัวขยายแสงแบบสารกึ่งตัวนำชนิดควอนตัมดอตเพื่อใช้ในโครงข่ายเข้าถึงข้อมูล. (Characteristics Improvement of Quantum Dot Semiconductor Optical Amplifier for Access Network) อ.ที่ปรึกษาหลัก : รศ. ดร.ดวงฤดี วรสุชีพ

วิทยานิพนธ์ฉบับนี้นำเสนอการปรับปรุงลักษณะเฉพาะและประเมินสมรรถนะของตัวขยายแสงแบบสารกึ่งตัวนำชนิดควอนตัมดอต (Quantum Dot Semiconductor Optical Amplifier, QD SOA) เพื่อนำไปใช้ในโครงข่ายเข้าถึงข้อมูล โดยแบ่งเป็น 3 ส่วน ได้แก่ 1) การทำให้ประสิทธิภาพควอนตัมภายในดีขึ้น 2) การเพิ่มอัตราการขยายของชิป และ 3) การนำ QD SOA ไปประยุกต์ใช้ในโครงข่ายเข้าถึงข้อมูลที่อัตราบิต 40 Gb/s วิทยานิพนธ์ส่วนแรกกล่าวถึงการใช้กระบวนการอบชุบด้วยความร้อนอย่างรวดเร็ว (Rapid thermal annealing) เพื่อเพิ่มประสิทธิภาพควอนตัมภายใน โดยเพิ่มได้มากถึง 1.4 เท่า เมื่อเปรียบเทียบกับกรณีไม่ได้ใช้กระบวนการดังกล่าว อีกทั้งยังให้ผลการสูญเสียทางแสงที่ต่ำ วิทยานิพนธ์ส่วนที่สองกล่าวถึงเทคนิคการชดเชยความตึงเครียดเพื่อเพิ่มอัตราการขยายของชิป QD SOA ซึ่งจะพิจารณาจำนวนชั้นควอนตัมดอตและกระแสขีดแบ่ง (Threshold current) ที่เหมาะสมของเลเซอร์ไดโอดชนิดควอนตัมดอต จากนั้นนำผลที่ได้ไปออกแบบ QD SOA โดยมีจำนวนชั้นควอนตัมดอต 25 ชั้น ความยาว 2 mm ทำให้ได้อัตราการขยายของชิปสูงถึง 35 dB และใช้กระแสไบแอสเพียง 400 mA ในส่วนสุดท้ายของวิทยานิพนธ์จะเป็นการประเมินสมรรถนะของตัวขยายแสงแบบสารกึ่งตัวนำชนิดทรานสดูดา 2 ตัว และ QD SOA 1 ตัว เมื่อนำไปใช้ในโครงข่ายเข้าถึงข้อมูลที่อัตราบิต 40 Gb/s โดยเริ่มต้นจากการเปรียบเทียบลักษณะเฉพาะของตัวขยายแสงทั้ง 2 ชนิด ซึ่ง QD SOA ให้ค่าตัวเลขสัญญาณรบกวนต่ำที่สุดเท่ากับ 4.59 dB เนื่องจากมีค่าโอเอสเอ็นอาร์ (Optical Signal to Noise Ratio, OSNR) สูงที่สุด อีกทั้ง QD SOA มีเวลาการตอบสนองเร็วที่สุดเท่ากับ 70 ps และมีผลกระทบรูปแบบข้อมูล (Data pattern effect) ต่ำที่สุดเมื่อใช้งานในช่วงอิมพัลส์ ซึ่งเหมาะกับการส่งเป็นชุดอย่างรวดเร็ว (Burst-mode transmission) ถัดไปได้ประเมินสมรรถนะของตัวขยายแสงเมื่อแทรกเข้าไปในโครงข่ายเข้าถึง และวัดค่าไอพีดีอาร์ (Input Power Dynamic Range, IPDR) ของตัวขยายแสงแบบสารกึ่งตัวนำทั้ง 3 ตัว สุดท้ายได้ทดลองใช้ตัวขยายแสงแบบสารกึ่งตัวนำ 2 ตัว มาต่อกัน เพื่อเพิ่มบงกำลังในโครงข่ายให้มากขึ้น ซึ่งสามารถรองรับจำนวนผู้ใช้งานได้มากถึง 128 ผู้ใช้งาน และส่งสัญญาณได้ระยะทางไกล 20 km ดังนั้นการนำ QD SOA มาใช้เป็นตัวขยายแสงลำดับที่ 2 ต่อจาก SOA ชนิดทรานสดูดาจะให้ค่าอัตราความผิดพลาดบิตที่น้อยกว่าการใช้ SOA ชนิดทรานสดูดา 2 ตัวต่อกัน เนื่องจาก QD SOA มีกำลังขาออกอิมพัลส์ที่สูงกว่าและมีผลกระทบรูปแบบข้อมูลที่ต่ำกว่าเมื่อใช้งานที่ค่ากำลังขาเข้าสูง ทั้งนี้ได้แทนค่าพารามิเตอร์ต่าง ๆ จากการทดลองลงในสมการสำหรับคำนวณค่าอัตราความผิดพลาดบิตและเปรียบเทียบเพื่อยืนยันผลการทดลองอันมีต้นเหตุมาจากการเสื่อมของโอเอสเอ็นอาร์และผลกระทบรูปแบบข้อมูล

สาขาวิชา วิศวกรรมไฟฟ้า
ปีการศึกษา 2563

ลายมือชื่อนิสิต
ลายมือชื่อ อ.ที่ปรึกษาหลัก

5971426621 : MAJOR ELECTRICAL ENGINEERING

KEYWORD: QD SOA, Conventional SOA, Internal quantum efficiency, Gain, 40 Gb/s access network

Budsara Boriboon : Characteristics Improvement of Quantum Dot Semiconductor Optical Amplifier for Access Network . Advisor: Assoc. Prof. Dr. Duang-rudee Worasuchep

This thesis presents the characteristics improvement and performance evaluation of Quantum Dot Semiconductor Optical Amplifier (QD SOA) in an access network. There are 3 parts: 1) improvement of internal quantum efficiency, 2) increase of chip gain and 3) implementation of QD SOA in 40 Gb/s access network. The first part, Rapid Thermal Annealing (RTA) is applied to improve internal quantum efficiency to be 1.4 times higher than without RTA and low optical loss. The second part, strain compensation technique is applied to increase the chip gain of QD SOA. Considering the design of Quantum Dot Laser Diode with optimized stacked QD layers and threshold current, then the same design is applied to QD SOA having 25-stacked QD layers and 2 mm long. It can achieve the maximum chip gain of 35 dB at 400-mA bias current. The last part of thesis, the performances of two conventional SOAs and one QD SOA are evaluated in 40 Gb/s access network. Starting from the characteristics between conventional SOAs and QD SOA are compared. QD SOA gives the lowest Noise Figure of 4.59 dB because of its highest Optical Signal to Noise Ratio (OSNR). Plus, QD SOA has the fastest response time of 70 ps with the lowest data pattern effect when operating in saturation region, which is suitable for burst-mode transmission. Next, the performance of single SOA transmission is evaluated, and the Input Power Dynamic Ranges (IPDR) of 3 SOAs are measured. Finally, the two-cascaded SOA is experimented to raise power budget of a network to successfully support 128 users and 20-km distance. Consequently, installing QD-SOA as 2nd-stage SOA following a conventional SOA provides lower Bit Error Rates (BERs) than two-cascaded conventional SOAs because QD SOA has higher saturation output power and lower data pattern effect when operating at high input power. Additionally, the BERs are computed by substituting all parameters from experiments into theoretical equations. They are compared to experimental BERs to confirm the root cause of OSNR degradation and data pattern effect.

Field of Study: Electrical Engineering

Student's Signature

Academic Year: 2020

Advisor's Signature

ACKNOWLEDGEMENTS

I would like to express my sincere gratitude to my advisor, Associate Professor Dr. Duangrudee Worasuchep, for her motivation, patience, and support. Her invaluable guidance encourages me to succeed in my Ph.D. study. It is very kind of her to teach me about everything in my life including my Ph.D. or my personal life.

I would like to thank all of my thesis committees for their useful suggestions and comments.

I would like to express appreciation to all researchers and staffs at Network Science & Convergence Device Technology Laboratory and Photonic Network System Laboratory under Network System Research Institute, National Institute of Information and Communications Technology of Japan (NICT) for the great experience to do the experiment research with high technology devices and equipment. I would like to thank NICT located at Engineering Centennial Memorial building at Chulalongkorn University for many devices and T&M equipment.

I am grateful to The 100th Anniversary Chulalongkorn University Fund for Doctoral Scholarship, The 90th Anniversary of Chulalongkorn University Fund (Ratchadaphiseksomphot Endowment Fund), and Overseas Research Experience Scholarship for Graduate Students from Graduate School Chulalongkorn University.

Finally, my special thanks must be given to my parents and my friends for giving me encouragement, moral support, and inspiration for many years. It means a lot to me to always be by my side.

จุฬาลงกรณ์มหาวิทยาลัย
CHULALONGKORN UNIVERSITY

Budsara Boriboon

TABLE OF CONTENTS

	Page
ABSTRACT (THAI).....	iii
ABSTRACT (ENGLISH).....	iv
ACKNOWLEDGEMENTS	v
TABLE OF CONTENTS	vi
List of Tables	x
List of Figures.....	xi
1. Introduction	1
1.1 Introduction.....	1
1.2 Background	2
1.3 Objectives	11
1.4 Scopes	11
1.5 Benefits and Applications.....	11
2. Characteristics-improvement of QD semiconductor optical amplifier using rapid-thermal annealing process.....	12
2.1 Introduction.....	13
2.2 Experiments.....	14
2.3 Results	16
2.4 Conclusion	19
2.5 Acknowledgment.....	19
3. Optimized design of QD-LD toward QD SOA to achieve 35-dB maximum chip gain with 400-mA injected current.....	21
3.1 Introduction.....	22

3.2 Experiments.....	24
3.2.1 Experimental setup of QD-LD & QD SOA chips	24
3.2.2 Experimental setups of QD SOA module	26
3.3 Results & Discussion	26
3.3.1 Results of QD-LD chips	27
3.3.2 Results of QD SOA chips	29
3.3.3 Results of QD SOA module.....	33
3.4 Conclusion	35
3.5 Acknowledgment.....	36
4. Performances of Conventional SOAs versus QD SOA in 1530-nm Upstream Transmission of 40 Gb/s Access Network.....	37
4.1 Introduction.....	38
4.2 SOA's Characteristics	40
4.2.1 Experimental Setup.....	40
4.2.2 Experimental Results.....	40
4.2.2.1 ASE Peak Wavelength & 3-dB Bandwidth	41
4.2.2.2 Gain, Saturation Output & Input Powers	42
4.2.2.3 Noise Figure (NF).....	43
4.3 SOA's Response Time and Data Pattern Effect	45
4.3.1 Experimental Setup.....	45
4.3.2 Experimental Results.....	46
4.4 Bit Error Rate (BER).....	49
4.4.1 Experimental Setup.....	49

4.4.2 Chromatic Dispersion (CD) Compensation in Link#1 & Link#2, and BER Performances of 3 SOAs.....	50
4.4.3 Single SOA Transmission & Input Power Dynamic Range (IPDR)	51
4.4.3.1 SOA#1 Transmission & IPDR	51
4.4.3.2 SOA#2 Transmission & IPDR	52
4.4.3.3 QD SOA Transmission & IPDR.....	53
4.4.4 Two-cascaded SOA Transmission	54
4.4.4.1 Two-cascaded SOA#1 & SOA#2.....	55
4.4.4.2 Two-cascaded SOA#1 & QD SOA	56
4.4.4.3 Verify the Performance of 2 nd -stage SOA	56
4.4.5 Theoretical Equations	58
4.4.5.1 Noise Terms	58
4.4.5.2 BER Calculation.....	58
4.4.6 Computed BER Results of SOA#1, SOA#2, and QD SOA	60
4.4.6.1 Computed and Experimental BERs of SOA#1	61
4.4.6.2 Computed and Experimental BERs of SOA#2	61
4.4.6.3 Computed and Experimental BERs of QD SOA	62
4.5 Conclusion	63
4.6 Acknowledgement	64
5. Conclusion.....	65
6. Appendix.....	67
6.1 As-grown structure	67
6.2 Fabrication process	68
6.2.1 Broad Area Laser Diode (BA-LD).....	68

6.2.2 Ridge Laser Diode (Ridge LD).....	70
ACRONYMS	73
PARAMETERS.....	76
REFERENCES	78
VITA.....	89



List of Tables

	Page
Table 1.1 ITU-T standards of G-PON, XG-PON, and NG-PON2.....	10
Table 4.1 Characteristics of 3 SOAs: SOA#1, SOA#2, and QD SOA.....	40
Table 4.2 All parameters and values for 2 nd -stage SOA.....	57
Table 4.3 Parameters and values for BER computation.....	60
Table 6.1 Parameters and values of as-grown structure.....	67



List of Figures

	Page
Figure 1.1 Applications of optical amplifier [1].....	2
Figure 1.2 Wavelength bands of a) fiber amplifiers and b) SOA [2].	3
Figure 1.3 Radiative processes of SOA: a) spontaneous emission, b) stimulated emission, and c) stimulated absorption or absorption [4]......	4
Figure 1.4 a) Double-heterostructure SOA and b) carrier & optical confinements in double-heterostructure SOA [4].	5
Figure 1.5 QD layer in QD SOA structure.	6
Figure 1.6 Density of state $D(E)$ for a) bulk, b) quantum well, c) quantum wire, and d) quantum dot [5].	6
Figure 1.7 Density of state of QD gain media [5].	7
Figure 1.8 Pump-probe curves: a) conventional SOA & c) QD SOA, and the change of carrier density: b) conventional SOA & d) QD SOA [5]......	8
Figure 2.1 (left) Structure of quantum dot laser and (right) a picture from AFM measurement.	15
Figure 2.2 PL spectrum of as-grown sample.....	16
Figure 2.3 L-I characteristic measurement of BA-LD, new BA-LD, and ridge LD.	16
Figure 2.4 External quantum efficiencies at different cavity lengths and RTA temperatures: a) BA-LD at 600 °C, b) BA-LD at 620 °C, c) BA-LD at 640 °C, d) BA-LD at 660 °C, e) new BA-LD at 640 °C, and f) ridge LD at 640 °C.....	17
Figure 2.5 a) Internal quantum efficiency vs. RTA temperature, and b) Optical loss vs. RTA temperature.	18
Figure 3.1 Structure of QD devices.	24
Figure 3.2 QD SOA chip's experimental setup.	25

Figure 3.3 Block diagrams: a) IPDR, b) pattern effect, and c) 40 Gb/s data transmission over 20-km SMF.	26
Figure 3.4 Threshold currents of QD-LDs (800 μm long) with 10, 14, 20 and 25 stacked QD layers at different temperatures.....	27
Figure 3.5 a) I-L plot of 25 stacked-layer QD-LD at different temperatures, and b) temperature dependence of threshold current.	28
Figure 3.6 a) Lasing spectra of 25 stacked-layer QD-LD at different temperatures, and b) plot of peak wavelength versus temperature.....	28
Figure 3.7 Chip gain versus injected current of 2-mm long QD SOA with pulse duty cycle of 1 % and 10 %.....	29
Figure 3.8 Chip gain versus injected current of 1.5-mm, 2-mm, and 2.4-mm long QD SOAs at +6 dBm input power.	30
Figure 3.9 I-L plot of 2-mm and 2.4-mm long QD SOAs.....	31
Figure 3.10 Characteristic of 2-mm long QD SOA: a) chip gain versus injected current at different input powers, b) chip gain versus output power at different injected currents, and c) chip gain versus wavelength at different injected currents.	32
Figure 3.11 ASE and NF of QD SOA module at 400-mA injected current with -13.91-dBm input power and +2.74-dBm output power.....	33
Figure 3.12 IPDR of QD SOA module at 320-mA injected current.....	33
Figure 3.13 Pattern effect of a) conventional SOA at 308-mA injected current and b) our QD SOA module at 320-mA injected current. (DCA scale: 7.5 mV/div with an offset of 15 mV)	34
Figure 3.14 Eye diagram of 40 Gb/s data over 20-km SMF. (DCA scale: 4.8 mV/div with an offset of 16 mV)	35
Figure 4.1 Block diagram of characteristic measurement.....	40
Figure 4.2 ASE spectra of QD SOA at 320 & 400-mA.....	41
Figure 4.3 Gain and saturation output power of QD SOA.....	42

Figure 4.4 NFs of 3 SOAs at lower & higher bias currents.	43
Figure 4.5 Output OSNRs versus input power of 3 SOAs.	43
Figure 4.6 Input and Output spectra of QD SOA.....	44
Figure 4.7 Block diagram to measure the response times.....	45
Figure 4.8 Output waveforms of 3 SOAs: small-signal gain, and saturation at lower & higher bias currents.	46
Figure 4.9 Parameters of a decay exponential curve.....	47
Figure 4.10 Estimated decay exponential curves of 3 SOAs at higher bias currents....	47
Figure 4.11 Outputs of SOA#1: a) lower & b) higher current at -5.11 dBm input, and c) lower & d) higher input at 360-mA (higher) current.	48
Figure 4.12 Block diagrams: a) link w/o SOA, b) single SOA w/o link, c) link w/ single SOA, and d) Link#1&2 w/ two-cascaded SOA.....	49
Figure 4.13 BER curves of different cases: B-B (PRBS15 & 23), Link#1, Link#2, SOA#1, SOA#2, and QD SOA.....	51
Figure 4.14 SOA#1 at 360 mA: a) BER curves of 6 cases and b) BER plot versus SOA's input showing IPDR.....	52
Figure 4.15 SOA#2 at 332 mA: a) BER curves of 6 cases and b) BER plot versus SOA's input showing IPDR.....	53
Figure 4.16 QD SOA at 400 mA: a) BER curves of 6 cases and b) BER plot versus SOA's input showing IPDR.....	54
Figure 4.17 BER curves of 2-cascaded SOA#1 & SOA#2.	55
Figure 4.18 BER curves of 2-cascaded SOA#1 & QD SOA.	56
Figure 4.19 BER curves of 2 nd -stage SOA with N splits.	57
Figure 4.20 Computed and experimental BERs of SOA#1.	61
Figure 4.21 Compute and experimental BERs of SOA#2.....	62
Figure 4.22 Computed and experimental BERs of QD SOA.	63

Figure 6.1 As-grown structure..... 67



1. Introduction

1.1 Introduction

This dissertation investigates the characteristic improvement and performance of QD SOA. There are 3 parts: 1) “Characteristics-improvement of QD semiconductor optical amplifier using rapid-thermal annealing process”, published in 2018 *SPIE Photonics West Conference (Section 2)*, 2) “Optimized design of QD-LD toward QD SOA to achieve 35-dB maximum chip gain with 400-mA injected current”, published in *Optics Communications Journal, vol. 475, 2020 (Section 3)*, and 3) “Performances of conventional SOAs versus QD-SOA in 1530-nm upstream transmission of 40 Gb/s access network”, to be submitted to *Engineering Journal (EJ) (Section 4)*. To improve the internal quantum efficiency in QD structure, Rapid Thermal Annealing (RTA) process is applied during QD growth process, as described in *Section 2*. Another important characteristic of QD SOA is gain. Therefore, *Section 3* shows the maximum chip gain of 35 dB by optimizing the stacked QD layers via strain compensation technique. Finally, two conventional SOAs (SOA1013S, SOA#1 and SOA1117S, SOA#2) and QD SOA are applied in 40 Gb/s access network to evaluate their effects and performances described in *Section 4*. The 3-dB bandwidth, ASE peak wavelength, small-signal gain, saturation output power, and Noise Figure (NF) are measured. Also, the response time and data pattern effect are reported, as well as the Input Power Dynamic Ranges (IPDRs) of conventional SOAs and QD SOA. The performances of 3 SOAs are evaluated by Bit Error Rate (BER) measurement. To increase power budget more than single SOA, the two-cascaded SOA is implemented in network. Finally, both computed and experimental BERs are plotted versus SOA’s input power to confirm the Optical Signal to Noise Ratio (OSNR) degradation and data pattern effect.

Part 1 and 2 were published in the international conference and international journal, respectively. Part 3 has been prepared to submit to the international journal. They are fulfillment of the requirements for Degree of Doctor of Philosophy in Electrical Engineering, Department of Electrical Engineering, Faculty of Engineering, Chulalongkorn University.

1.2 Background

An optical amplifier is extremely useful to apply in various applications shown in Figure 1.1. The in-line amplifier is inserted in a middle of network to amplify signal as shown in Figure 1.1 a). It is generally used in a long-haul system to compensate for total loss. Also, it is used in Wavelength Division Multiplexing (WDM). Moreover, multiple amplifiers are applied as cascaded amplifiers to increase the power budget of network. Figure 1.1 b) shows the preamplifier inserted before an optical receiver to improve an optical receiver's sensitivity as well as increase the power budget. The power booster amplifier is applied after an optical transmitter as shown in Figure 1.1 c). This amplifier increases transmitted power and power budget. Figure 1.1 d) illustrates the LAN booster amplifier inserted in a middle of network similar to an in-line amplifier. This amplifier is generally used in the Passive Optical Network (PON).

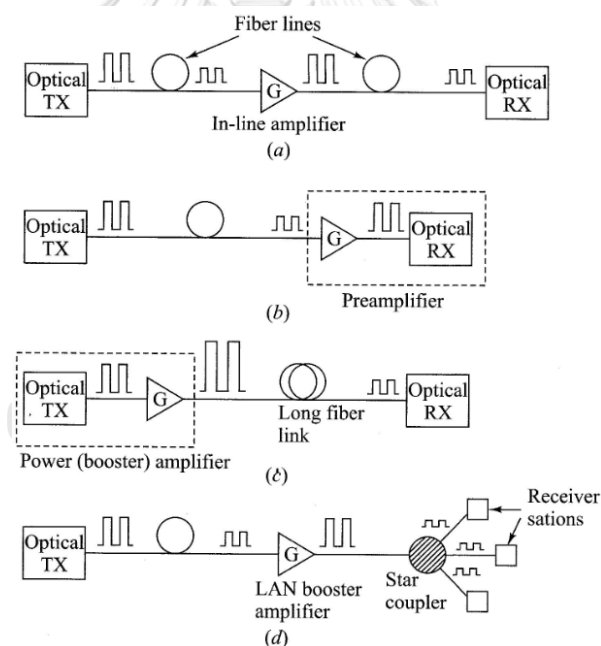


Figure 1.1 Applications of optical amplifier [1].

There are three main types of optical amplifiers: 1) Erbium-Doped Fiber Amplifier (EDFA), 2) Raman amplifier, and 3) Semiconductor Optical Amplifier (SOA). EDFA is doped by Erbium element. It gives high gain and low Noise Figure (NF). However, EDFA can operate in only C-band (1530 nm – 1565 nm) as shown in Figure

1.2 a). Raman amplifier has very high gain and can operate outside C-band. However, it is expensive and has high power consumption.

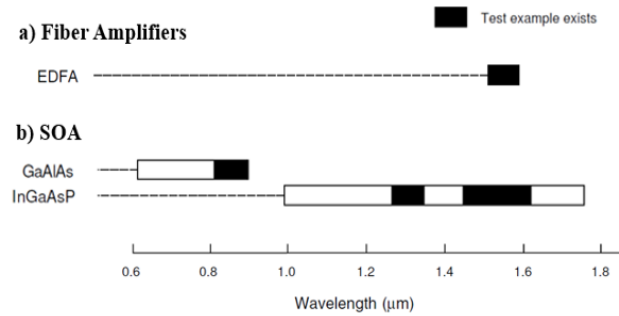


Figure 1.2 Wavelength bands of a) fiber amplifiers and b) SOA [2].

SOA is a good option to be used for several bands. The operating wavelength ranges depend on doped elements. Figure 1.2 b) shows the operating wavelengths of GaAlAs and InGaAsP substrates, which can fabricate different SOAs operating in various wavelength ranges. Furthermore, SOA has lower cost and is more compact size compared to other amplifiers. Moreover, it can be easily integrated with semiconductor devices such as laser and modulator. The nonlinear effects of SOA, such as cross-gain modulation and cross-phase modulation, can be applied for wavelength conversion [3]. The radiative processes of SOA are described as follows.

Radiative Processes [4]

The energy gap (E_g) of semiconductor material is important factor for emitted wavelength according to equation (1.1) [4].

$$E_g = h\nu = \frac{hc}{\lambda} \quad (1.1)$$

where h is Planck's constant ($= 6.626 \times 10^{-34}$ J-s), ν is frequency (Hz), c is velocity of light ($\approx 3 \times 10^8$ m/s), and λ is wavelength (nm).

There are 3 radiative processes of SOA as shown in Figure 1.3 [4]. The lowest conduction band (E_2) and highest valence band (E_1) are considered. The energy gap of SOA is equal to $E_g = h\nu = E_2 - E_1$.

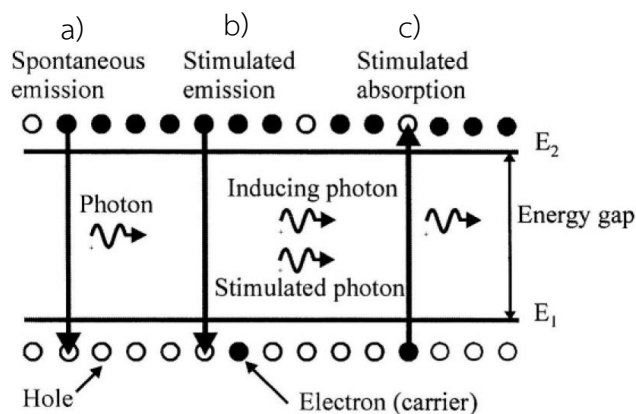


Figure 1.3 Radiative processes of SOA: a) spontaneous emission, b) stimulated emission, and c) stimulated absorption or absorption [4].

- The spontaneous emission is displayed in Figure 1.3 a). The electrons in conduction band are released to valence band depending on carrier lifetime. Therefore, this process produces background noise that cannot be avoided.
- The stimulated emission process is important for amplification in SOA as shown in Figure 1.3 b). This process requires the empty states in valence band. The inducing photons trigger electrons from a conduction band to relax to a valence band, then stimulated photons occur.
- The stimulated absorption or absorption process is shown in Figure 1.3 c). This process requires the empty states in conduction band. The electrons in a valence band are excited to a conduction band by inducing photons. The absorption process is important to photodiodes.

Additionally, the current from external current source is injected into SOA to increase more electrons or carriers in a conduction band. Therefore, the stimulated photons of stimulated emission process can be increased because of high carriers. For this reason, it results in the amplification of SOA.

SOA's Structure [4]

The double-heterostructure SOA shown in Figure 1.4 a) illustrates a basic structure of SOA. The compound III-V semiconductor, such as GaAs and InP, is used as SOA's substrate for wavelength emissions in optical communication. Light emits from the active layer, which is intrinsic semiconductor grown between p-type and n-

type semiconductors. The current is injected into SOA at current stripe, then electrons spread into active layer to increase carriers. Anti-Reflection (AR) coatings must be applied at the end of both facets to eliminate high reflectivity.

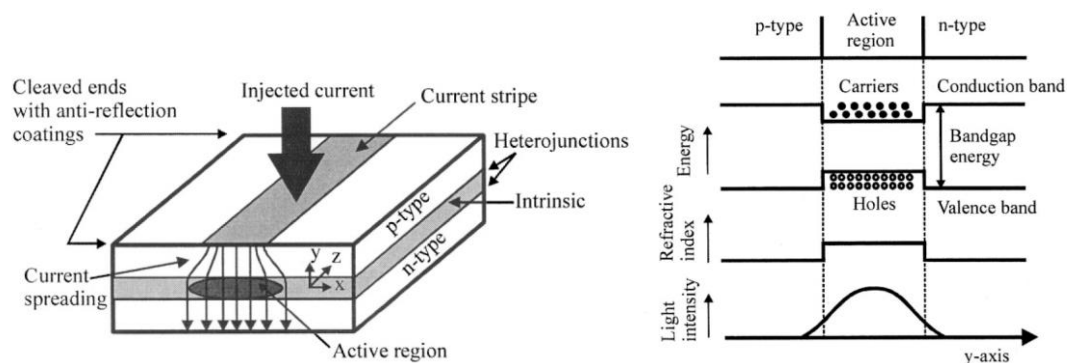


Figure 1.4 a) Double-heterostructure SOA and b) carrier & optical confinements in double-heterostructure SOA [4].

The p-type and n-type semiconductors are cladding layers. The cladding layers must have higher energy gap and lower refractive index than active layer in order to have carrier and optical confinements as shown in Figure 1.4 b). Therefore, the highest light intensity occurs in active region. The width of waveguide has to be narrow to avoid higher-order transverse mode. SOA has nonlinear effects such as self-phase modulation and chirp. They are undesirable effects for an access network. Consequently, Quantum Dot Semiconductor Optical Amplifier (QD SOA) is developed to reduce those effects.

The QD SOA is interesting device in many researches. This amplifier is developed from SOA by using Quantum technology. Both structures of SOA and QD SOA are almost the same. However, QD SOA has the QD layer grown in active layer as shown in Figure 1.5. QD layer improves some characteristics of semiconductors.

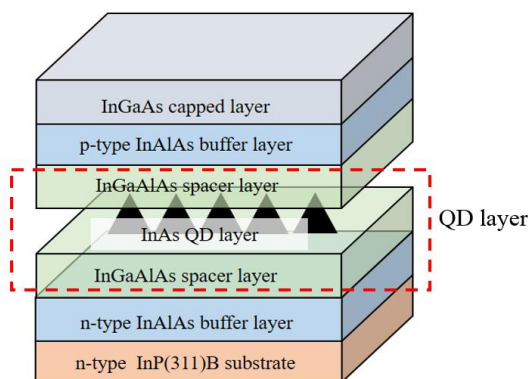


Figure 1.5 QD layer in QD SOA structure.

Nano Structure [5]

Bulk, Quantum Well (QW), Quantum Wire, and Quantum Dot (QD) have the density of states $D(E)$ as shown in Figure 1.6. First, the bulk structure has three dimensions (3D) and continuous density of state. Second, the QW structure has two dimensions (2D). And, its density of state is step function. Third, the Quantum Wire has one dimension (1D) and density of state shown in Figure 1.6 c). Last, the QD structure has dimensionless (0D) and discrete density of state. Therefore, the QD provides better carrier confinement compared to other structures.

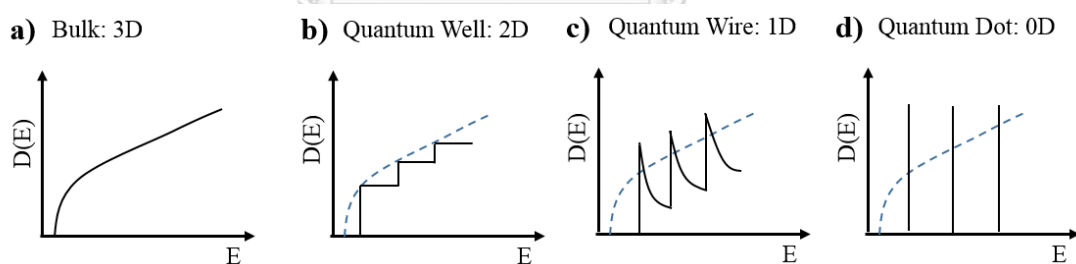


Figure 1.6 Density of state $D(E)$ for a) bulk, b) quantum well, c) quantum wire, and d) quantum dot [5].

Figure 1.7 displays the density of state of QD gain media. Bulk and QW act as carrier reservoirs. The QD Excited State (QD ES) is additional state. The most important state is QD Ground State (QD GS), which affects response time of SOA.

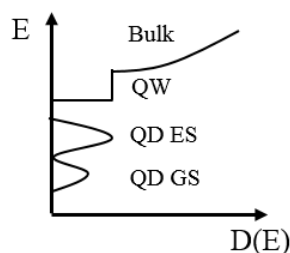


Figure 1.7 Density of state of QD gain media [5].

Dynamic Properties [5]

Two main dynamic processes are intra-band and inter-band processes. The intra-band process is dynamic carrier within each band, while the inter-band process has generation and recombination of carriers (electron or hole) between valence and conduction bands. Moreover, the carrier injection from external current source causes inter-band process.

The dynamic properties are related to gain recovery time or response time of SOA. Its response time is important factor for many applications such as burst-mode transmission, optical signal processing, wavelength conversion, and optical switching. Therefore, the individual process is necessary to consider SOA's response time. According to Ref. [5], they measured the response time by pump-probe configuration. The pump signal is short and strong pulse to force gain media out of steady-state. Furthermore, the probe signal is short and weak pulse. The probe signal detects gain and phase change after pump pulse. Then, it traces gain and system recovery back to steady-state.

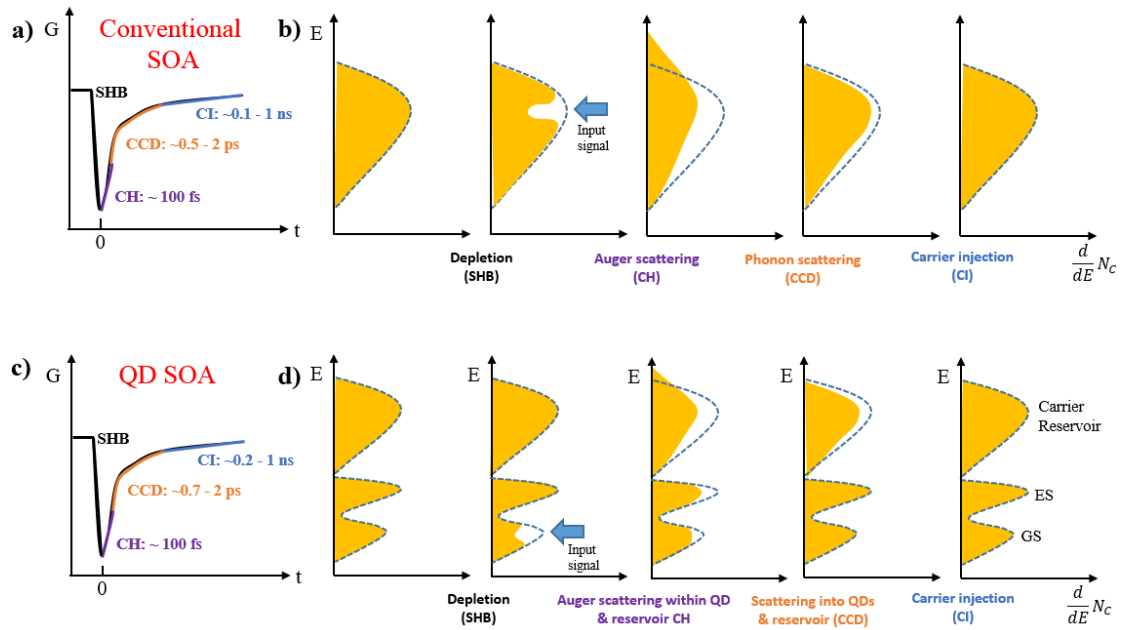


Figure 1.8 Pump-probe curves: a) conventional SOA & c) QD SOA, and the change of carrier density: b) conventional SOA & d) QD SOA [5].

The pump-probe curves and the change of carrier density ($\frac{d}{dE}N_C$) of conventional SOA are shown in Figure 1.8 a) and b), respectively. According to this pump-probe measurement, the pump signal is applied to SOA as gain compression, which results in carrier depletion or Spectral Hole Burning (SHB). Next, the Auger scattering or Carrier Heating (CH), which is intra-band process occurs at about 100 fs to close spectral hole. Furthermore, the carrier distribution has to be equal to Fermi distribution. After that, the phonon scattering or Carrier Cool Down (CCD), which is intra-band process, occurs in a few ps for a relaxation of carrier distribution. Last, the carrier injection from external current source, which is inter-band process, needs 1 ns to refill carrier density in a conduction band. Consequently, the response time in conventional SOA is approximately 1 ns.

The pump-probe curves and the change of carrier density of QD SOA are shown in Figure 1.8 c) and d), respectively. The gain media of QD SOA are different from conventional SOA. They have additional states: Ground State (GS) and Excited State (ES). According to Figure 1.8 d), the upper band is used for carrier reservoir, which needs carrier density higher than in QD at least 10^4 times. First, the gain

compression results in SHB similar to conventional SOA. But, the SHB in QD SOA occurs only at GS. Next, the reservoir CH results in carrier refilling from reservoir into GS and ES about 100 fs. After that, the carrier distribution occurs from CCD leading to closure of spectral hole in GS. Therefore, QD SOA has gain recovery within a few ps without carrier injection that needs long time to refill carrier density in conduction band. As a result, the QD SOA has response time less than 1 ns.

At present, the QD SOA has many advantages such as ultra-fast gain response, low Noise Figure (NF), low data pattern effect, low power consumption, and low cost [6]. The typical operating wavelengths used in optical communication are O-band and C-band. The typical substrates of QD SOA are GaAs [7] for O-band and InP [8] for C-band. The Stranski–Krastanov growth (S-K growth) is applied for QD layer growth because of ultralow threshold current, temperature stability, high modulation bandwidth, and low chirp. However, this S-K growth technique cannot be suitable for more than ten layers of QD. For this reason, the strain compensation technique [9, 10] has been proposed to increase QD layers and QD density. To improve the characteristics of QD, Rapid Thermal Annealing (RTA) is applied during growth process. The threshold current of annealed devices is better than as-grown devices. The external quantum efficiency (η_d) and internal quantum efficiency (η_i) of lasers under RTA process are also improved [7, 11].

Nowadays, the number of users in an access network increases every year. Many applications require large bandwidth and high-speed internet. The optical access network with high bit rate is installed to support many users and extended distance. The Passive Optical Network (PON) plays an important role in many countries to support many users and high bit rate at least 1 Gb/s. Therefore, the optical amplifier is inserted to increase power budget in PON. The details of Gigabit-capable Passive Optical Networks (G-PON), 10-Gigabit-capable Passive Optical Networks (XG-PON), and 40-Gigabit-capable Passive Optical Networks (NG-PON2) based on ITU-T standards are listed in Table 1.1.

Table 1.1 ITU-T standards of G-PON, XG-PON, and NG-PON2

Standard	Name	Upstream bit rate	Downstream bit rate
ITU-T G.984.1 [12]	G-PON	2488.32 Mb/s@1310 nm	2488.32 Mb/s@1490 nm
ITU-T G.987.1 [13]	XG-PON	10 Gb/s@1270 nm	10 Gb/s@1577 nm
ITU-T G.989.1 [14]	NG-PON2	40 Gb/s@1524–1544 nm	40 Gb/s@1596–1603nm

First, the G-PON based on ITU-T G.984.1 has upstream and downstream wavelengths at 1310 nm and 1490 nm, respectively. The bit rates of both upstream and downstream transmissions are up to 2488.32 Mb/s. And, the number of users is up to 64 users. The power budget classes are class A (5 – 20 dB), class B (10 – 25 dB), and class C (15 – 30 dB). According to GPON: Reach extension based on ITU-T G.984.6 [15], the reach extension is up to 60 km by using optical amplifiers or repeaters. Next, the XG-PON based on ITU-T G.987.1 has upstream and downstream wavelengths at 1270 nm and 1577 nm, respectively. The bit rates of upstream and downstream transmission are 10 Gb/s. The distance can be extended from 20 km to 60 km by using optical amplifiers. The power budget classes are N1 class (14 – 29 dB), N2 class (16 – 31 dB), E1 class (18 – 33 dB), and E2 class (20 – 35 dB). Last, the NG-PON2 follows ITU-T G.989.1. It uses Time & Wavelength Division Multiplexed (TWDM) PON and Point-to-Point (PtP) WDM to increase bandwidth. The bit rates of upstream and downstream transmission are up to 40 Gb/s. The upstream and downstream wavelengths are 1524 – 1544 nm and 1596 – 1603 nm, respectively [16]. The power budget classes are the same as XG-PON.

1.3 Objectives

1. Study the fabrication of a ridge laser diode to be implemented as Quantum Dot Semiconductor Optical Amplifier (QD SOA) and improve the characteristics of QD SOA.
2. Study and measure the characteristics of conventional SOAs and QD SOA as follows: amplifier gain, optical spectrum, output saturation power, and Noise Figure (NF).
3. Apply amplifiers in an access network, expecting at least 2 times of power budget above the standard. Measurements are repeated to analyze the Bit Error Rate (BER) at 10^{-3} .

1.4 Scopes

1. Study 40 Gb/s bit rate access network at C-band wavelength.
2. Measure the characteristics of 3 optical amplifiers as follows: (1) C-band conventional SOA1013S (SOA#1), (2) C-band conventional SOA1117S (SOA#2), (3) C-band QD SOA.
3. Evaluate the performances of 3 optical amplifiers in 40 Gb/s data transmission, which must achieve 10^{-3} BER according to standard. Their results are analyzed the data pattern effect.

1.5 Benefits and Applications

1. The internal quantum efficiency of ridge LD increases to be 66.39 % with low optical loss at 9.36 cm^{-1} by Rapid Thermal Annealing (RTA).
2. The maximum chip gain is 35 dB with 400-mA bias current. The high gain of QD SOA is important parameter to increase power budget in a network.
3. QD SOA successfully gives the fastest response time of 70 ps and less data pattern effect, which are suitable for burst-mode transmission.
4. The cascaded SOA#1 and QD SOA can support 128 users and distance at 20 km in 40 Gb/s access network. And, the power budget is at least 2 times above standard.

2. Characteristics-improvement of QD semiconductor optical amplifier using rapid-thermal annealing process

Budsara Boriboon¹, Duang-rudee Worasuchep¹, Atsushi Matsumoto², Kouichi Akahane², Naokatsu Yamamoto², Naoya Wada²

¹Department of Electrical Engineering, Chulalongkorn University, Thailand

²National Institute of Information and Communications Technology, Japan

Published in international conference: *Proc. SPIE 10528*, Optical Components and Materials XV, 105280F (22 February 2018); doi: 10.1117/12.2288608

<https://doi.org/10.1117/12.2288608>

We investigated the effect of Rapid Thermal Annealing (RTA) process on Quantum Dot Semiconductor Optical Amplifiers (QD SOAs). The devices are composed of 30-layer stacks of InAs quantum dot by using strain compensation method. The lateral size and height of QD are 30 nm and 4 nm, respectively. Our QD SOAs have emission wavelengths within 1.5 μm -band. We applied RTA process to improve the characteristics of internal quantum efficiency (η_i) and optical loss (α_i) of ridge laser diode for QD SOAs. In this case, the operating temperatures of RTA process were set at 600 °C, 620 °C, 640 °C and 660 °C for 30 seconds each. In addition, the devices are cleaved to form a cavity length at 0.06 cm, 0.08 cm, 0.10 cm, 0.12 cm and 0.14 cm. According to the L-I characteristic result of ridge laser diode structure for QD SOAs at 640 °C, the best minimum threshold current (I_{th}) is 47.93 mA. Moreover, according to the plot between η_{d}^{-1} (external quantum efficiency) and cavity length, we can optimize the internal quantum efficiency and optical loss for a ridge laser diode structure to be 66.39 % and 9.87 cm^{-1} , respectively at 640 °C RTA's temperature. Finally, The RTA process helps to achieve 1.4 times higher in internal quantum efficiency as well as a minimal increase in internal optical loss comparing to without RTA.

2.1 Introduction

The number of Internet users is rising every year and their residences are spreading outwards. Many applications also require large bandwidth. The installed optical access networks must offer a high bit rate transmission covering a broader subscribed area with more power budget. The standard G-PON [17] and XG-PON [18] play an important role in many countries to support bit rates up to 10 Gb/s. But, the limited power budget prohibit those networks to offer both a large number of subscribers and long distance. For this reason, an optical amplifier is needed to compensate for more losses from splitters and fiber attenuation. For example, Semiconductor Optical Amplifier (SOA) is widely used since it can work at any wavelength depending on its dopant, unlike Erbium Doped Fiber Amplifier (EDFA) only works in C-band. However, SOA consumes more power than EDFA at the same output gain. SOA also has data pattern dependent effect. Hence, Quantum Dot Semiconductor Optical Amplifiers (QD SOAs) will be used instead because of better performance, such as lower power consumption and no pattern dependent effect.

The Quantum Dot (QD) semiconductor is applied in many optical devices. The Stranski–Krastanov growth (S-K growth) is an excellent technique for QD layer growth. This technique has a lot of advantages such as ultralow threshold current, temperature stability, high modulation bandwidth, and low chirp. According to quantum dot lasers with S-K growth technique, the improvement of a threshold current density, characteristic temperature, differential gain, linewidth enhancement factor, and internal quantum efficiency were observed [19]. However, this S-K growth technique cannot be suitable for more than ten layers of QD. Therefore, the layers and density of quantum dot will be limited. For this reason, the highly stacked layers with strain compensation technique [9, 10] has recently been proposed to improve the performance of quantum dot density. The 30-layer InAs quantum dot grown on InP substrate at 1.5 μm -band wavelength with high characteristic temperature was reported [20]. Furthermore, a ridge laser diode with highly stacked layers was already proposed in [21]. Finally, the QD SOAs can be assembled from a ridge Laser Diode (LD) structure [8].

The Rapid Thermal Annealing (RTA) process has been applied to improve performance in many applications such as Quantum Dot Laser, Quantum Dot Infrared Photodetector (QDIP) [22, 23], and solar cell [24]. In papers [7, 11, 22, 23, 25-27], the RTA process on QD laser with GaAs substrate at 1.3 μm wavelength was investigated. Instead, we use InP substrate at 1.5 μm -band wavelength with RTA process, which is different from those reported papers. This annealing process improves the characteristic of QD structure. In addition, the threshold current of annealed devices is better than as-grown devices. The external quantum efficiency (η_{ext}) and the internal quantum efficiency (η_{int}) of lasers under RTA process are also improved [7, 11]. Nevertheless, the internal optical loss (α_{i}) was slightly increased during RTA in our case. Then, we suppressed this optical loss by using a better growth condition of new Broad Area Laser Diode (BA-LD) and ridge LD. The thermal annealing results in blue-shift effect and a narrower Full Width at Half Maximum (FWHM). During RTA process, the devices are capped by SiO_2 sputtering on both sides to protect its surface substrate [28, 29].

In this paper, we investigate the effect of RTA process on BA-LD and ridge LD for QD SOAs. The devices are composed of 30 stacked-layer InAs quantum dot operating at 1.5 μm wavelength band for CATV broadcast according to ITU-T G.984.5 G-PON standard [30]. The improvement in characteristics of annealed devices are compared to as-grown devices. We can achieve a significantly high internal quantum efficiency and low internal optical loss for BA-LD and ridge LD under RTA process.

2.2 Experiments

There are 4 experiment steps: (1) Quantum Dot growth, (2) RTA process, (3) laser diode fabrication and (4) measurements. First, we grew 30-layers stacks of InAs quantum dot on InP(311)B substrate by Molecular Beam Epitaxy (MBE), as shown in Figure 2.1 (left). Then, this highly stacked QD layer was applied the strain compensation method. The QD density is $5.24 \times 10^{10} \text{ cm}^{-2}$, measured by Atomic Force Microscope (AFM) as shown in Figure 2.1 (right). The average lateral size and height of QDs are 30 nm and 4 nm respectively. The n-InAlAs buffer layers are composed of 100-nm thick layer of lattice-matched Si-doped n-type. Also, a 2000-

nm thick of p-type InAlAs buffer layer was grown. The InAs QDs are separated by 20-nm thick InGaAlAs as spacer layers. An InGaAs capped layer follows the buffer layer. Next step, we did RTA process on as-grown samples to improve the characteristics of QD SOAs. The temperature conditions of RTA process were performed in Ar ambient at 600 °C, 620 °C, 640 °C, and 660 °C for 30 seconds. During RTA process, the devices were capped by sputtered SiO₂ on both sides to prevent In desorption. Later, this SiO₂ coating was removed by Buffered Hydrofluoric Acid (BHF).

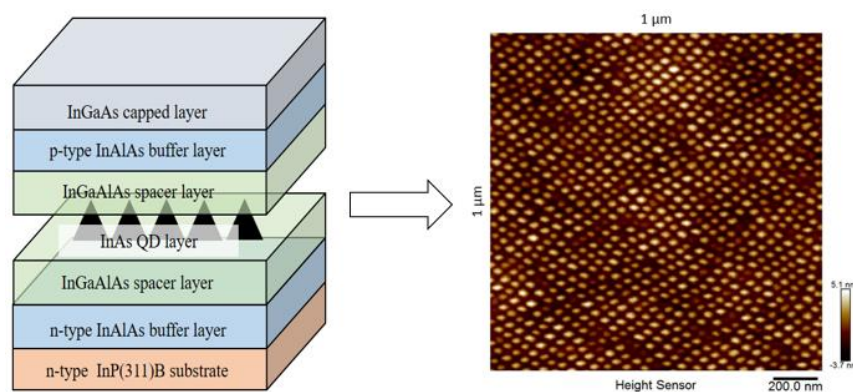


Figure 2.1 (left) Structure of quantum dot laser and (right) a picture from AFM measurement.

The 3rd step, we fabricated 2 types of laser diode: Broad Area Laser Diode (BA-LD) and ridge laser diode. In case of BA-LD, SiO₂ was coated on as-grown samples, followed by an ohmic contact layer which is Ti-Pt-Au n-type. Likewise, a ridge laser diode structure consists of the same SiO₂ and ohmic type, but it has Benzocyclobutene (BCB) as an insulator layer. The devices were cleaved at 0.06 cm, 0.08 cm, 0.10 cm, 0.12 cm and 0.14 cm cavity lengths. For measurement step, the optical spectrum of as-grown samples were measured by Photoluminescence (PL), which was set at 77 Kelvin temperatures. The 514-nm laser diode and InGaAs photodetector were used in PL measurement. According to L-I characteristics measurement, the plot shows light output power versus injection current. We can obtain the threshold current (I_{th}) from this L-I relationship. The pulse width and duty cycle of Laser Diode (LD) tester were set at 1 μs and 1 %, respectively. In this paper, we tested three cases: (1) BA-LD, (2) new BA-LD with better conditions of QD growth, and (3) ridge LD.

2.3 Results

Figure 2.2 shows the plot of Photoluminescence (PL) intensity and wavelength of as-grown sample before Rapid Thermal Annealing (RTA) process. The peak wavelength of PL spectrum was measured to be 1580 nm.

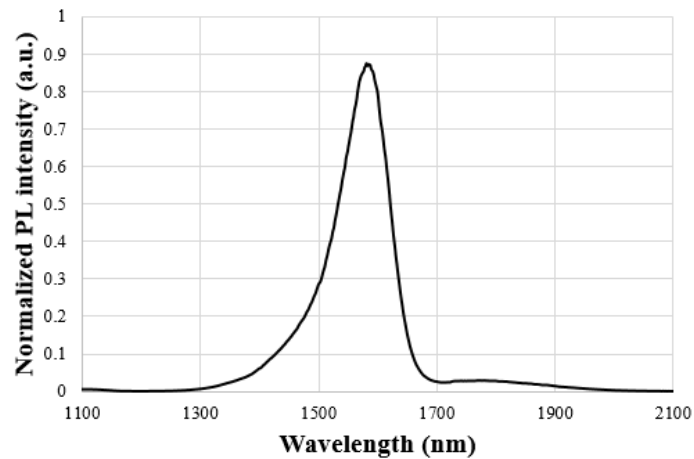


Figure 2.2 PL spectrum of as-grown sample.

According to the L-I results in Figure 2.3, the significant improvement of threshold current when using RTA process can be distinctively observed, comparing to the threshold current of 1366.35 mA for devices without RTA. Figure 2.3 shows the threshold currents of 650.93 mA for BA-LD and 315.13 mA for new BA-LD, at 640 °C RTA temperature. In addition, the ridge LD has the lowest threshold current of 47.93 mA, which is better than BA-LDs under the same conditions.

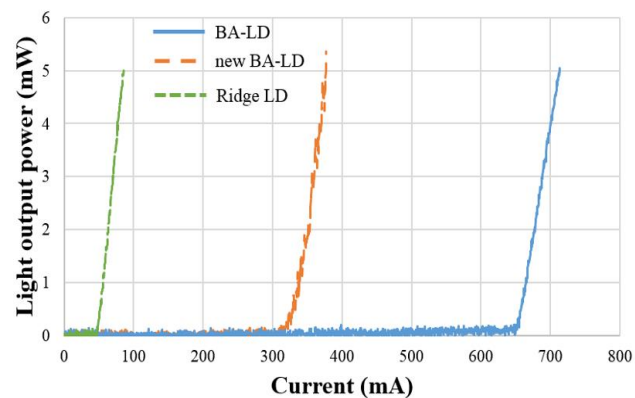


Figure 2.3 L-I characteristic measurement of BA-LD, new BA-LD, and ridge LD.

The external quantum efficiency (η_d) was derived from a slope of L-I plot in Figure 2.3. We repeated L-I measurement of many samples, and found the external quantum efficiencies of LDs at different cavity lengths and RTA temperatures. Figure 2.4 a) – d) display the external quantum efficiency results of BA-LD samples at 600 °C, 620 °C, 640 °C and 660 °C RTA temperatures, respectively. Figure 2.4 e) displays the results of new BA-LD samples at 640 °C, and Figure 2.4 f) shows the results of ridge LD samples at 640 °C RTA temperature.

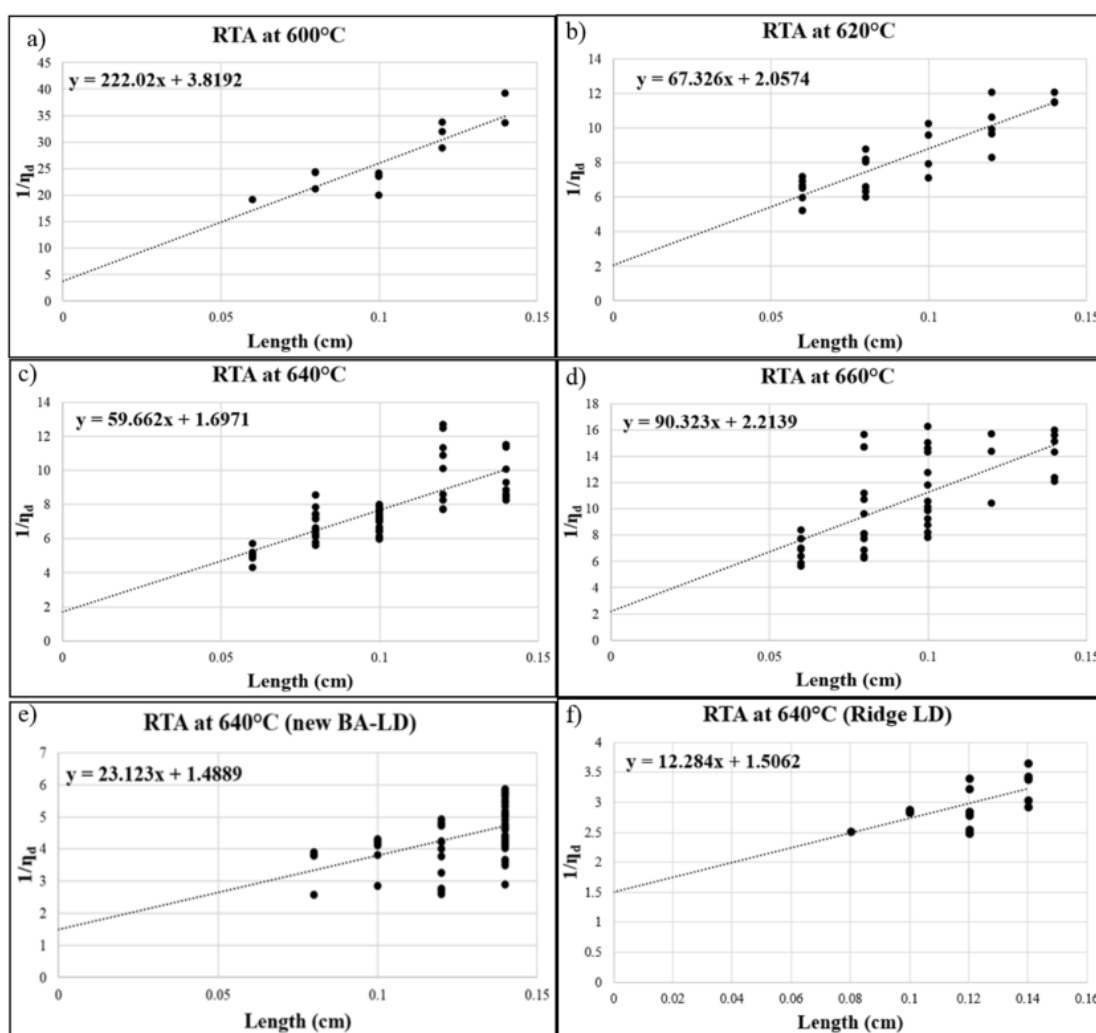


Figure 2.4 External quantum efficiencies at different cavity lengths and RTA temperatures: a) BA-LD at 600 °C, b) BA-LD at 620 °C, c) BA-LD at 640 °C, d) BA-LD at 660 °C, e) new BA-LD at 640 °C, and f) ridge LD at 640 °C

A relationship between external quantum efficiency and cavity length leads to the internal quantum efficiency (η_i) and optical loss (α_i) as given in equation (2.1).

$$\frac{1}{\eta_d} = \frac{1}{\eta_i} \left[\frac{\alpha_i L}{\ln\left(\frac{1}{R}\right)} + 1 \right] \quad (2.1)$$

where L and R are cavity lengths and reflectivity of laser cavity, respectively. In this case, R is equal to 0.298, and L are equal to 0.06 cm, 0.08 cm, 0.10 cm, 0.12 cm, and 0.14 cm.

Based on all those dot results in Figure 2.4, the dotted line was drawn in each plot to approximate equation (2.1). Hence, the internal quantum efficiency and optical loss were extracted and plotted versus different RTA temperatures as illustrated in Figure 2.5. The solid reference line is also shown for devices without RTA process as the lower bound.

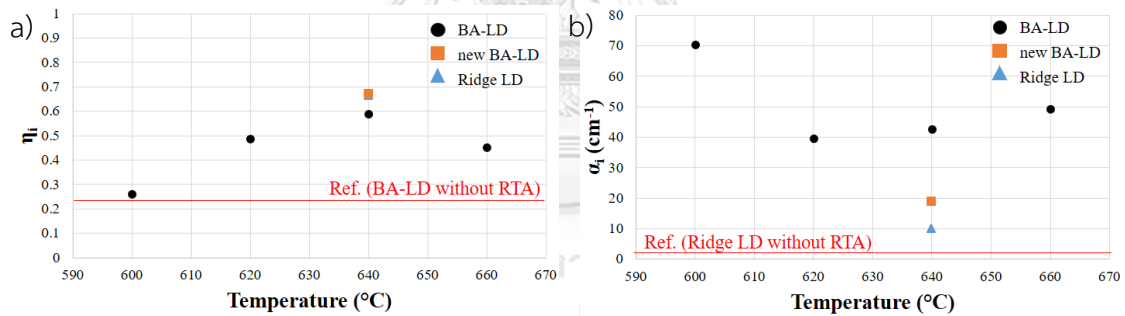


Figure 2.5 a) Internal quantum efficiency vs. RTA temperature, and b) Optical loss vs. RTA temperature.

In Figure 2.5, the results of BA-LD, new BA-LD, and ridge LD are displayed as circle, square, and triangle, respectively. The internal quantum efficiencies of annealed devices are higher than devices without RTA. Clearly, this efficiency is highest at 640 °C due to the reduction of non-radiative recombination and density of defects. However, a too high RTA temperature at 660 °C caused dislocation of quantum dots. According to Figure 2.5 a), the improvement of internal quantum efficiency jumps from 24.71 % (BA-LD without RTA) to 58.92 % for BA-LD, and rises

from 50.36 % (without RTA) to 67.16 % for new BA-LD, both at 640 °C RTA temperature.

In Figure 2.5 b), the internal optical losses at different RTA temperature are shown. Again, these losses of annealed devices are higher than devices without RTA. The highest loss at 600 °C RTA temperature was caused by a too low annealing temperature, which is unsuitable condition for QD structure in annealed devices. Consequently, the optimized internal optical losses at 640 °C RTA temperature are 42.56 cm⁻¹ for BA-LD and 18.80 cm⁻¹ for new BA-LD.

In case of ridge LD at 640 °C RTA temperature, its internal quantum efficiency rises from 46.13 % (without RTA) to 66.39 %. And in Figure 2.5 b), the internal optical loss also increases from 2.24 cm⁻¹ (ridge LD without RTA) to 9.87 cm⁻¹. Comparing these results of internal quantum efficiency and optical loss, the ridge LD outperforms BA-LD.

2.4 Conclusion

We successfully fabricated 30-layer stacks of InAs Quantum Dot Semiconductor Optical Amplifiers (QD SOAs) by using strain compensation method. The devices have emission wavelengths within 1.5 μm-band. The Rapid Thermal Annealing (RTA) process at 640 °C temperature can improve the characteristics of internal quantum efficiency (η_i) and optical loss (α_i) for a ridge laser diode structure equal to 66.39 % and 9.87 cm⁻¹, respectively. The RTA process helps to achieve 1.4 times higher in internal quantum efficiency as well as a minimal increase in internal optical loss comparing to without RTA.

2.5 Acknowledgment

The authors are grateful to all staffs for their helps at Photonic Device Laboratory (PDL), National Institute of Information and Communications Technology of Japan (NICT), as well as International Affairs Department for summer internship program, which gave a great opportunity to use equipment and gain research experience at Network System Research Institute. We would like to express

appreciation to researchers and technical staffs, especially Mr. Shinya Nakajima, for helps and advices at Network Science and Convergence Device Technology Laboratory. Our special thanks must be given to the 100th Anniversary Chulalongkorn University Fund for Doctoral scholarship. This work was partly conducted as part of a research project supported by the Japanese Government funding for “R&D to Expand Radio Frequency Resources” by the Ministry of Internal Affairs and Communications. Lastly, the authors would like to thank NICT located at Engineering Centennial Memorial building at Chulalongkorn University for many devices and T&M equipment, especially 1.5 μm -band QD SOA for characteristic study.



3. Optimized design of QD-LD toward QD SOA to achieve 35-dB maximum chip gain with 400-mA injected current

Budsara Boriboon¹, Duang-rudee Worasucheep¹, Atsushi Matsumoto², Kouichi Akahane², Naokatsu Yamamoto², Naoya Wada²

¹Department of Electrical Engineering, Chulalongkorn University, Thailand

²National Institute of Information and Communications Technology, Japan

Published in international journal: *Optics Communications*, vol. 475, p. 126238, 2020/11/15/ 2020.

<https://doi.org/10.1016/j.optcom.2020.126238>

We measured the characteristics of Quantum Dot Semiconductor Optical Amplifiers (QD SOA) with 25 stacked layers of InAs/InGaAlAs QDs grown on InP(311)B substrate. The temperature dependence of threshold current and lasing peak wavelength in C-band of QD-Laser Diode (QD-LD) were analyzed over its operating range of 15 – 80 °C. The chip gains of 3 device lengths (1.5, 2 and 2.4 mm) were compared under varied injected currents up to 500 mA. To avoid overheat and chip damage during measurements, the pulse current source with 1 % and 10 % duty cycles was used. Based on our best results of 2-mm long QD SOA with 25 stacked QD layers, the 1 % pulse is preferable because of its lower heating and additional chip gain of 11.9 dB. Hence, the highest chip gain of 35 dB was achieved at 400-mA injected current, as well as the highest 3-dB saturation output power at 20.9 dBm. According to the plot of chip gain versus wavelength, it shows 3-dB gain spectrum over 20 nm and the highest peak at 1570-nm wavelength with 500-mA injected current. In addition, the results of another QD SOA module showed 15.4-dB Input Power Dynamic Range (IPDR), faster response time due to less pattern effect and error-free transmission of 40 Gb/s data over 20-km Single Mode Fiber (SMF) link.

3.1 Introduction

The Quantum Dot technology has become more interesting in R&D mainly in optical communication. Many devices integrate QD, such as QD-LD since 1997 [19], QD SOA [6] and photodetector [31]. In case of QD-LDs, some techniques are applied to improve performances. For example, the Rapid Thermal Annealing (RTA) process can increase lasers' internal quantum efficiency (η_i) with low optical loss (α_i) [32]. This efficiency also increases with the higher number of stacked QD layers [33]. However, the number of QD layers must be optimized because of the self-heating effect that occurs under too many QD layers [34].

In case of QD SOAs, they are attractive due to many advantages, such as ultra-fast gain response, low noise figure [6], and high efficiency of Four Wave Mixing (FWM) or Cross Gain Modulation (XGM) for wavelength conversion [35-38] as well as Cross Phase Modulation (XPM) for all-optical signal processing, e.g. logic (XOR & AND) gates [39, 40], 2x2 switch [41], and D flip-flop [42]. Plus, the QD SOAs can be applied in very high bit-rate up to 40 Gb/s [35-38, 43] in various applications using different modulation formats, such as QPSK, 8-PSK [36], 16-QAM [36, 43], and PAM-4 [37, 38]. Similar to QD-LD [44], the extremely stable temperature characteristic of QD SOA can be achieved by proper growth conditions of QD layers. The key parameter of QD SOA is amplifier gain, which can be increased by the number of stacked QD layers, for instance, QD SOA operating at O-band [45, 46] and C-band [43, 47]. Based on prior work [47], the highest chip gain of 1550-nm QD SOA (with 20 stacked InAs/InGaAlAs QD layers) is 35 dB at 500-mA injected current. In this paper, we can reach the same gain, but at a lower current and higher stacked QD layers, which are very complicated to fabricate. To the best of our knowledge, the maximum gain is 41 dB around 1480-nm wavelength as reported in [48], from the QD SOA applied in 16-QAM amplification; but it required very high injected current of 1.85 A.

Here are the benefits of SOAs and QD SOAs. They can be applied in fiber networks to amplify any wavelength depending on their doped semiconductor elements. They are very compact and consume less power as compared to Erbium Doped Fiber Amplifier (EDFA). The QD SOAs have better performance of frequency

chirp as well as less data pattern effect than conventional SOAs [49, 50]; and thus they are more suitable for the burst-mode upstream transmission in Passive Optical Network (PON) as well as for optical signal processing. The QD SOA can increase link distance and splitting ratios in access networks, such as in Ref. [51] that applied QD SOAs as stand-alone units in 1.3- μm upstream and 1.5- μm downstream transmissions of GPON [17] to extend fiber distance up to 60 km. Moreover, the QD SOAs can be integrated together with pin- or QD-photodiode for their higher responsivities of receiver modules [52, 53].

In this paper, we initially investigate 4 different stacked QD layers of QD-LD: 10, 14, 20 and 25 layers. The plots of injected current versus output power, so called I-L plot, at various temperatures are measured. Then, their lowest threshold currents are reported to be related to temperature according to its equation. These QD-LDs can operate at high temperature up to 80 °C. Secondly, after optimizing the structure of QD-LD and the best number of stacked QD layers was found, we apply these profiles to the structure of QD SOAs in order to obtain very high gains over C-band. Three device lengths of QD SOA are evaluated at room temperature: 1.5, 2 and 2.4 mm. To investigate QD SOAs' potential, the simple chip state is typically used with a pulse current source to measure chip gain. Without mounting those chips on heat sink as in assembled modules, the self-heating effect will occur under a high DC operation. For this reason, the pulse current source is set at 1 % and 10 % duty cycles to avoid heating and chip damage during measurements [9, 10, 44, 54-56]. Finally, due to its higher gain results, only the 2-mm QD SOA chip is chosen for more tests of maximum gain's conditions, saturation output power, and 3-dB gain spectrum in C-band. Furthermore, another QD SOA chip with almost same design, which was assembled into a module, is evaluated for its dynamic properties, such as Input Power Dynamic Range (IPDR), pattern effect, and 40 Gb/s data transmission over 20-km Single Mode Fiber (SMF).

3.2 Experiments

3.2.1 Experimental setup of QD-LD & QD SOA chips

Our QD devices were fabricated using a simple ridge structure as shown in Figure 3.1. The active layer consists of InAs QD layers separated by 20-nm thick InGaAlAs spacing layers. All layers were grown on InP(311)B substrate in Molecular Beam Epitaxy (MBE). One of the most important feature of our design is the strain compensation technique based on previous works [10, 57], such that we can fabricate the highly stacked QD-LD & QD SOA with tensile strain-induced spacer layer. From the profile of QD devices in Figure 3.1, the thickness and doping concentration of n-InAlAs cladding layer are 150 nm and $8 \times 10^{17} \text{ cm}^{-3}$, respectively. The thickness and doping concentration of p-InAlAs cladding layer are 1.6 – 2 μm and $5 \times 10^{17} \text{ cm}^{-3}$, respectively. The BCB (Benzo Cyclo Butene) is an insulator layer. The top p⁺-InGaAs layer is 100 nm thick with a doping concentration of $2.4 \times 10^{19} \text{ cm}^{-3}$. Both p- and n-contact electrode layers are made of Ti-Pt-Au. The typical QD sheet density is estimated to be $7.0 - 9.5 \times 10^{10} \text{ cm}^{-2}$, whereas the average lateral size and height of QDs are approximately 35 nm and 3 nm, respectively. The width and height of ridge waveguide are 2.5 μm and 1.4 – 1.8 μm , respectively.

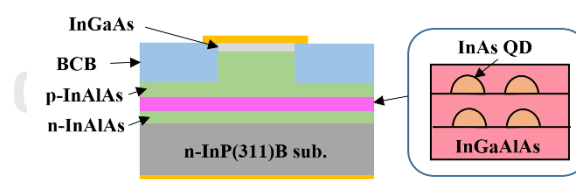


Figure 3.1 Structure of QD devices.

The first part focuses on QD-LD chips. Their temperature characteristics were observed via I-L plot measurement at different temperatures from 15 to 80 °C. There are 4 cases of stacked QD layers: 10, 14, 20 and 25 layers. All QD-LD chips are 800 μm long. Also, the lasing spectra of 25 stacked-layer QD-LD were recorded as temperature increased.

The second part focuses on QD SOA chips. Their structures are almost the same as QD-LD chips, but only the 25 stacked layers were used in QD SOA. Both

facets were cleaved 6° tilted from its ridge waveguide structure by the conventional photolithography and dry etching. In addition, the Anti-Reflection (AR) coating with TiO_2 and SiO_2 was applied on both facets by sputtering process to reduce their reflectivities less than 0.1 %. We evaluated three lengths of QD SOA chips: 1.5, 2 and 2.4 mm.

The characteristics of QD SOA, such as chip gain and saturation output power, were tested by our setup in Figure 3.2. A Tunable Laser Diode (TLD) generated an input power, $P_{in,dBm}$, into a bare QD SOA chip, here called a Device Under Test (DUT). The power level of input and polarization were adjusted by Variable Optical Attenuator (VOA) and Polarization Controller (PC), respectively. The Polarization Dependent Gain (PDG) of DUT is roughly 5 – 10 dB based on prior work [58]. Our design aims for extremely high gain, leaving the PDG not optimized. Of course, it can be reduced by the strain-controlled columnar QDs (SC-CQDs) technique [59]. All QD SOA chips were individually set on base in optical fiber alignment machine to measure their characteristics.

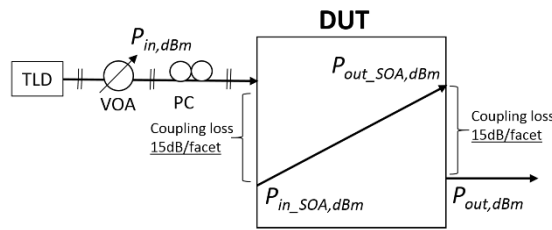


Figure 3.2 QD SOA chip's experimental setup.

According to those parameters shown in Figure 3.2, the chip gain of QD SOA can be estimated from equation (3.1) – (3.3) at any input wavelength from TLD; where G_{chip} is chip gain of QD SOA, $P_{out_SOA,dBm}$ is output power of SOA, $P_{in_SOA,dBm}$ is input power of SOA, $P_{out,dBm}$ is output power of SOA after including the coupling loss, CL_{facet} , at each facet, and $P_{in,dBm}$ is input power before PC. The pulse current source injected current into QD SOA chip with its Pulse Duty Cycle, PDC , of 1 % and 10 %.

$$G_{chip} = P_{out_SOA,dBm} - P_{in_SOA,dBm} \quad (3.1)$$

$$P_{out_SOA,dBm} = P_{out,dBm} + CL_{facet,dB} - 10\log_{10}(PDC) \quad (3.2)$$

$$P_{in_SOA,dBm} = P_{in,dBm} - CL_{facet,dB} \quad (3.3)$$

3.2.2 Experimental setups of QD SOA module

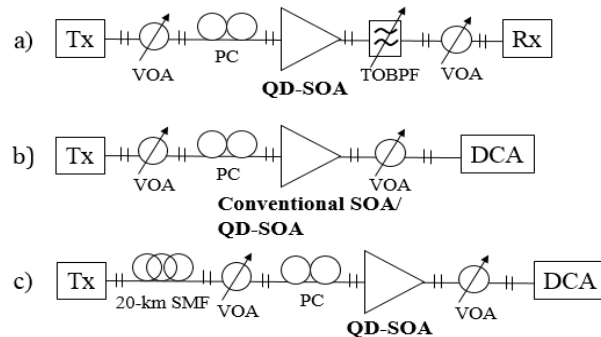


Figure 3.3 Block diagrams: a) IPDR, b) pattern effect, and c) 40 Gb/s data transmission over 20-km SMF.

To prove its application, one QD SOA chip was assembled into a module and evaluated for Input Power Dynamic Range (IPDR), pattern effect, and error-free transmission over 20-km SMF. Their block diagrams are shown in Figure 3.3. The transmitter (Tx) consists of a tunable laser set at 1530 nm, 4 channel Pulse Pattern Generator (PPG) & Multiplexer to generate 40 Gb/s data, PC, and Mach-Zehnder Modulator. The PPG was programmed to generate 3 patterns: Pseudo-Random Binary Sequence $2^{23}-1$ (PRBS23) for IPDR, 64 consecutive bits of '1' followed by 64 consecutive bits of '0' for pattern effect, and $2^{31}-1$ (PRBS31) for 20-km transmission. The receiver (Rx) consists of Photodetector, Clock Recovery, Demultiplexer, and Error Detector. The 2-nm Tunable Optical Band Pass Filter (TOBPF) was added in IPDR test, but not in latter two tests to observe worse performance. VOA and PC help adjust optical power and polarization, respectively. Digital Communication Analyzer (DCA) can capture the data patterns and 40 Gb/s eye diagrams.

3.3 Results & Discussion

The 1st part reports results of QD-LD chips: I-L plot, threshold current and temperature characteristic. Once the structure of QD layers was optimized in QD-LDs, the same was applied in QD SOA's fabrication. Then, the 2nd part reports results of QD SOA chips: chip gain of 3 device lengths, saturation output power and 3-dB gain spectrum at different injected currents. The last part reports results of QD SOA

module: IPDR, response time of data pattern effect, and eye diagram of 20-km SMF transmission.

3.3.1 Results of QD-LD chips

The I-L plots of QD-LDs (800 μm long) with 10, 14, 20 and 25 stacked QD layers were measured at 15, 20, 25, 30, 40, 50, 60, 70 and 80 $^{\circ}\text{C}$ temperatures. Next, their corresponding threshold currents were plotted in Figure 3.4. Evidently, these threshold currents increase with temperature. And, the best number of stacked QD layers is 25 due to its lowest threshold currents across all temperatures. The higher QD density gives more carriers to reach threshold. Thus, the threshold current is lower at higher QD layers or QD density [9, 33, 55]. For this reason, all results afterwards will focus on 25 stacked QD layers.

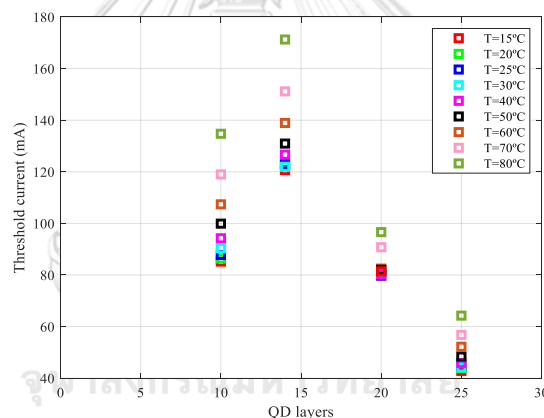


Figure 3.4 Threshold currents of QD-LDs (800 μm long) with 10, 14, 20 and 25 stacked QD layers at different temperatures.

A closer look at I-L plot of 25 stacked-layer QD-LD in Figure 3.5 a), the threshold currents are 42.8, 43.8, 44.4, 44.2, 45.8, 48.3, 52.1, 56.7 and 64.2 mA at 15, 20, 25, 30, 40, 50, 60, 70 and 80 $^{\circ}\text{C}$, respectively. In this paper, all threshold currents are lower than 78 mA (at room temperature) as reported in prior work [21]. At 25 $^{\circ}\text{C}$, the threshold current density is 2,220 A/cm^2 , computed from 800- μm length and 2.5- μm width of ridge waveguide. So, each QD layer of 25 stacked-layer QD-LD has the threshold current density of 88.8 A/cm^2 . Moreover, this laser can operate over a wide range of temperature up to 80 $^{\circ}\text{C}$.

From equation (3.4) [60], Figure 3.5 b) shows the temperature dependence of threshold current as 2 dash lines. The characteristic temperatures (T_0) over lower (15 – 30 °C) and higher (40 – 80 °C) temperature regions are 473 K and 118 K, respectively, which is higher than 102 K in prior work.

$$I_{th} = I_0 \exp(T / T_0) \quad (3.4)$$

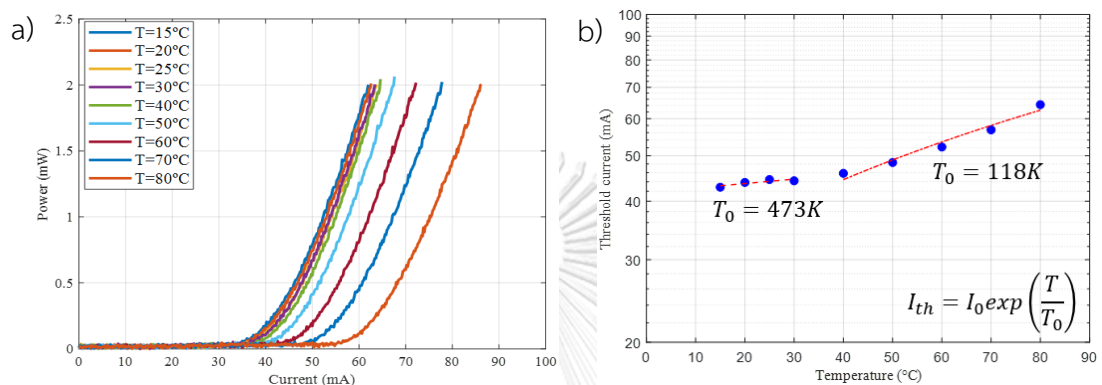


Figure 3.5 a) I-L plot of 25 stacked-layer QD-LD at different temperatures, and b) temperature dependence of threshold current.

The output lasing spectra of 25 stacked-layer QD-LD were repeatedly recorded as shown in Figure 3.6 a) at 15, 20, 25, 30, 40, 50, 60, 70 and 80 °C temperatures. As temperature increases, its peak wavelength linearly shifts to longer wavelengths at the rate of 0.56 nm/°C, estimated from Figure 3.6 b), due to the reduction of bandgap energy of laser. Also, the peak amplitude of each spectrum slightly decreases owing to more heat accumulation inside a laser.

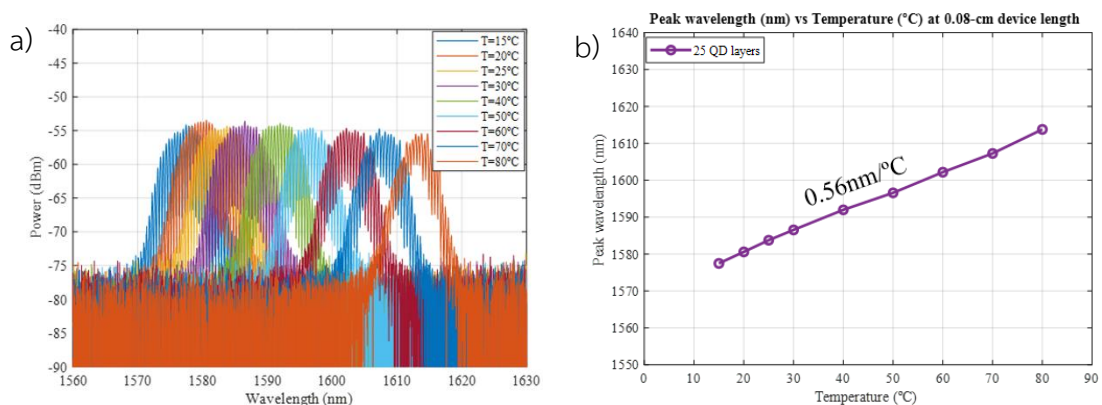


Figure 3.6 a) Lasing spectra of 25 stacked-layer QD-LD at different temperatures, and b) plot of peak wavelength versus temperature.

3.3.2 Results of QD SOA chips

Based on the results of QD-LD chips from part 1, 25 stacked QD layers showed the lowest threshold currents across its temperature range. Hence, the QD SOA chips with 25 stacked QD layers were fabricated having 2-mm and 2.4-mm device lengths. One more sample is 1.5-mm long, but with 20 stacked QD layers. After AR coating process of 3 samples, the chip gains, saturation output powers, and 3-dB gain spectra at different injected currents were measured using a pulse current source with duty cycles of 1 % and 10 %. Due to self-heating effect, a constant DC source cannot be used here because the injected current and power consumption of QD SOA are much higher than QD-LD, despite the high characteristic temperature (T_0) of QD-LD. To effectively reduce this self-heating effect, the QD SOA chip must be mounted on a heat sink with the Thermo Electric Cooler (TEC) and a temperature control circuit in order to remove the amount of accumulated heat. The input wavelength, input power, and injected current of QD SOA chips were set at 1580 nm, +6 dBm, and 200 – 500 mA, respectively. The chip gain was estimated by those equation (3.1) – (3.3), and plotted in Figure 3.7 for the case of 2-mm long QD SOA. Noticeably, the 1 % pulse has 11.9-dB higher chip gain than 10 % pulse due to its lower heating. Thus, it was applied in all later tests.

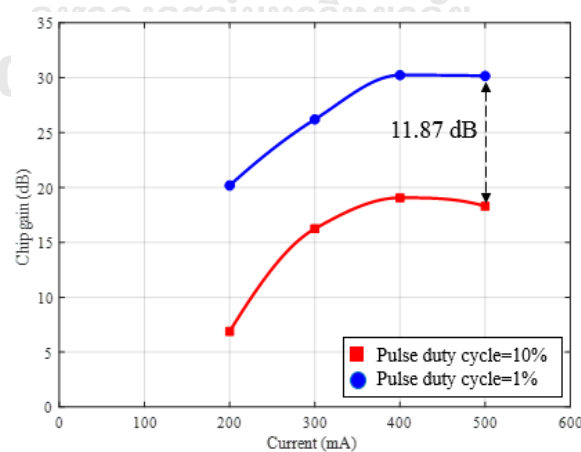


Figure 3.7 Chip gain versus injected current of 2-mm long QD SOA with pulse duty cycle of 1 % and 10 %.

Figure 3.8 shows the chip gain versus current of 3 QD SOA samples using 1 % pulse cycle, +6-dBm input power and 1580-nm wavelength. Clearly, these gains increase with currents. The maximum gains of 1.5-mm and 2.4-mm lengths occur at 500 mA to be 22.6 and 24.8 dB, respectively, whereas the 2-mm length gives higher maximum gain of 30.2 dB at 400 mA. The lower gain of 1.5-mm length is due to its shorter device length and a lower number of stacked QD layers. Next, comparing between 2-mm and 2.4-mm lengths with the same number of stacked QD layers, we expected a longer device should have more gain but we found the opposite.

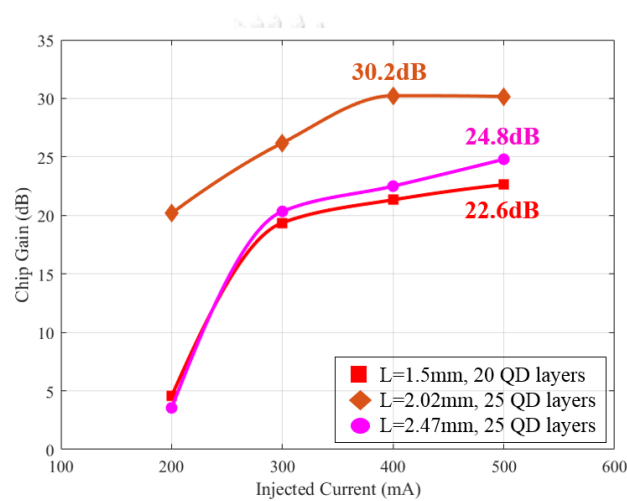


Figure 3.8 Chip gain versus injected current of 1.5-mm, 2-mm, and 2.4-mm long QD SOAs at +6 dBm input power.

Their I-L plots in Figure 3.9 reveals the reason. The 2-mm length behaves like a conventional SOA because of no clear threshold current, but the 2.4-mm length behaves like a laser based on its ascending line. A root cause was the manually improper positioning of these devices during their AR coating process, which causes the reflectivity of some areas over both facets of QD SOA chips to be above a desired 0.1 %. Consequently, the 2-mm QD SOA chip having a better AR coating can provide the highest maximum chip gain. So, we will focus on this 2-mm device length from now on.

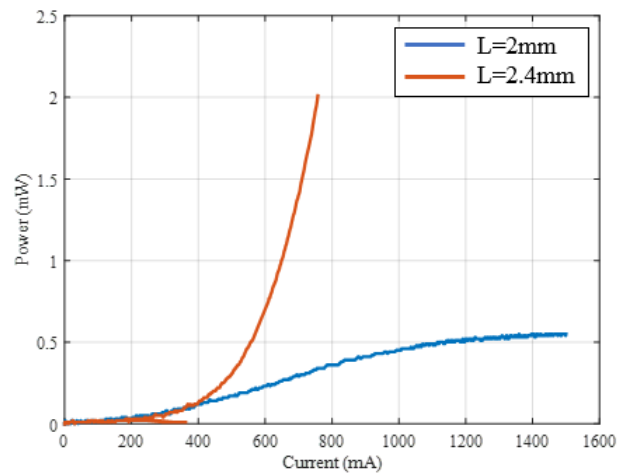


Figure 3.9 I-L plot of 2-mm and 2.4-mm long QD SOAs.

Besides the injected current, two more parameters that effect the chip gain of QD SOA are studied. The first parameter is its input power, which was reduced from +6 dBm down to -2 dBm at 1580-nm wavelength. The chip gains of 2-mm long QD SOA at 5 injected currents (100, 200, 300, 400 and 500 mA) are plotted in Figure 3.10 a). These gains increase as the input power is reduced. The maximum chip gain is 35 dB (exactly at 34.4 dB) occurring at the injected current of 400 mA and at such a high input power of -2 dBm. In summary, this QD SOA chip can achieve the same gain as in prior work [47] but consume less current.

Next, in order to find the saturation output power of QD SOA chip, we replotted those results in Figure 3.10 a) again in Figure 3.10 b), which is chip gain versus output power at 3 injected currents: 300, 400 and 500 mA. To properly identify the 3-dB saturation output power, more results of lower input powers should be added. However, due to the difficulty of measurement setup of fiber alignment machine, only the -3.19 dBm input power is included to become 5 data points per current. At this lower input, the results of 300-mA and 400-mA currents do not give a constant high gain as expected, owing to the highly sensitivity of fiber aligner setup and input polarization that cause more losses. After neglecting such lower input data points and focusing on the remaining high input data points in Figure 3.10 b), the saturation gain occurs at higher input powers and as the injected current approaches 500 mA as shown in Figure 3.10 a). According to curves in Figure 3.10 b), the highest 3-dB saturation output power is 20.9 dBm at 400-mA injected current.

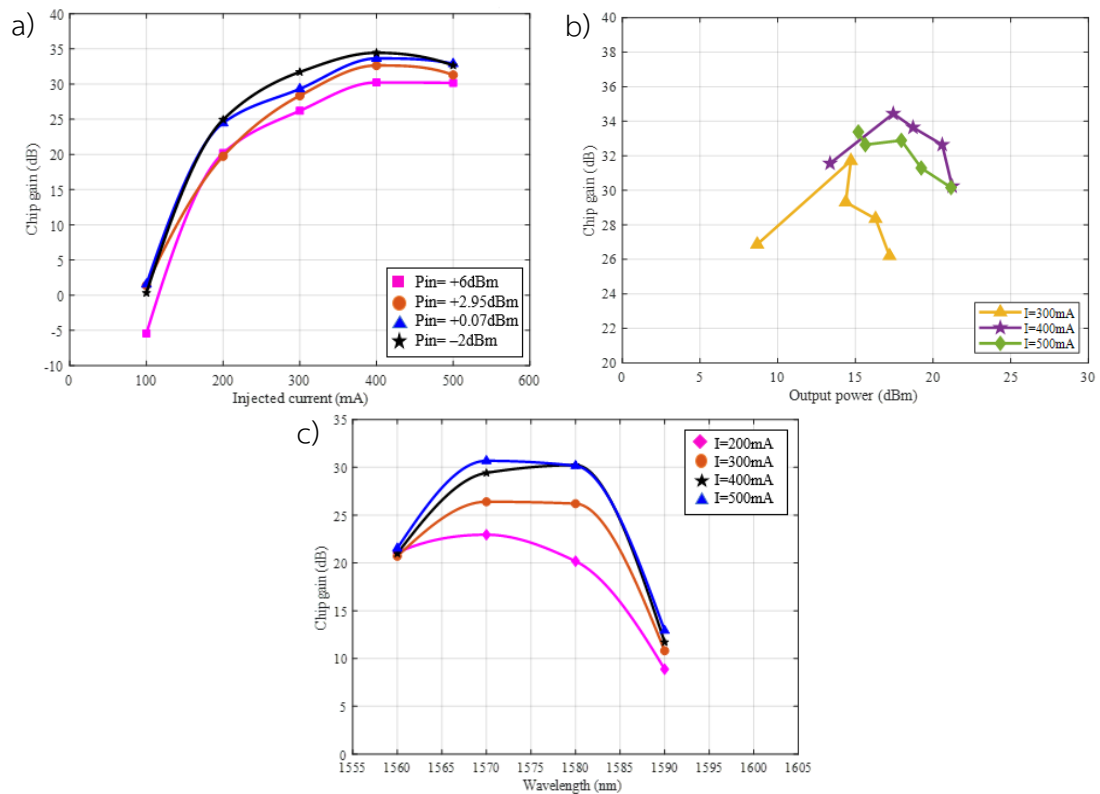


Figure 3.10 Characteristic of 2-mm long QD SOA: a) chip gain versus injected current at different input powers, b) chip gain versus output power at different injected currents, and c) chip gain versus wavelength at different injected currents.

Another parameter that effects chip gain is the input wavelength of QD SOA. Instead of the previous 1580-nm input, others wavelength were also tested: 1560, 1570 and 1590 nm, as in Figure 3.10 c). The input power was set at +6 dBm. The results show gain peaks between 1570 nm to 1580 nm for all injected currents. Consequently, the 3-dB gain spectrum is over 20 nm wide having its highest peak at 1570-nm wavelength and 500-mA injected current.

Finally, Noise Figure (NF) is the most important parameter of all optical amplifiers. But, in this case, it cannot be measured as being in chip state. Instead, we measured this NF using the QD SOA module to be 5 dB at 400-mA injected current via Optical Spectrum Analyzer (OSA) with 0.1-nm resolution bandwidth. Figure 3.11 shows the NF and Amplified Spontaneous Emission (ASE) noise floor at -36.05 dBm together with its amplified output at $+2.74$ dBm when the input of QD SOA module is -13.91 dBm.

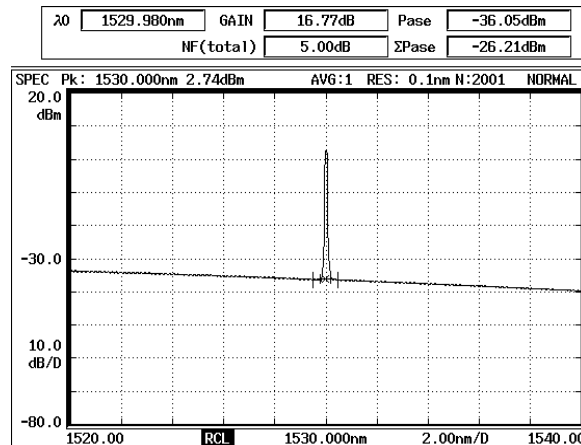


Figure 3.11 ASE and NF of QD SOA module at 400-mA injected current with -13.91 -dBm input power and $+2.74$ -dBm output power.

3.3.3 Results of QD SOA module

The IPDR of QD SOA module at 10^{-10} BER is 15.4 dB as shown in Figure 3.12, which is the plot of Bit Error Rate (BER) versus input power of QD SOA. The bias current of QD SOA module was 320 mA while the received power at Rx was fixed at -4 dBm for all BER measurements. According to Figure 3.12, the input power of QD SOA at -13.91 dBm gives the lowest BER. The rising BERs on left & right sides are due to Amplified Spontaneous Emission (ASE) noise and severe pattern effect, respectively. Hence, we can identify the optimum input power and IPDR of QD SOA module for its proper operation in a fiber link.

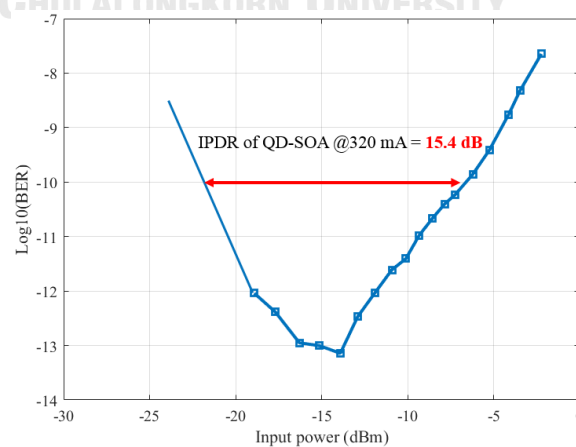


Figure 3.12 IPDR of QD SOA module at 320-mA injected current.

In Figure 3.13, we compare the data pattern effect between conventional SOA and our QD SOA module. Their bias currents were 308 and 320 mA, respectively, to give the same 14.5-dB gain. In this case, their input powers were fixed at -2.17 dBm (much higher than its optimum input power), in order to operate in the saturation regime and cause pattern effect. This effect is significant if the SOAs are applied in optical signal processing. Based on our testing data sequence (64 consecutive bits of '1' and 64 consecutive bits of '0'), we measured the response time at 37 % from its peak according to a decay exponential equation. As a result, the conventional SOA and QD SOA module have response times of 98 ps and 84 ps, respectively. Plus, the *Signal to Overshoot ratios* of conventional SOA and QD SOA module are 0.75 and 1.15, respectively. Obviously, our QD SOA has faster response time and lower overshoot than conventional SOA. Therefore, our QD SOA module has less data pattern effect than conventional SOA, making it more suitable for the burst-mode upstream transmission in PON as well as for optical signal processing with fast response.

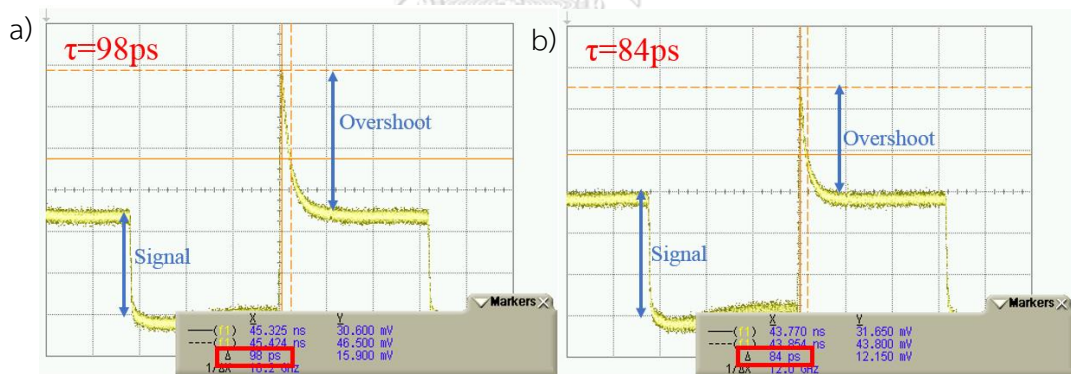


Figure 3.13 Pattern effect of a) conventional SOA at 308-mA injected current and b) our QD SOA module at 320-mA injected current. (DCA scale: 7.5 mV/div with an offset of 15 mV)

The last test is 40 Gb/s PRBS31 data transmission over 20-km SMF and QD SOA, as shown in Figure 3.3 c) block diagram. The bias current of QD SOA was 400 mA. Its input power was reduced by 1st VOA to be -16 dBm, assuming to include 12-dB loss from 1:16 splitter and 4-dB loss from 20-km SMF with an output from Tx at 0 dBm. This chosen input is close to the optimum input power found earlier. As a

result, the measured eye diagram in Figure 3.14 shows a clear eye opening, even after a long SMF and at high bit rate. Consequently, this error-free transmission proves the applications of our QD SOA module for high-speed fiber networks.

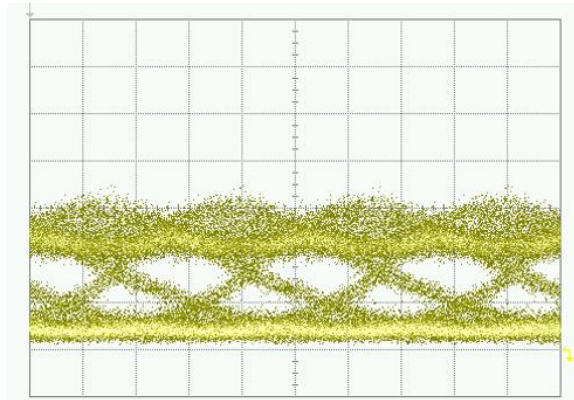


Figure 3.14 Eye diagram of 40 Gb/s data over 20-km SMF. (DCA scale: 4.8 mV/div with an offset of 16 mV)

3.4 Conclusion

We investigated the characteristics of QD-LDs in order to choose the best conditions for QD SOA's fabrication. Both QD-LDs and QD SOAs consist of InAs QD layers grown on InP(311)B substrate. The QD-LD with 25 stacked QD layers gives the lowest threshold current as compared to 10, 14 and 20 layers. Its characteristic temperatures over lower (15 – 30 °C) and higher (40 – 80 °C) temperature regions are 473 K and 118 K, respectively. Also, the peak wavelength of lasing spectrum shifts linearly with temperature at the rate of 0.56 nm/°C over 15 – 80 °C and within C-band. Then, 3 QD SOA chips were evaluated: 2-mm & 2.4-mm device lengths with 25 stacked QD layers, and 1.5-mm device length with 20 stacked QD layers. The 1 % pulse duty cycle was applied in all measurements of QD SOA chips to have more chip gain and avoid self-heating effect. The 2-mm long QD SOA reports higher chip gains than 1.5-mm and 2.4-mm lengths due to its longer device length, higher stacked QD layers, and better AR coating. Thus, it is chosen for more tests of the maximum gain's conditions, saturation output power, and 3-dB gain spectrum in C-band. The highest 3-dB saturation output power is 20.9 dBm at 400-mA injected current. Plus, its 3-dB gain spectrum is over 20 nm wide with the highest peak at

1570-nm wavelength. Finally, our QD SOA chip can achieve the highest chip gain of 35 dB at -2 -dBm input power and 400-mA current, lower than prior work of 500 mA. In addition, another QD SOA chip with same design was assembled into a module to be able to measure its dynamic properties. The IPDR is 15.4 dB at 10^{-10} BER and its optimum input is -13.91 dBm. Also, the QD SOA module shows less pattern effect than a conventional SOA with faster response time of 84 ps and higher *Signal to Overshoot ratios* of 1.15. Moreover, the measured eye-diagram proves that our QD SOA module can be applied in high bit rate of 40 Gb/s over 20-km SMF transmission.

3.5 Acknowledgment

The authors are grateful to The 100th Anniversary Chulalongkorn University for Doctoral Scholarship, The 90th Anniversary of Chulalongkorn University Fund (Ratchadaphiseksomphot Endowment Fund), and Overseas Research Experience Scholarship for Graduate Students from Graduate School Chulalongkorn University. This work was partly conducted as part of a research project supported by the Japanese Government funding for “R&D to Expand Radio Frequency Resources” by the Ministry of Internal Affairs and Communications.

4. Performances of Conventional SOAs versus QD SOA in 1530-nm Upstream Transmission of 40 Gb/s Access Network

Budsara Boriboon¹, Duang-rudee Worasuchep¹, Satoshi Shimizu², Satoshi Shinada²,
Hideaki Furukawa², Atsushi Matsumoto², Kouichi Akahane², Naokatsu Yamamoto²,
Naoya Wada²

¹Department of Electrical Engineering, Chulalongkorn University, Thailand

²National Institute of Information and Communications Technology, Japan

Prepare the manuscript to submit in international journal: *Engineering Journal (EJ)*

SOA is the key device for burst-mode upstream transmission of 40 Gb/s access network to extend distance and increase a number of users. We evaluate two conventional SOAs and our QD SOA in networks, consisting of 20-km Single Mode Fiber (SMF) and splitters (1:8, 1:16 & 1:32). First, their characteristics are reported: 3-dB bandwidth, ASE peak wavelength, gain, saturation output, and Noise Figure (NF). QD SOA gives the lowest NF of 4.59 dB at -20-dBm input due to its highest Optical Signal to Noise Ratio (OSNR). It also has the fastest response time (70 ps) with less data pattern effect when operating in saturation region. Besides the measurement of Input Power Dynamic Range (IPDR) of 3 SOAs, their performances of single versus two-cascaded SOA transmissions are evaluated by Bit Error Rate (BER) in many cases of SMF and splitters. In case of having 1:8 splitter between two cascaded SOAs, the performance of 2nd-stage QD SOA has lower BERs than 2nd-stage conventional SOA due to its higher saturation output and less pattern effect when operating at high input. Finally, both experimental and computed BERs are plotted versus SOA's input to confirm the OSNR degradation and data pattern effect.

4.1 Introduction

The optical amplifiers, such as Erbium-Doped Fiber Amplifier (EDFA) and Semiconductor Optical Amplifier (SOA), can be applied in Passive Optical Network (PON) to extend distance and support a large number of users. The advantages of SOA over EDFA are lower cost, less power consumption, more compact size, and simpler integration with other components and electronic boards. Plus, it can amplify any wavelength range depending on doped elements. To improve characteristics of SOA, the Quantum Dot SOA (QD SOA) has been developed with superior properties, e.g., low Noise Figure (NF), less chirp, fast response time, and less pattern effect [6]. The faster response of QD SOA is beneficial to many applications, such as all-optical signal processing [61, 62] and wavelength conversion [35-38]. The QD features are improved by some techniques. For example, the Rapid Thermal Annealing (RTA) in Ref. [32] helps to obtain a high internal quantum efficiency of 66.39 % and low optical loss of 9.87 cm^{-1} in QD-laser. Using the strain compensation technique, the 35-dB highest chip gain was achieved in QD SOA with 25 stacked QD layers at 400-mA bias current [63] based on previous works [10, 57]. In addition, QD SOA can operate at very high bit rates up to 40 Gb/s and support several modulation formats, such as 8-PSK [36], 16-QAM [36, 43] and PAM4 [37, 38]. Also, the nonlinear effects like Cross Gain Modulation (XGM) and Four-Wave-Mixing (FWM) were applied in wavelength conversion up to 40 Gb/s bit rate [35-38], while the Cross Phase Modulation (XPM) effect was used in all-optical signal processing such as logic XOR & AND gates, 2x2 switches, and D flip-flop. Besides, the input polarization dependence of QD SOA was resolved by using the strain-controlled columnar QDs technique to be a polarization-insensitive QD SOA as in Ref. [59].

According to the burst-mode upstream transmission in NG-PON2 [14], SOA can be placed between Optical Network Unit/Optical Network Terminal (ONU/ONT) and Optical Distribution Network (ODN) to increase the power budgets of access links as well as a trunk line in between ODN and Optical Line Terminal (OLT). Ref. [64] demonstrated the configurations of a bi-directional SOA at OLT: single SOA per downstream channel as a booster amplifier and a preamplifier SOA followed by

avalanche photodiode, to give the best signal performance. In Ref. [65], QD SOAs were applied in T-band (1000 – 1260 nm) WDM/TDM access network, as path switches for self-restoring system because of fast response and power loss compensation. Also, QD SOAs were used in GPON with 1.5- μm downstream & 1.3- μm upstream transmissions to increase distance of 60 km and 32 users [51]. To gain more budget, the cascaded SOAs were proposed. In Ref. [66], a non-gated parallel cascade of linear SOAs was set up in long-reach-high-split PON to support 100 km and 2048 users. Moreover, the cascaded SOAs were used in PAM4 transmission of PON uplink with 1024 splits & 70 km [67]. In case of QD SOA, the performance of 11-cascaded QD SOAs were evaluated in recirculating loop as in [68], showing the Q-factor less than 10^{-9} BER.

In this paper, we compare the performances of our QD SOA versus 2 conventional SOAs (SOA#1 & #2) in 40 Gb/s per channel of upstream transmission for future access network. Based on NG-PON2 [69], the 1530-nm wavelength is chosen for all setups. First, we measure their characteristics: 3-dB bandwidth, ASE peak wavelength, small-signal gain, saturation output & input, and NF, including the response time and data pattern effect. Next, we evaluate the performance of single SOA transmission by BER measurements in 6 combination cases: splitter 1:8, 1:16 & 1:32, and with & without 20-km SMF. The BER plot versus SOA's input reveals its Input Power Dynamic Range (IPDR). Also, the two-cascaded SOA transmission is set up in 4 cases: splitter 1:32 +40-km SMF, 1:128 +20-km, 1:32 +20-km, and only 1:128 splitter. SOA#1 is fixed as the 1st-stage SOA due to its highest saturation output. Either SOA#2 or QD SOA is placed as the 2nd-stage SOA to compare their performances. Finally, we compute the BERs according to theoretical equations and compare to experimental results in BER plots versus SOA's input, in order to confirm the Optical Signal to Noise Ratio (OSNR) degradation and data pattern effect.

4.2 SOA's Characteristics

All parameters of SOA#1, SOA#2 and our QD SOA are measured as shown in Table 4.1. For a fair comparison, their bias currents are set at different values as listed in the 2nd column of Table 4.1, since they will be later applied in different transmission cases for their exact same gains: a lower gain of ~14.5 dB and a higher gain of 17 dB.

4.2.1 Experimental Setup

Figure 4.1 shows our block diagram. A Laser Diode (LD), which is a tunable Distributed Feedback (DFB) laser, emits 1530-nm wavelength without data modulation. The SOAs' input power and polarization are adjusted by a Variable Optical Attenuator (VOA) and a Polarization Controller (PC), respectively. The SOAs' output spectra are recorded by an Optical Spectrum Analyzer (OSA) with 0.1-nm resolution bandwidth, and then all parameters are found. In case of the 3-dB bandwidth measurement, no input is needed.

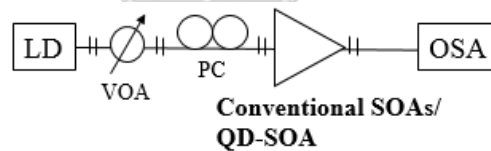


Figure 4.1 Block diagram of characteristic measurement.

4.2.2 Experimental Results

Table 4.1 Characteristics of 3 SOAs: SOA#1, SOA#2, and QD SOA

Optical Amplifier	Bias Current	3-dB Bandwidth	ASE Peak λ	Small Signal Gain	Saturation Output Power	Saturation Input Power	Saturation Input Power (Mod.)	Noise Figure ($P_{in} = -20\text{dBm}$)
SOA1013S	308mA	72nm	1521nm	14.8dB	9.2dBm	-2.6dBm	-6.0dBm	7.10dB
	360mA	72nm	1516nm	17.0dB	9.8dBm	-4.2dBm	-7.0dBm	6.70dB
SOA1117S	285mA	59nm	1546nm	14.3dB	5.6dBm	-5.6dBm	-9.0dBm	9.92dB
	332mA	60nm	1551nm	17.0dB	6.5dBm	-7.5dBm	-12.0dBm	9.58dB
QD SOA	320mA	42nm	1504nm	14.5dB	7.3dBm	-4.2dBm	-8.5dBm	4.87dB
	400mA	43nm	1500nm	17.0dB	8.0dBm	-6.0dBm	-10.8dBm	4.59dB

Table 4.1 lists all parameters of 3 SOAs. Their details will be discussed in the following sub-sections. In addition, the saturation input powers without and with 40 Gb/s data modulation are included in the 7th and 8th columns, respectively. By a definition, the saturation input/output is power level that causes its gain to reduce by 3 dB from the highest small-signal gain. Any input/output above it will be in saturation operation. In this case, the higher saturation inputs without data modulation are used to compare SOA's characteristic, while the lower saturation inputs with data modulation are used in Section 4.3 SOA's Response Time & Data Pattern Effect.

4.2.2.1 ASE Peak Wavelength & 3-dB Bandwidth

All SOA's output spectra have their operating ranges covering 1530 nm. The 3-dB bandwidth and ASE peak wavelength are given in the 3rd & 4th columns, respectively. Clearly, SOA#1 has the widest bandwidth of 72 nm. Figure 4.2 shows our QD SOA's ASE spectra at 320 and 400-mA currents. Its 3-dB bandwidths are the narrowest (43 nm), but still wider than 35 nm of typical EDFAs. In this case, the QD structure is almost homogeneous QDs, resulting in its high gains but with a narrow bandwidth. The design of our QD SOA aims to amplify wavelengths outside the C-band (1530 – 1565 nm) of EDFAs.

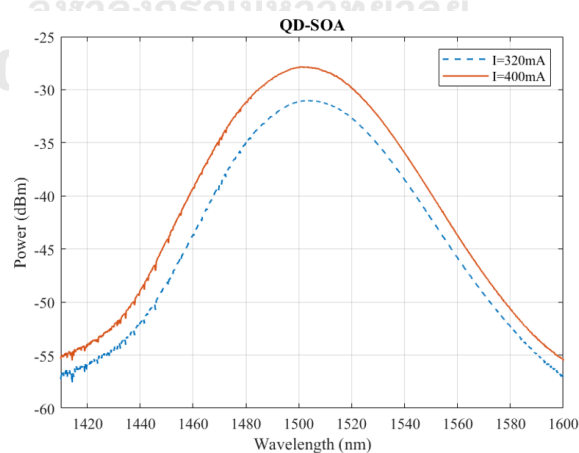


Figure 4.2 ASE spectra of QD SOA at 320 & 400-mA.

4.2.2.2 Gain, Saturation Output & Input Powers

More gain and higher saturation output are the keys to boost a link's budget. Table 4.1 column 5 – 8 list the small-signal gain, saturation output, and saturation input powers (without & with Mod.). Among all saturation outputs, SOA#1 has the highest power of 9.8 dBm at 360-mA current. Figure 4.3 plots the gain curves of QD SOA at 320 and 400-mA currents, showing both small-signal gain and saturation output ($P_{out, sat}$). Its 8-dBm saturation is in between those outputs of 2 conventional SOAs. However, this saturation output of QD SOA can be increased up to 23 dB [70] by the tapered gain section [4].

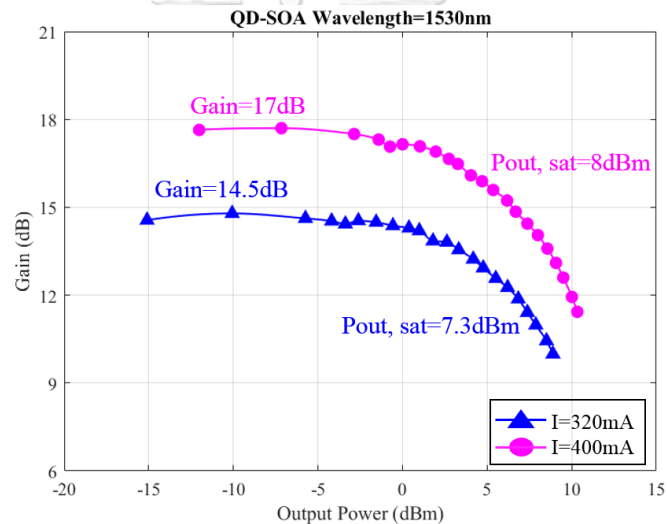


Figure 4.3 Gain and saturation output power of QD SOA.

4.2.2.3 Noise Figure (NF)

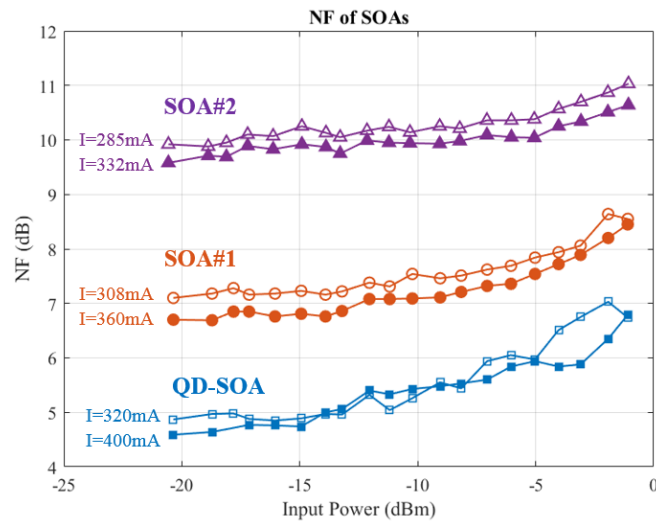


Figure 4.4 NFs of 3 SOAs at lower & higher bias currents.

Last column of Table 4.1 lists all NFs measured by OSA at -20 dBm input of SOA. Both NFs of SOA#1 & #2 are close to 8 & 10 dB, reported in their data sheets [71, 72]. When the input of SOA increases above saturation, its NF gradually rises as in Figure 4.4. Evidently, our QD SOA gives the lowest NF across all inputs due to its higher OSNR at output as plotted in Figure 4.5. For example, in case of SOA#2 at 332-mA current, two insets in Figure 4.5 show the lowest $OSNR_{out}$ of 18.21 dB at -30.09 -dBm input and the highest $OSNR_{out}$ of 46.11 dB at -1.07 -dBm input, respectively.

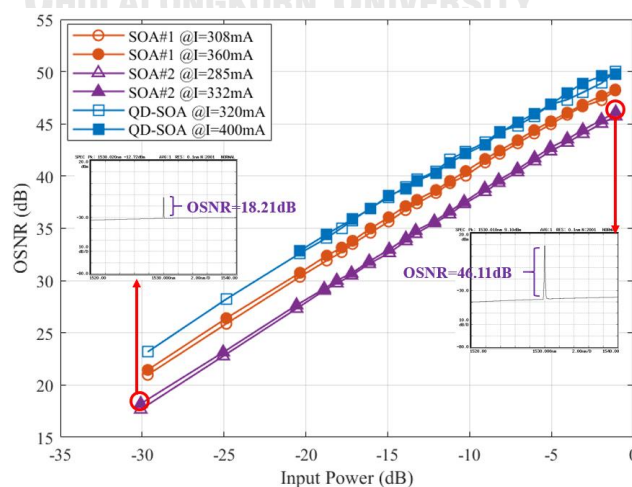


Figure 4.5 Output OSNRs versus input power of 3 SOAs.

Here is our analysis. The NF strongly depends on input power of SOA, P_{in} , and $OSNR_{out}$ following equation (4.1) without a shot-noise term originated from [73].

$$NF = \frac{2P_{in}}{h\nu B_{ref}} \left[\frac{1}{OSNR_{out}} \right] \quad (4.1)$$

where h is the Planck's constant ($= 6.626 \times 10^{-34}$ J-s), ν is frequency of SOA's input wavelength, and B_{ref} is frequency band converted from an OSA's resolution bandwidth. When operating under the small-signal gain region, the output OSNR is linearly proportional to input power as shown in Figure 4.5, resulting in almost a constant NF. In contrast, as input increases across saturation region, the OSNR slightly tapers off, causing a slow rise of NF. Plus, the lower current has little lower OSNR due to less gain and Amplified Spontaneous Emission (ASE) noise. From equation (4.1), it causes slightly higher NFs as seen in Figure 4.4.

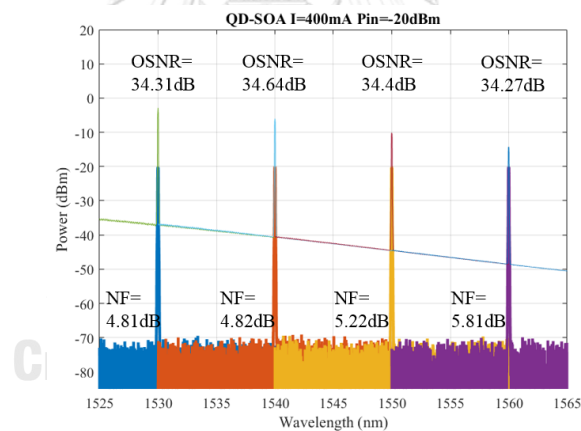


Figure 4.6 Input and Output spectra of QD SOA.

In addition, we examine the wavelength dependency of NF by measuring input and output spectra of 3 QD-SOA at 1530, 1540, 1550 and 1560 nm, in order to find OSNRs and corresponding NFs. For instance, Figure 4.6 shows the input and output spectra of QD SOA at 400-mA current and -20 dBm input. As a result, NFs provide low wavelength dependency in this wavelength range.

4.3 SOA's Response Time and Data Pattern Effect

The SOAs are well-known to have faster response times than those fiber-based amplifiers, like EDFA. Thus, they are suitable for burst-mode applications, for example as amplifiers in upstream PON transmission. However, when operating as boosters with high input powers (aka. in saturation region), the unwanted overshoots due to data pattern effect may occur. And, this will affect the length of overhead bits in time-slot sharing of upstream PON. In this study, we compare the response times of SOA#1, SOA#2, and QD SOA at lower & higher bias currents in both small-signal gain and saturation regions.

4.3.1 Experimental Setup

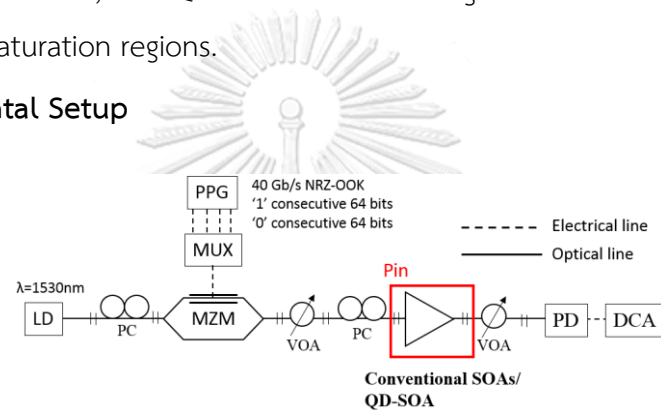


Figure 4.7 Block diagram to measure the response times.

In Figure 4.7, data pattern is generated by 4 Ch x 10 Gb/s Pulse Pattern Generator (PPG), 4 to 1 Multiplexer (MUX), 1530-nm LD, and Mach-Zehnder Modulator (MZM), to be the long consecutive 64 zeros and 64 ones alternatively. Later, this same setup was used for the BER tests of 40 Gb/s Pseudo-Random Binary Sequence (PRBS) data in Section 4.4 Bit Error Rate (BER). The input polarizations of MZM and SOA are adjusted by PCs, while the input powers of SOA and Digital Communications Analyzer (DCA) are varied by VOAs. The SOA's output waveforms is detected by a photo-detector (PD) and an electrical port of DCA. Based on the saturation input (Mod.) in Table 4.1 column 8, each SOA's input is set accordingly at a lower power for the small-signal gain operation, and at a higher power (4 – 5 dB above) for the saturation operation.

4.3.2 Experimental Results

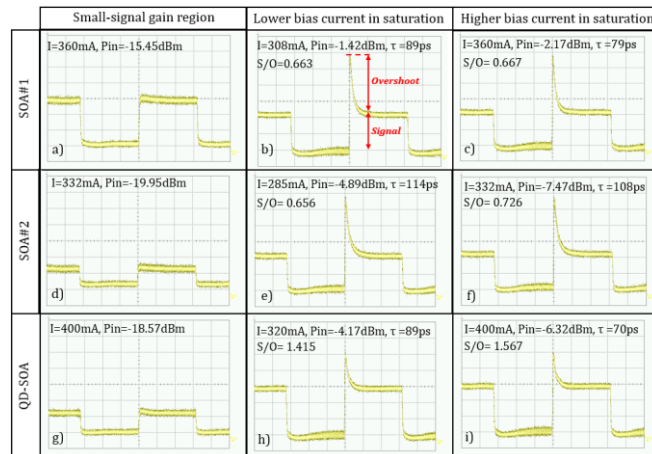


Figure 4.8 Output waveforms of 3 SOAs: small-signal gain, and saturation at lower & higher bias currents.

Figure 4.8 compares output responses of 3 SOAs. The 1st column (small-signal gain operation at higher current, omitting same results at lower current), has no overshoot and thus no pattern effect. But, they are prominent under saturation operation as in the 2nd & 3rd columns. So, we focus on them to determine the response time. Figure 4.8 b) illustrates the amount of Signal versus Overshoot that we define as *Signal to Overshoot ratio (S/O)*. The higher *S/O* in QD SOA reflects less pattern effect, while both SOA#1 & SOA#2 show strong effect.

The response time, τ , can be approximated by a decay exponential equation as in equation (4.2) and Figure 4.9, where y is voltage, V_{SS} is steady-state voltage, A is peak amplitude, and t is time in picosecond.

$$y = V_{SS} + Ae^{-\frac{t}{\tau}} \quad (4.2)$$

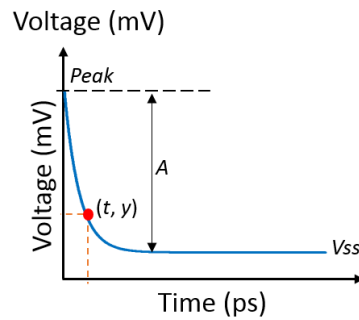


Figure 4.9 Parameters of a decay exponential curve.

All response times and S/O under saturation are listed in Figure 4.8. QD SOA gives the fastest response of 70 ps and the highest $S/O = 1.567$ at higher bias current. For a better view, Figure 4.10 plots the decay exponential curves estimating 3 waveforms in the last column of Figure 4.8. Clearly, the QD SOA has a lower overshoot and faster recovery than conventional SOAs due to the Ground State that gives ultra-fast recovery time within a few picoseconds, while a typical recovery time of SOA is longer than 10 ps [74]. In this case, our results display the overall response time without separating the ultra-fast or fast parts from slow response, unlike a clear picture shown in [5].

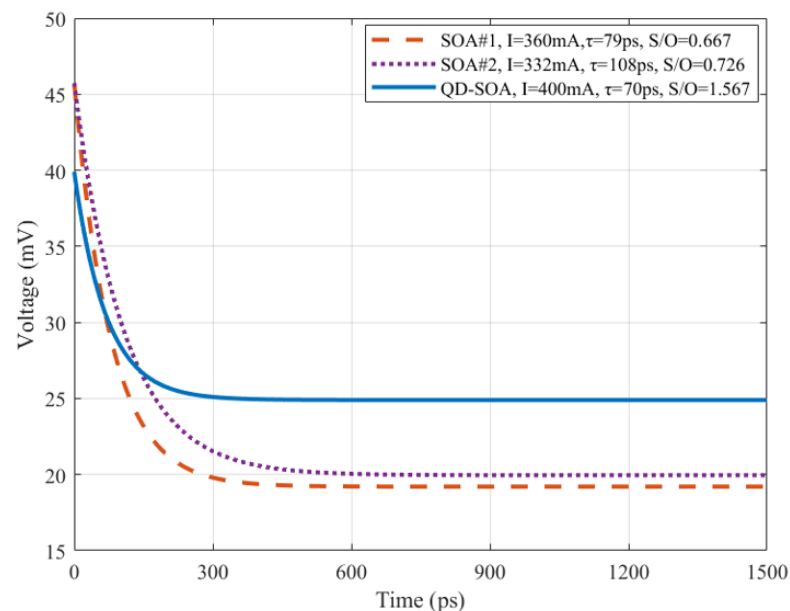


Figure 4.10 Estimated decay exponential curves of 3 SOAs at higher bias currents.

The overshoot responses of 3 SOAs under saturation at different input powers and bias currents are also studied. For example, Figure 4.11 compares the outputs of SOA#1. In Figure 4.11 a) & b) at same input, the higher current gives a lower response time owing to more carrier density injected to an active layer, and thus higher population inversion and faster refilling carrier density [75]. In Figure 4.11 c) & d) at same current, the response time reduces as input increases because of higher stimulated emission rate [76].

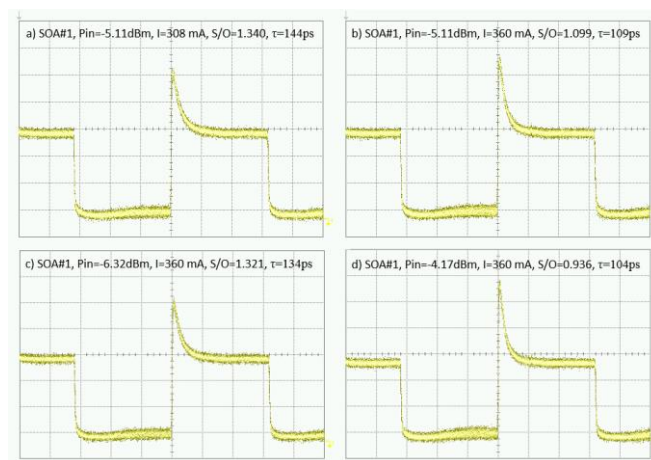


Figure 4.11 Outputs of SOA#1: a) lower & b) higher current at -5.11 dBm input, and c) lower & d) higher input at 360 -mA (higher) current.

A high overshoot is related to frequency chirp [49], which depends on the linewidth enhancement factor, α , as in equation (4.3) [77],

$$\alpha = -\frac{4\pi}{\lambda} \frac{(\partial n / \partial N)}{\Gamma A_g} \quad (4.3)$$

where n is refractive index, N is carrier density, λ is wavelength, Γ is confinement factor, and A_g is differential gain ($A_g = \partial g / \partial N$, g is material gain). When operating in saturation region, this α is positive due to carrier depletion ($\Delta N < 0$) [77] that causes a change in refractive index. The overshoot or pattern effect gets worse under high input power and bias current as seen in Figure 4.11. In Ref. [78], the α of QD SOA is lower than conventional SOA.

4.4 Bit Error Rate (BER)

The performances of 2 conventional SOAs and QD SOA in a network link are evaluated by BER tests in 2 cases: single SOA and two-cascaded SOA. Also, a Back-to-Back (B-B) case is included as reference. Link#1 and Link#2 both consist of 20-km Standard Single Mode Fiber (SSMF) and Dispersion Compensation Fiber (DCF) to remove Chromatic Dispersion (CD). Their total losses are 6.69 and 8.43 dB, respectively. The BER performance depends on SOA's input power, and thus the IPDR of 3 SOAs are found. Lastly, to verify experimental results, the theoretical equations are presented to compute BERs.

4.4.1 Experimental Setup

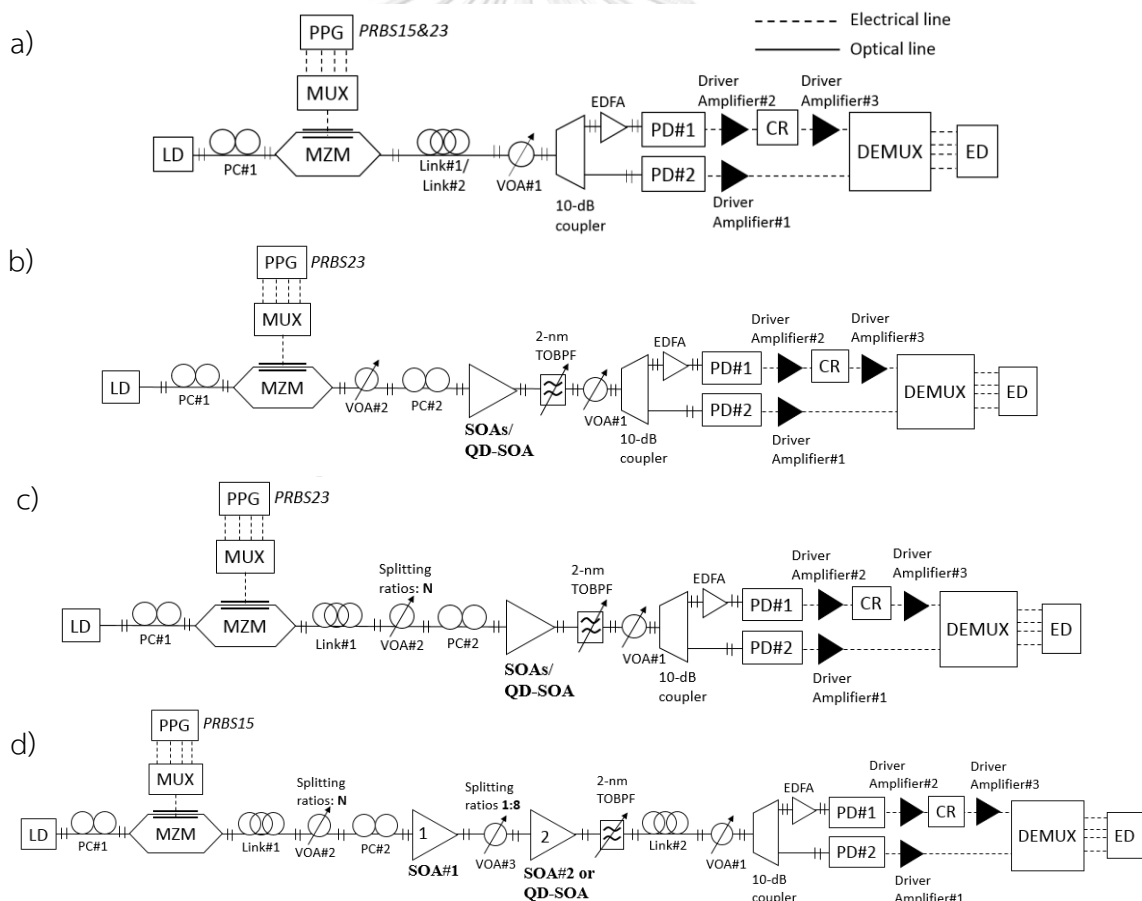


Figure 4.12 Block diagrams: a) link w/o SOA, b) single SOA w/o link, c) link w/ single SOA, and d) Link#1&2 w/ two-cascaded SOA.

Figure 4.12 shows 4 block diagrams using same transmitter as in Section 4.3. All 40-Gb/s data are PRBS23, except in Figure 4.12 d) using PRBS15 for better BERs [79]. The input of receiver (Rx) is varied by VOA#1 and split by 10-dB coupler to be clock & data signals in upper & lower paths, respectively. The upper path with less power needs an EDFA. Next, both clock & data signals are detected by 2 PDs and amplified by Driver Amplifiers before entering 1 to 4 Demultiplexer (DEMUX). The 40 GHz clock is retrieved by a Clock Recovery (CR) for BER measurement at Error Detector (ED). Figure 4.12 a) studies only CD effect in Link#1 & #2. Figure 4.12 b) focuses on BER and IPDR of either SOA#1, SOA#2 or QD SOA without a link. The ASE noise of SOA is limited by a 2-nm Tunable Optical Band Pass Filter (TOBPF). Figure 4.12 c) combines SOA with Link#1, so called the single SOA transmission, and uses VOA#2 as 1:N splitter ($N = 8, 16$ and 32). Figure 4.12 d) adds Link#2 in the two-cascaded SOA transmission: SOA#1 followed by SOA#2 or QD SOA. Here, VOA#3 acts as 1:8 splitter between 1st & 2nd stage SOAs, while VOA#2 reduces its splitter down to 4 and 16 due to budget limit.

4.4.2 Chromatic Dispersion (CD) Compensation in Link#1 & Link#2, and BER Performances of 3 SOAs

Based on Figure 4.12 a) and b), the BER results of Link#1, Link#2, and single SOA (SOA#1, SOA#2 or QD SOA) are plotted in Figure 4.13, with B-B cases of PRBS15 & 23. Since Link#1 & #2 have different losses, the budget limits BER results below the received powers of -6.67 & -8.12 dBm respectively. The partial curve of Link#1 case still follows B-B curves, proving the DCFs can compensate CD of SSMFs. All SOAs are set at higher bias currents and same input of -16.94 dBm. In Figure 4.13, the power penalties of SOA#1, SOA#2, and QD SOA at 10^{-12} BER are 0.14, 1.51 and 1.23 dB, respectively. SOA#1 has the least penalty owing to its highest saturation output of 9.8 dBm as in Table 4.1, and thus having lower data pattern effect.

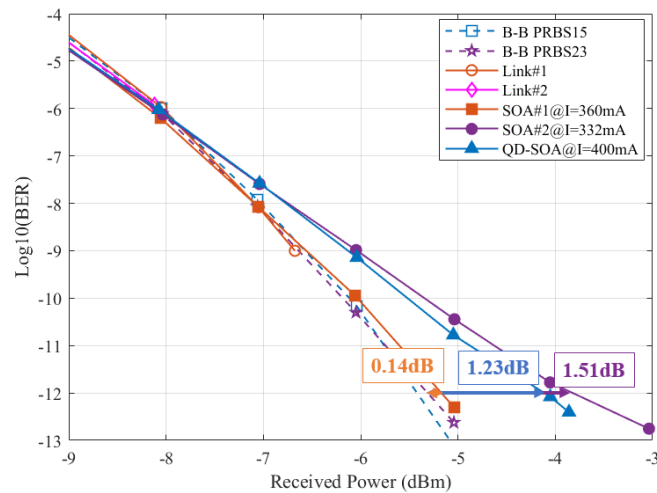


Figure 4.13 BER curves of different cases: B-B (PRBS15 & 23), Link#1, Link#2, SOA#1, SOA#2, and QD SOA.

4.4.3 Single SOA Transmission & Input Power Dynamic Range (IPDR)

As in Figure 4.12 c), we evaluate the 40 Gb/s upstream transmission of each SOA with access Link#1. Also, the BER results versus SOA's input is plotted to identify its IPDR. All SOAs are set at higher bias currents, with & without Link#1, and 3 splitting ratios: 1:8, 1:16, and 1:32. These ratios have different Insertion Losses (IL) that will vary the input of SOA. Here, there are 6 cases: i) 8 splits, ii) 16 splits, iii) 32 splits, iv) 8 splits with Link#1, v) 16 splits with Link#1, and vi) 32 splits with Link#1.

4.4.3.1 SOA#1 Transmission & IPDR

Figure 4.14 a) shows the BER curves of B-B using PRBS23 and 6 cases with different SOA's input powers due to IL of splitter and total loss of Link#1. Case i) - v) have their penalties of 1.16, 0.32, 0.1, 0.15 and 0.68 dB at 10^{-12} BER, respectively. But, in case vi), no BER below 10^{-9} could be measured due to a high IL of 32 splits. So, it shows 0.48-dB penalty at 10^{-7} BER instead. Based on these BER curves, they rely on the SOA's inputs. Then, using the setup in Figure 4.12 b) to find IPDR, we measure BERs at many SOA's inputs, while the received power at receiver (Rx) is kept at -4 dBm by VOA#1. Figure 4.14 b) shows the lowest BER of 3.9×10^{-14} at SOA's input of -15.11 dBm, and the IPDR of 18.36 dB at 10^{-9} BER. On the left side of BER curve, they get worse due to OSNR degradation as shown in Figure 4.5 [80]. However, on the right

side, they get worse owing to data pattern effect. Notice that the BER results in Figure 4.14 a) with 6 different inputs are related to the BER curve in Figure 4.14 b). Therefore, case iii) to vi) are dominated by OSNR degradation, while case i) and ii) are dominated by pattern effect.

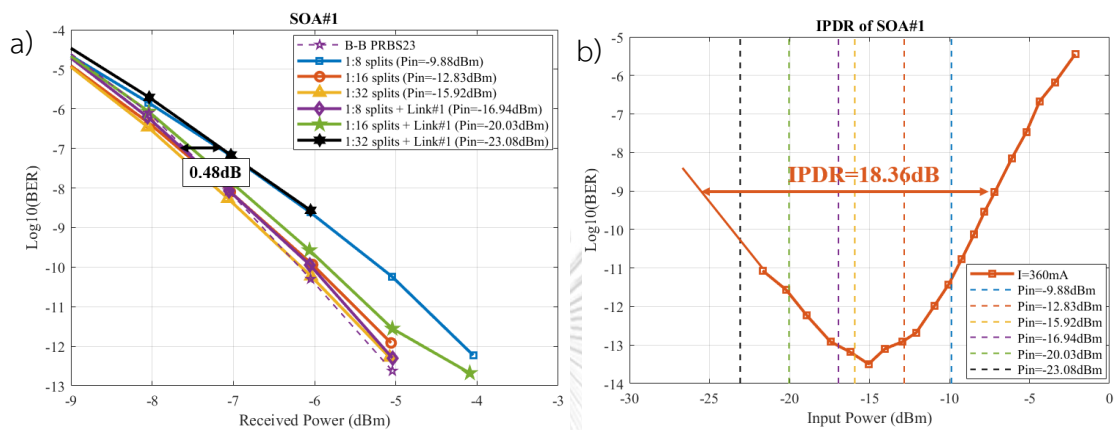


Figure 4.14 SOA#1 at 360 mA: a) BER curves of 6 cases and b) BER plot versus SOA's input showing IPDR.

4.4.3.2 SOA#2 Transmission & IPDR

SOA#2 is evaluated under the same conditions as SOA#1. All BER curves are displayed in Figure 4.15 a), being worse than those of SOA#1 due to inferior characteristics: NF and saturation output power. Case i) – v) have higher penalties of 2.55, 1.84, 1.61, 1.52, and 2.32 dB at 10⁻¹² BER, respectively. Again, in case vi), no BER below 10⁻⁸ could be measured. So, it shows 1.45-dB penalty at 10⁻⁷ BER. In Figure 4.15 b), the SOA's input of -17.47 dBm gives the lowest BER of 7.7 × 10⁻¹². Its IPDR at 10⁻⁹ BER is 12 dB, which is less than 18.36 dB of SOA#1, indicating the worse OSNR degradation and data pattern effect. Hence, case v) to vi) are dominated by OSNR degradation, while case i) to iii) are dominated by pattern effect.

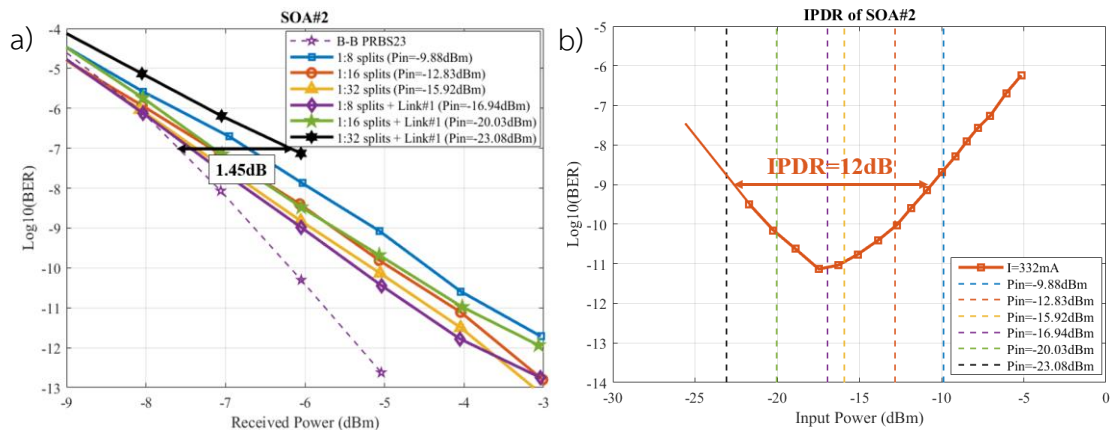


Figure 4.15 SOA#2 at 332 mA: a) BER curves of 6 cases and b) BER plot versus SOA's input showing IPDR.

4.4.3.3 QD SOA Transmission & IPDR

Similar to SOA#1 & #2, the same conditions and 6 cases are set for QD SOA. Its BER curves are given in Figure 4.16 a). They are slightly better than those of SOA#2, and much lower BERs over high received powers ($> -5 \text{ dBm}$). However, SOA#1 has the best BER curves because of its high performance. In fact, there are several techniques to improve SOAs to be high performance [81]. The penalties of case i) – v) are 1.5, 1.39, 1.03, 1.24, and 1.61 dB at 10^{-12} BER, respectively. Again, in case vi), no BER below 10^{-8} could be measured. So it shows 1.3-dB penalty at 10^{-7} BER. Similar to SOA#2, case v) to vi) are dominated by OSNR degradation, while case i) to iii) are dominated by pattern effect. In Figure 4.16 b), the input power of -17.69 dBm gives the lowest BER of 3.0×10^{-13} . The IPDR at 10^{-9} BER is 17.73 dB, close to 18.36 dB of SOA#1. When this input of QD SOA is higher than -8 dBm , its BERs are better than those of SOA#1. In other words, our QD SOA can operate over high input powers with less pattern effect as compared to conventional SOAs.

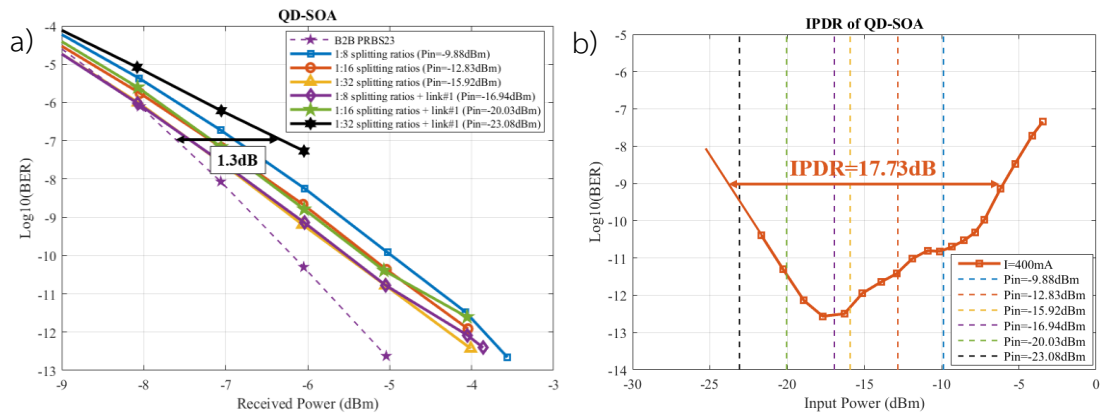


Figure 4.16 QD SOA at 400 mA: a) BER curves of 6 cases and b) BER plot versus SOA's input showing IPDR.

4.4.4 Two-cascaded SOA Transmission

Any access network will require the higher budget to support more users (splitter) and longer distance. Thus, the two-cascaded SOA is proposed to raise such budget. Its block diagram for an upstream transmission is already presented in Figure 4.12 d). Link#1 acts as an access link connecting ONU/ONT to ODN, whereas Link#2 acts as a main link connecting ODN to OLT. In this case, our ODN consists of a fixed 1:8 splitter in between 1st & 2nd-stage SOA, and a 1:N splitter ($N = 4$ or 16) locating after Link#1. SOA#1 is chosen as the 1st-stage SOA because of higher saturation output and superior BER results. Its current is set at typical 500 mA (higher than in Table 4.1) for more gain of 19 dB. The 2nd-stage SOA is either SOA#2 or QD SOA, both at higher bias currents. Since this 2-cascaded SOA transmission has worse ASE noise, PRBS15 is used instead of PRBS23 in 4 cases: i) 32 splits with Link#1 & #2, ii) 128 splits with Link#2, iii) 32 splits with Link#1, and iv) 128 splits. Case i) is common, while case ii) removes access Link#1 to have more users ($N=16$). In contrast, case iii) & iv) remove main Link#2 as if OLT is placed nearby ODN, and the 2nd-stage SOA acts as a preamplifier. Based on the minimum BER in a BER plot versus SOA#1's input at 500-mA current (excluding here, but similar to Figure 4.14 b), the input of 1st-stage SOA#1 is fixed at -14.02 dBm . With 19 dB gain, its output is about 5 dBm. After 1:8 splitter ($IL \approx 9 \text{ dB}$), the input of 2nd-stage SOA#2 or QD SOA is about -4.84 dBm . Later, in Section 4.4.4.3 Verify Performance of 2nd-stage SOA, the 1:8 splitter is replaced by 1:16 & 1:32 to vary input of 2nd-stage SOA, resulting in 6 combination cases: SOA#2

with 8, 16 & 32 splits, and QD SOA with 8, 16 & 32 splits. All BER curves are measured to report the corresponding power penalties of different splitting ratios (8, 16 & 32), as well as the output powers of 2nd-stage SOA.

4.4.4.1 Two-cascaded SOA#1 & SOA#2

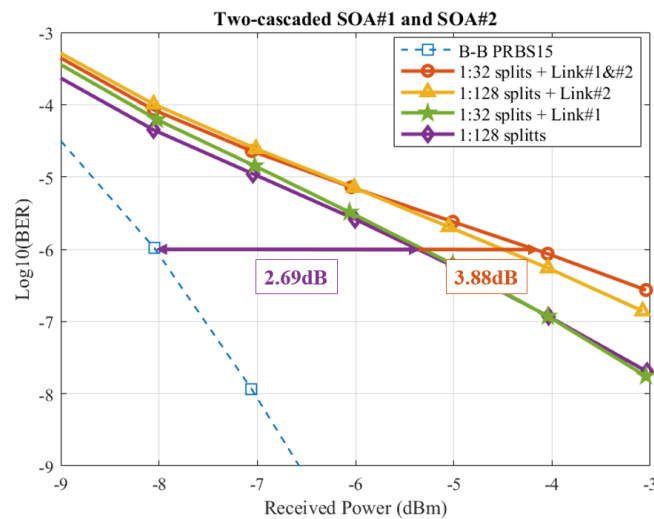


Figure 4.17 BER curves of 2-cascaded SOA#1 & SOA#2.

Figure 4.17 plots BER curves of B-B (PRBS15) and 4 cases. Due to budget limit, the highest received power is -3 dBm, and so the power penalty is read at 10^{-6} BER instead. For case i) to iv), their corresponding penalties are 3.88, 3.53, 2.76 and 2.69 dB, respectively. Case i) has the most penalty due to its longer 40-km SSMF despite CD compensation by DCF. When Link#1 is removed for more splits (1:128) in case ii) & iv), its total loss (6.69 dB) is almost equal to an extra IL (~ 6 dB) of replacing 1:4 splitter by 1:16. So, the input of 1st-stage SOA#1 is unchanged, resulting in similar BER curves. However, when Link#2 is removed in case iii) & iv), their penalties reduce about 1 dB, possibly as a result of less perfect CD compensation than Link#1. Focusing at -4 dBm received power, all BER results are between 10^{-7} and 10^{-6} BER, which are in agreement with the BER in Figure 4.15 b) read at SOA#2's input of -5 dBm (close to -4.84 dBm input power of 2nd-stage SOA).

4.4.4.2 Two-cascaded SOA#1 & QD SOA

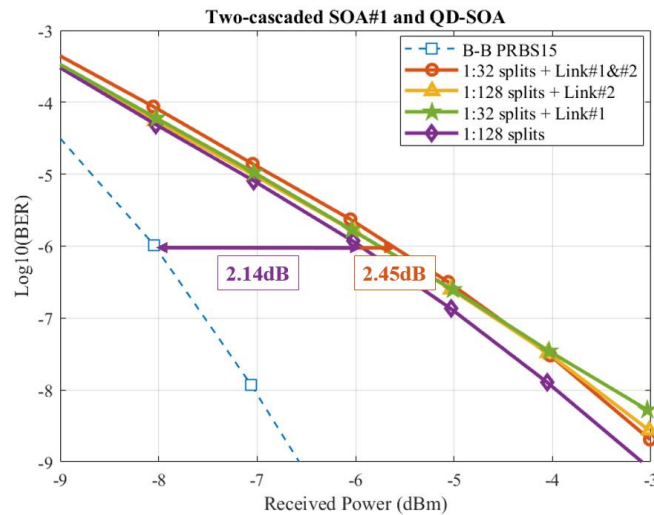


Figure 4.18 BER curves of 2-cascaded SOA#1 & QD SOA.

Likewise, Figure 4.18 shows the BER curves and power penalties at 10^{-6} BER for case i) to iv) to be 2.45, 2.31, 2.31 & 2.14 dB respectively. Again, case i) has the most penalty, while case iv) with only splitters has the least penalty. In case iii) & iv), the imperfect CD compensation of Link#2 shows little penalties. Noting at -4 dBm received power, all BERs are between 10^{-8} and 10^{-7} BER, which are close to the BER in Figure 4.16 b) at -4.84 dBm input of QD SOA.

The performance of 2-cascaded SOA#1 & QD SOA is better than 2-cascaded SOA#1 & SOA#2, because QD SOA gives lower BERs than SOA#2 according to Figure 4.15 b) & Figure 4.16 b) when operating at high input as 2nd-stage SOA. Plus, it has higher saturation output and less pattern effect when operating in saturation as shown in Section 4.3. Based on our experiments, we achieve either 40-km SSMF with 32 splits or 128 splits without a long SSMF. Thus, this scenario of 2-cascaded SOAs can be implemented to increase the power budget of upstream transmission.

4.4.4.3 Verify the Performance of 2nd-stage SOA

We verify the performance of 2nd-stage SOA (SOA#2 or QD SOA) by varying a splitting ratio between 1st & 2nd-stage SOAs as 8, 16 & 32, while the input and output of 1st-stage SOA#1 are fixed at -14.02 & 5 dBm respectively. So, the inputs of 2nd-stage SOA are -4.84 , -7.91 & -10.87 dBm for 8, 16, and 32 splits, respectively. Two

parameters of 2nd-stage SOA are focused. First, the higher output (P_{out}) with same input reflects more power budget. Second, the lower penalty represents better performance, depending on SOA's input. Consequently, we define ($P_{out} - Penalty$) @ 10^{-7} BER to compare the performance of 2nd-stage SOA; of course, the higher the better. Table 4.2 lists all parameters. According to its higher saturation output in Table 4.1, our QD SOA gives a higher output P_{out} than SOA#2 when operating at high input, corresponding to a lower split 1:8. Figure 4.19 shows BER curves of 6 cases. All Penalty @ 10^{-7} BER in Table 4.2 are measured relative to the reference case: QD SOA+8split. For example, the case of SOA#2+8split has 1 dB more penalty than the reference. But, the case of SOA#2+16split has 0.4 dB less penalty than the reference (a negative value in Table 4.2).

Table 4.2 All parameters and values for 2nd-stage SOA.

Amplifier	Splits	P_{out}	Penalty at 10^{-7} BER	$P_{out} - Penalty$ @ 10^{-7} BER
SOA1117S	8	5.61 dBm	1 dB	4.61 dB
	16	3.93 dBm	-0.4 dB	4.33 dB
	32	2.78 dBm	-1 dB	3.78 dB
QD SOA	8*	6.23 dBm	0 dB	6.23 dB
	16	4.32 dBm	-0.9 dB	5.22 dB
	32	2.75 dBm	-1 dB	3.75 dB

*Reference case

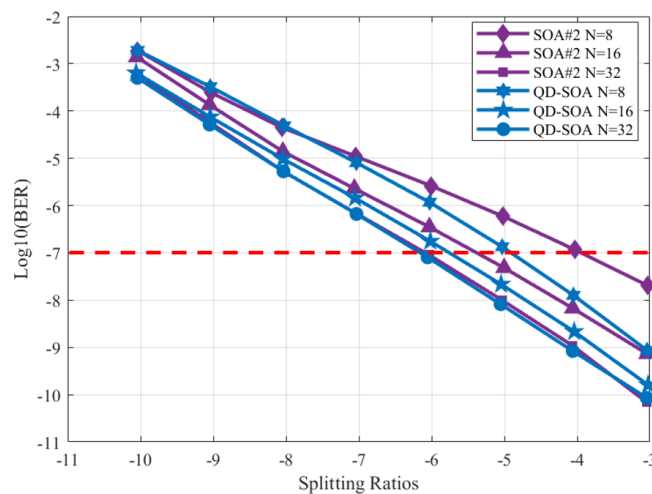


Figure 4.19 BER curves of 2nd-stage SOA with N splits.

From the last column of Table 4.2, the QD SOA with 8 & 16 splits have very high ($P_{out} - Penalty$) as expected, because of higher outputs and less penalties when operating at high input as compared to SOA#2. Especially, in another scenario of 2-cascaded SOAs without any splitter in between them, a high output of 1st-stage SOA will demand 2nd-stage SOA to support such a high input with less signal degradation. Hence, the QD SOA will give the best performance at high input (in saturation region).

4.4.5 Theoretical Equations

This section lists the equations to compute BERs. Starting with 5 noises, all parameters related to our experiments are applied to approximate the Signal-to-Noise Ratio (SNR), Q-factor, and finally BERs of 3 SOAs.

4.4.5.1 Noise Terms

At a receiver (Rx), there are 5 noises [82]: shot, signal-ASE beat, ASE-ASE beat, thermal, and dark current. All parameters and their values are declared in next section Table 4.3.

$$\langle i_{shot}^2 \rangle = \sigma_{shot}^2 = 2q \left[\Re[P_r + P_{ASE}] B_e \right] \quad (4.4)$$

$$P_{ASE} = S_{ASE} \times B_O \quad (4.5)$$

$$S_{ASE} = \frac{P_{ASE-OSA}}{RBW_{OSA}} \quad (4.6)$$

$$\langle i_{S-ASE}^2 \rangle = \sigma_{S-ASE}^2 = 4\Re^2 P_r S_{ASE} B_e \quad (4.7)$$

$$\langle i_{ASE-ASE}^2 \rangle = \sigma_{ASE-ASE}^2 = 4\Re^2 S_{ASE}^2 B_O B_e \quad (4.8)$$

$$\langle i_T^2 \rangle = \sigma_T^2 = \left(\frac{4k_B T}{R_L} \right) B_e \quad (4.9)$$

$$\langle i_d^2 \rangle = \sigma_d^2 = 2q I_d B_e \quad (4.10)$$

4.4.5.2 BER Calculation

The BER is calculated from SNR in equation (4.11), which is a ratio of signal power of photo-current from PD, $\langle i_p^2 \rangle$ in equation (4.12), over the noise summation scaled up by NF of electrical amplifier, F_n [83].

$$SNR = \frac{\langle i_P^2 \rangle \times (\text{Ratio}_{OSNR} \text{ or } \text{Ratio}_{pattern})}{(\sigma_{shot}^2 + \sigma_{S-ASE}^2 + \sigma_{ASE-ASE}^2 + \sigma_T^2 + \sigma_d^2) \times F_n} \quad (4.11)$$

$$\langle i_P^2 \rangle = (\mathfrak{R}P_r)^2 \quad (4.12)$$

To include both OSNR degradation and pattern effect, we introduce the Ratio_{OSNR} and $\text{Ratio}_{pattern}$ to reduce signal power, such that the BERs in its plot versus SOA's input as in Figure 4.14 b) will rise accordingly. So, those BER points on the left side of minimum BER will be scaled up by Ratio_{OSNR} defined as in equation (4.13),

$$\text{Ratio}_{OSNR} = \frac{\Delta G_{OSNR}}{\Delta OSNR + \Delta G_{OSNR}} \quad (4.13)$$

where ΔG_{OSNR} is gain difference between such point and the minimum BER, and $\Delta OSNR$ is OSNR difference between such point and adjacent point. Moreover, the right side of minimum BER will be scaled up by $\text{Ratio}_{pattern}$ defined as in equation (4.14),

$$\text{Ratio}_{pattern} = \frac{\Delta G_{pattern}}{\Delta P_{in} + \Delta G_{pattern}} \quad (4.14)$$

where $\Delta G_{pattern}$ has same definition as ΔG_{OSNR} , and ΔP_{in} is input difference between such point and adjacent point.

Finally, the Q-factor & BER are related to SNR by equation (4.15) & (4.16), where $erfc$ is complementary error function.

$$Q = \frac{1}{2} \sqrt{SNR} \quad (4.15)$$

$$BER = \frac{1}{2} erfc \left[\frac{Q}{\sqrt{2}} \right] \quad (4.16)$$

In the B-B case, its BER is calculated from SNR equation without ASE noise terms. In next Section, all computed BER points are plotted along with experimental results in the BER plot versus SOA's input of 3 SOAs.

4.4.6 Computed BER Results of SOA#1, SOA#2, and QD SOA

From the equations in Section 4.4.5 and parameters in Table 4.3, the BERs are computed at fixed -4 dBm received power of each SOA biased at high current and with same setup as in Figure 4.12 b). This power is same as experimental cases in Section 4.4.3 that shows IPDR.

Table 4.3 Parameters and values for BER computation.

Parameter	Symbol	Value	Unit
Electron Charge	q	1.6021×10^{-19}	C
Responsivity	R	0.65	A/W
Electrical Bandwidth	B_e	40	GHz
Dark Current	I_d	200	nA
Boltzmann Constant	k_B	1.38054×10^{-23}	J/K
Temperature	T	298	K
Load Resistance	R_L	50	Ω
Electrical Amplifier's NF	F_n	3.98	
Wavelength	λ	1530	nm
OSA's Resolution Bandwidth	RBW_{OSA}	0.2	nm
Optical Bandwidth	B_o	2 [84]	nm

4.4.6.1 Computed and Experimental BERs of SOA#1

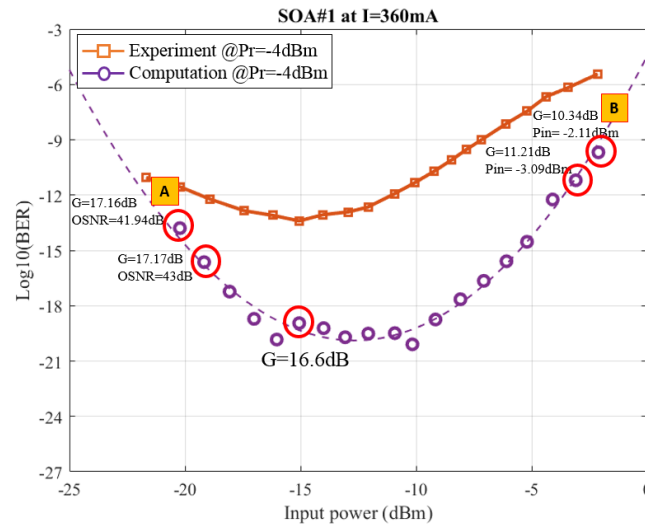


Figure 4.20 Computed and experimental BERs of SOA#1.

Figure 4.20 is the BER plot of SOA#1, showing computed and experimental results. As mentioned earlier, the OSNR degradation and pattern effect cause worse BERs on the left and right sides of minimum BER, respectively. Thus, either $Ratio_{OSNR}$ or $Ratio_{pattern}$ is multiplied in equation (4.11). For example, $Ratio_{OSNR}$ at A point and $Ratio_{pattern}$ at B point are calculated by those values shown in Figure 4.20. Based on the experiment of SOA#1, its gain is 16.6 dB at minimum BER. According to equation (4.13), ΔG_{OSNR} is 1.138 ($17.16 - 16.6 = 0.56$ dB) and $\Delta OSNR$ is 0.783 ($41.9 - 43 = -1.06$ dB). So, $Ratio_{OSNR}$ is 0.592. Also, $Ratio_{pattern}$ is 0.159 calculated from $\Delta G_{pattern} = 0.237$ and $\Delta P_{in} = 1.253$. As a result, the trend of computed and experimental BERs are almost the same with OSNR degradation and pattern effect.

4.4.6.2 Computed and Experimental BERs of SOA#2

The BER plot of SOA#2 is shown in Figure 4.21 with same calculations of $Ratio_{OSNR}$ and $Ratio_{pattern}$ as in SOA#1. The gain of SOA#2 is 15.79 dB at minimum BER. The ΔG_{OSNR} , $\Delta G_{pattern}$, $\Delta OSNR$ and ΔP_{in} are 1.081, 0.22, 0.653 and 1.23 respectively, resulting in the $Ratio_{OSNR}$ at A point and $Ratio_{pattern}$ at B point of 0.623 and 0.152. In Figure 4.21, the computed BERs at lower inputs show high BER due to its high P_{ASE_OSA} that causes such high signal-ASE noise term. In this case, we use the minimum BER

point according to experiment. But, the minimum BER from computation does not match it, because of the $Ratio_{OSNR}$ and $Ratio_{pattern}$ multiplication that depend on each BER point.

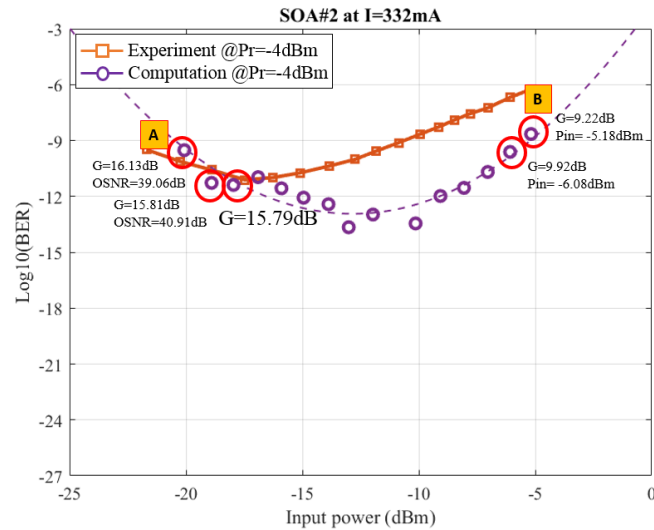


Figure 4.21 Compute and experimental BERs of SOA#2.

4.4.6.3 Computed and Experimental BERs of QD SOA

Figure 4.22 shows the BER plot of QD SOA, with same calculations as in 2 conventional SOAs. The gain of QD SOA is 16.05 dB at minimum BER. The ΔG_{OSNR} , $\Delta G_{pattern}$, $\Delta OSNR$ and ΔP_{in} are 1.14, 0.228, 0.82 and 1.256 respectively. So, the $Ratio_{OSNR}$ at A point and $Ratio_{pattern}$ at B point are 0.582 and 0.153. Similarly, the trend of computed and experimental BERs are almost the same.

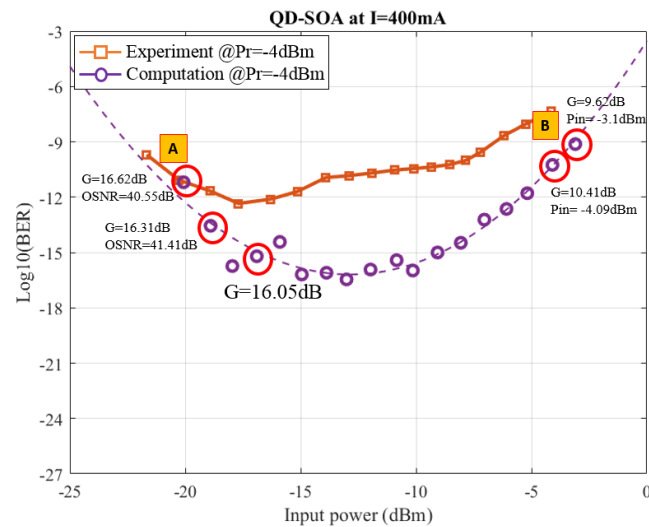


Figure 4.22 Computed and experimental BERs of QD SOA.

4.5 Conclusion

We evaluate the performances of two conventional SOAs (#1 & #2) and our QD SOA in 1530-nm Upstream Transmission of 40 Gb/s access network over two 20-km SSMF with DCF (Link#1 & #2) and splitters (8, 16 & 32). Among the characteristic results of 3 SOAs, QD SOA gives the lowest NF of 4.59 dB at -20-dB input, as well as the fastest response of 70 ps and highest S/O of 1.567. Hence, it is more suitable for burst-mode amplification. Based on the single SOA transmission in 6 combination cases (3 splitters with & without Link#1), the BER curves of 3 SOAs depend on their inputs, proven by BER plots versus SOA's input showing IPDR. SOA#1 has superior BER results and higher saturation output, and thus is applied as 1st-stage SOA. In 2-cascaded SOA transmission using either SOA#2 or QD SOA as 2nd-stage, there are 4 cases: 32 splits with Link#1 & #2, 128 splits with Link#2, 32 splits with Link#1, and 128 splits. All BER results of QD SOA are lower with less power penalty than SOA#2 due to its higher saturation output and less pattern effect. Also, we verify the performance of 2nd-stage SOA with different splitters (8, 16 & 32) between 1st & 2nd-stage SOA. The 2nd-stage QD SOA with 8 & 16 splits have very high ($P_{out} - Penalty$) @ 10^{-7} BER, owing to its higher outputs and less penalties when operating at high input as compared to SOA#2. Finally, we compute the BERs of 3 SOAs and compare to experimental results. In a BER plot versus SOA's input, the left side of minimum BER

gets worse by OSNR degradation, whereas the right side of minimum BER gets worse by data pattern effect.

4.6 Acknowledgement

The authors are grateful to The 100th Anniversary Chulalongkorn University Fund for Doctoral Scholarship, The 90th Anniversary of Chulalongkorn University Fund (Ratchadaphiseksomphot Endowment Fund), and Overseas Research Experience Scholarship for Graduate Students from Graduate School Chulalongkorn University. We would like to express appreciation to researchers and technical staffs, especially Mr. Hiroyuki Sumimoto, for their helps and advices at Photonic Network System Laboratory, NICT.



5. Conclusion

This thesis demonstrates the characteristic improvement of QD SOA. The performances of conventional SOAs and QD SOA are evaluated in an access network. The high internal quantum efficiency of QD SOA can be achieved at 66.39 % by Rapid Thermal Annealing (RTA) process. The strain compensation technique is applied to increase maximum chip gain at 35 dB. The characteristics of 2 conventional SOAs and 1 QD SOA are measured. QD SOA gives the lowest NF of 4.59 dB at -20-dBm input power and 400-mA bias current. Moreover, the response times and data pattern effects of 3 SOAs are measured. QD SOA provides the fastest response time of 70 ps and lowest pattern effect with *Signal to overshoot ratio (S/O)* at 1.567. Therefore, QD SOA is suitable to apply in burst-mode upstream transmission. The performances of conventional SOAs and QD SOA are evaluated in 40 Gb/s access network. The single SOA transmission and Input Power Dynamic Range (IPDR) are measured. QD SOA gives 17.73-dB IPDR, which is slightly lower than SOA1013S (SOA#1). Moreover, the BER curves of 3 SOAs depend on their input powers. According to a plot of Bit Error Rate (BER) versus SOA's input power, BERs get worse due to the Optical Signal to Noise Ratio (OSNR) degradation when SOA operates in low input power; while BERs get worse owing to data pattern effect when SOA operates in high input power. After that, the two-cascaded SOA transmission is applied to increase power budget more than single SOA transmission. Consequently, the cascaded SOA1013S & QD SOA provides lower BER than cascaded SOA1013S & SOA1117S, because QD SOA has higher saturation output power and lower pattern effect than SOA1117S. The two-cascaded SOA transmission can provide splitting ratios up to 128 splits (more than 64 splits compared to standard) and distance of 20 km. Finally, both experimental and computed BERs are plotted versus SOA's input power to confirm the OSNR degradation and data pattern effect.

Research Limitation

Author needs to conduct this research at higher bit rate than 10 Gb/s. Therefore, it is necessary to do the researches and experiments of 40 Gb/s bit rate with many expert researchers at National Institute of Information and Communications Technology (NICT) in Japan.



6. Appendix

6.1 As-grown structure

As-grown structure is shown in Figure 6.1. Plus, the parameters and values are shown in Table 6.1.

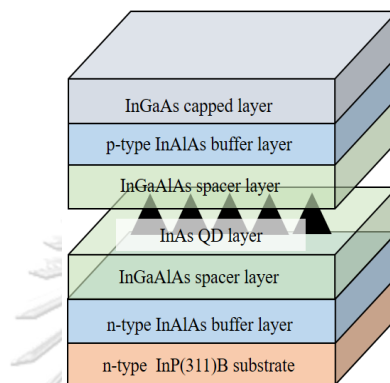


Figure 6.1 As-grown structure

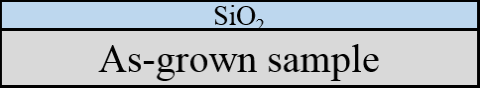
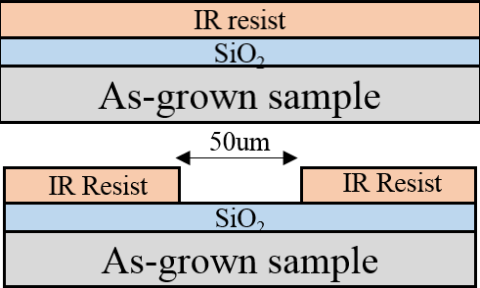
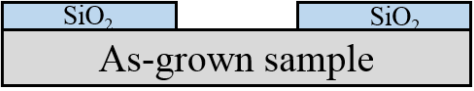
Table 6.1 Parameters and values of as-grown structure

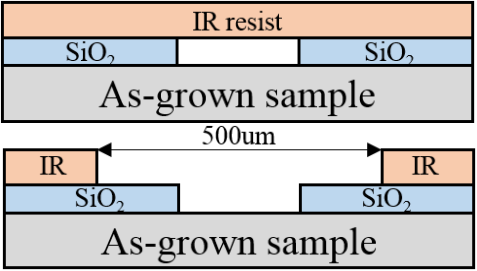
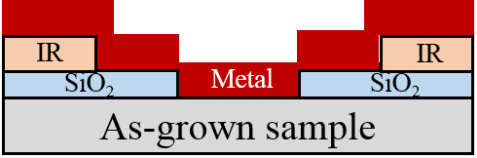


Parameter	Value
InAs QD layers	10 - 30 layers
QD density	$5.24 - 9.5 \times 10^{10} \text{ cm}^{-2}$
Lateral size of QD	30 - 35 nm
Height of QD	3 - 4 nm
Spacer layer: InGaAlAs	20 nm
Substrate: InP(311)B	
Cladding layer: n-InAlAs	100 - 150 nm
Cladding layer: p-InAlAs	1600 - 2000 nm
Contact layer: InGaAs	100 nm

6.2 Fabrication process

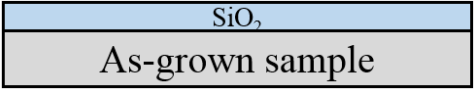
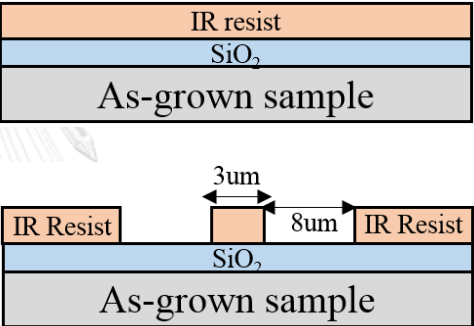
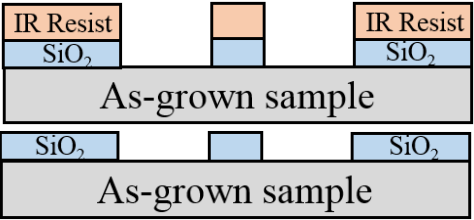

The fabrication processes of Broad Area Laser Diode (BA-LD) and ridge laser diode are investigated. To focus on the fabrication process, as-grown sample shown in Figure 6.1 is applied in this section.



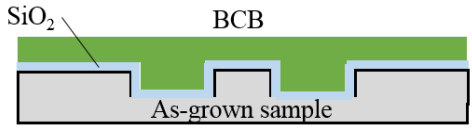


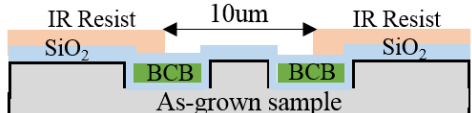
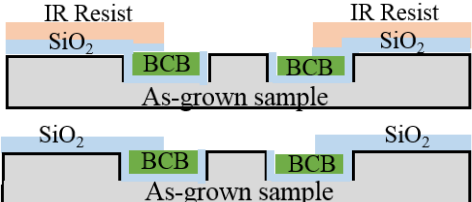
6.2.1 Broad Area Laser Diode (BA-LD)

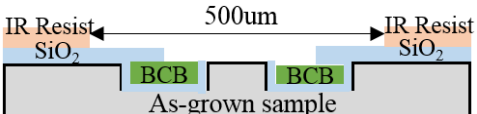
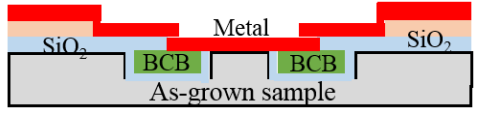
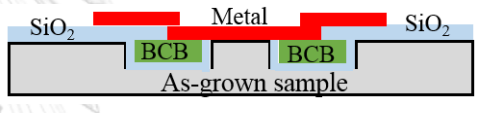
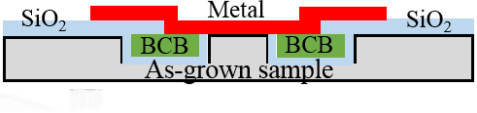

<p><u>1. SiO₂ deposition</u> : Chemical Vapor Deposition (CVD) is used to deposit SiO₂. After SiO₂ deposition process, we need to check a thickness of SiO₂ by using a spectroscopic ellipsometer. Equipment: CVD machine and spectroscopic ellipsometer.</p>	 <p>The diagram shows a cross-section of a substrate labeled 'As-grown sample' (grey). A uniform layer of SiO₂ (blue) is deposited on top of the substrate.</p>
<p><u>2. Photolithography (for BA-LD)</u> : This is an UV exposure process. We use a glass mask with the Image Reversal (IR) resist. After UV exposure process, resist will be removed with 50 μm width on SiO₂ surface. Equipment: Mask Aligner (MA) and a glass mask</p>	 <p>The diagram shows two stages of photolithography. In the first stage, an 'IR resist' (orange) layer is applied on top of the 'SiO₂' (blue) layer on the 'As-grown sample' (grey). In the second stage, the resist is patterned into two rectangular blocks, with a double-headed arrow between them indicating a width of '50um'. The SiO₂ layer and substrate remain unchanged.</p>
<p><u>3. Remove SiO₂ of selected area</u> : This process is a wet etching process. We use the chemical liquid to remove SiO₂ in selected area and resist. After that, we do arching to perfectly remove SiO₂ by using O₂ gas. Chemical liquid: Buffered Hydrofluoric Acid (BHF), Acetone, and Ethanol</p>	 <p>The diagram shows the final etched structure. The SiO₂ (blue) layer has been removed from the areas where the resist was present, leaving two rectangular pits on the 'As-grown sample' (grey) substrate. The remaining SiO₂ is shown as two separate blocks on either side of the pits.</p>

<p>Equipment: Arching machine</p>	
<p><u>4. Photolithography (for lift-off)</u> : After UV exposure process, resist will be removed with 500 μm width on SiO_2 surface. Equipment: MA and a glass mask</p>	
<p><u>5. Metal deposition (top side)</u> : Ti (Titanium), Pt (Platinum), and Au (Gold) are deposited, one at a time, on SiO_2 layer. Equipment: Electron-beam (e-beam) machine</p>	
<p><u>6. Lift-off</u> : We use the resist remover to perfectly remove resist. Chemical liquid: Resist remover, IPA (Isopropyl Alcohol, $(\text{CH}_3)_2\text{CH}(\text{OH})$), Acetone, and Ethanol</p>	
<p><u>7. Metal deposition (back side)</u> : Repeat step 5 Equipment: E-beam machine</p>	
<p><u>8. Cracked and cleaved</u> : We crack and cleave wafers to be a piece of samples with various cavity lengths. Equipment: Crack and cleave machines Cavity length: 600 μm, 800 μm, 1000 μm, 1200 μm, and 1400 μm</p>	

6.2.2 Ridge Laser Diode (Ridge LD)

<p><u>1. SiO₂ deposition</u></p> <p>: Chemical Vapor Deposition (CVD) is used to deposit SiO₂. After SiO₂ deposition process, we need to check a thickness of SiO₂ by using a spectroscopic ellipsometer.</p> <p>Equipment: CVD machine and spectroscopic ellipsometer.</p>	
<p><u>2. Photolithography (for ridge LD)</u></p> <p>: This is an UV exposure process. We use a glass mask with the Image Reversal (IR) resist. After UV exposure process, resist will be removed with 3 μm (for ridge LD) and 8 μm width on SiO₂ surface.</p> <p>Equipment: Mask Aligner (MA) and a glass mask</p>	
<p><u>3. Remove SiO₂ of selected area</u></p> <p>: This is a dry etching process using an etching machine to carefully remove SiO₂ and resist, respectively.</p> <p>Equipment: Inductively Coupled Plasma-Reactive Ion Etching (ICP-RIE) by Fluorine (F) source</p> <p>Chemical liquid: Resist remover</p>	
<p><u>4. Remove InP surface of selected area</u></p> <p>: This is a dry etching process to carefully remove InP. In this process, we use Chlorine (Cl) source, instead of F</p>	

<p>source, because InP cannot be removed by F source.</p> <p>Equipment: ICP-RIE by Cl source</p>	
<p><u>5. Remove SiO₂</u></p> <p>: SiO₂ can be removed by the acid liquid.</p> <p>Chemical liquid: Buffered Hydrofluoric Acid (BHF)</p>	
<p><u>6. SiO₂ deposition</u></p> <p>Equipment: CVD machine</p>	
<p><u>7. BCB coating</u></p> <p>: This process is coating Benzocyclobutene (BCB) on SiO₂ layer.</p> <p>Equipment: Spin coater, and Baker machine</p>	
<p><u>8. Remove BCB in selected area</u></p> <p>: This is a dry etching process to remove BCB by using an etching machine.</p> <p>Equipment: ICP-RIE by F source</p>	
<p><u>9. SiO₂ deposition</u></p> <p>Equipment: CVD machine</p>	
<p><u>10. Photolithography</u></p> <p>: After UV exposure process, resist will be removed with 10 μm width on SiO₂ surface.</p> <p>Equipment: MA and a glass mask</p>	
<p><u>11. Remove SiO₂ of selected area</u></p> <p>: SiO₂ can be removed by acid liquid.</p> <p>Chemical liquid: BHF</p>	

<p><u>12. Photolithography (for lift-off)</u></p> <p>: After UV exposure process, resist will be removed with 500 μm width on SiO_2 surface.</p> <p>Equipment: MA and a glass mask</p>	
<p><u>13. Metal deposition (top side)</u></p> <p>: Ti (Titanium), Pt (Platinum), and Au (Gold) are deposited, one at a time, on SiO_2 layer.</p> <p>Equipment: E-beam machine</p>	
<p><u>14. Lift-off</u></p> <p>: We use a resist remover to perfectly remove resist.</p> <p>Chemical liquid: Resist remover, IPA (Isopropyl Alcohol, $(\text{CH}_3)_2\text{CH}(\text{OH})$), Acetone, and Ethanol</p>	
<p><u>15. Polishing</u></p> <p>: Cleaning surface of back side</p> <p>Equipment: Polishing machine</p>	
<p><u>16. Metal deposition (back side)</u></p> <p>: Repeat step 13</p> <p>Equipment: E-beam machine</p>	
<p><u>17. Cracked and cleaved</u></p> <p>: We crack and cleave wafers to a piece of samples with various cavity lengths.</p> <p>Equipment: Crack and cleave machines</p> <p>Cavity length: 600 μm, 800 μm, 1000 μm, 1200 μm, and 1400 μm</p>	

ACRONYMS

AFM	Atomic Force Microscopy
AR	Anti-Reflection
ASE	Amplified Spontaneous Emission
BA-LD	Broad Area Laser Diode
B-B	Back to Back
BCB	Benzocyclobutene
BER	Bit Error Rate
BHF	Buffered Hydrofluoric Acid
CATV	Cable Television
CD	Chromatic Dispersion
CR	Clock Recovery
DCA	Digital Communications Analyzer
DCF	Dispersion Compensation Fiber
DEMUX	Demultiplexer
DFB	Distributed Feedback
DUT	Device Under Test
ED	Error Detector
EDFA	Erbium-Doped Fiber Amplifier
FWHM	Full Width at Half Maximum
FWM	Four Wave Mixing
G-PON	Gigabit-capable Passive Optical Networks
IL	Insertion Loss
IPDR	Input Power Dynamic Range
LD	Laser Diode
MBE	Molecular Beam Epitaxy
MUX	Multiplexer
MZM	Mach-Zehnder Modulator
NF	Noise Figure
NG-PON2	40-Gigabit-capable Passive Optical Networks

ODN	Optical Distribution Network
OLT	Optical Line Terminal
ONT	Optical Network Terminal
ONU	Optical Network Unit
OSA	Optical Spectrum Analyzer
OSNR	Optical Signal to Noise Ratio
PAM-4	Pulse Amplitude Modulation 4-level (PAM4)
PC	Polarization Controller
PD	Photo-Detector
PDC	Pulse Duty Cycle
PDG	Polarization Dependent Gain
PL	Photoluminescence
PON	Passive Optical Network
PPG	Pulse Pattern Generator
PRBS	Pseudo Random Bit Sequences
PSK	Phase Shift Keying
PtP	Point-to-Point
QAM	Quadrature Amplitude Modulation
QD SOA	Quantum Dot Semiconductor Optical Amplifier
QDIP	Quantum Dot Infrared Photodetector
QD-LD	Quantum Dot Laser Diode
QPSK	Quadrature Phase Shift Keying
RTA	Rapid Thermal Annealing
SC-CQD	Strain-Controlled Columnar QD
S-K growth	Stranski-Krastanov growth
SNR	Signal-to-Noise Ratio
SSMF	Standard Single Mode Fiber
TEC	Thermo Electric Cooler
TLD	Tunable Laser Diode
TOBPF	Tunable Optical Band Pass Filter
TWDM	Time and Wavelength Division Multiplexed

VOA	Variable Optical Attenuator
WDM	Wavelength Division Multiplexing
XGM	Cross Gain Modulation
XG-PON	10-Gigabit-capable Passive Optical Networks
XPM	Cross Phase Modulation



PARAMETERS

Symbol	Parameter
η_i	Internal quantum efficiency
η_d	External quantum efficiency
α_i	Internal optical loss
I_{th}	Threshold current
L	Device's length
G_{chip}	Chip Gain
CL_{facet}	Coupling loss at each facet
T_0	Characteristic Temperature
S/O	Signal to Overshoot ratio
h	Planck's constant ($=6.626 \times 10^{-34}$ J·s)
ν	Frequency of SOA's input wavelength
B_{ref}	Frequency band converted from an OSA's resolution bandwidth
τ	Response time
V_{ss}	Steady-state voltage
A	Peak amplitude
α	Linewidth enhancement factor
n	Refractive index
N	Carrier density
λ	Wavelength
Γ	Confinement factor
A_g	Differential gain
P_{out}	Output power
q	Electron Charge ($=1.60218 \times 10^{-19}$ C)
R	Responsivity ($=0.65$ A/W)
B_e	Electrical Bandwidth ($=40 \times 10^9$ Hz)
I_d	Dark current ($=200 \times 10$ nA)
k_B	Boltzmann constant ($=1.38054 \times 10^{-23}$ J/K)

Symbol	Parameter
T	Temperature
R_L	Load resistance (=50 Ω)
RBW_{OSA}	OSA Resolution bandwidth at 1530 nm
B_O	Optical bandwidth at 1530 nm
P_r	Received power
P_{ASE}	ASE power of SOA
S_{ASE}	Spectral density of ASE noise
P_{ASE_OSA}	ASE power measured by SOA
F_n	Noise figure (electrical amplifier)
σ_{shot}^2	Shot noise
σ_{S-ASE}^2	Signal-ASE beat
$\sigma_{ASE-ASE}^2$	ASE-ASE beat
σ_T^2	Thermal noise
σ_d^2	Dark current noise
$\langle i_p^2 \rangle$	Signal power
Q	Q-factor

REFERENCES

- [1] G. Keiser, Optical Fiber Communication, 5 ed. Singapore: McGraw-Hill, 2015.
- [2] H. Ghafouri-Shiraz, The Principles of Semiconductor Laser Diodes and Amplifiers: Analysis and Transmission Line Laser Modeling: Imperial College Press, 2004.
- [3] Comparison Of Different Optical Amplifiers [Online]. Available: <http://www.fiber-optic-tutorial.com/comparison-of-different-optical-amplifiers.html>
- [4] M. J. Connelly, Semiconductor Optical Amplifiers: Springer US, 2002.
- [5] H. Schmeckebier, Quantum-Dot-Based Semiconductor Optical Amplifiers for O-Band Optical Communication, 1 ed.: Springer International Publishing, 2017.
- [6] T. Akiyama, M. Sugawara, and Y. Arakawa, "Quantum-Dot Semiconductor Optical Amplifiers," *Proceedings of the IEEE*, vol. 95, pp. 1757 - 1766, 2007.
- [7] Q. Cao, C. Tong, S. F. Yoon, C. Liu, and C. Y. Ngo, "Improved Performance of 1.3- μm Multilayer P-Doped InAs/InGaAs Quantum Dot Lasers Using Rapid Thermal Annealing," *IEEE Transactions on Nanotechnology*, vol. 11, pp. 231-235, 2012.
- [8] A. Matsumoto, K. Akahane, T. Sakamoto, T. Umezawa, A. Kanno, and N. Yamamoto, "Dynamic characteristics of 20-layer stacked QD-SOA with strain compensation technique by ultrafast signals using optical frequency comb " *Physica Status Solidi A: Applications and Materials Science*, vol. 214, No. 3, 2017, p. 1600557.
- [9] K. Akahane, Y. Naokatsu, and K. Tetsuya, "Characteristics of highly stacked quantum dot laser fabricated on InP(311)B substrate," in *2009 IEEE International Conference on Indium Phosphide & Related Materials*, 2009, pp. 73-74.
- [10] K. Akahane, N. Yamamoto, and T. Kawanishi, "Highly stacked quantum dot lasers fabricated by a strain-compensation technique," in *IEEE Photonic Society 24th Annual Meeting*, 2011, pp. 163-164.
- [11] H. X. Zhao, S. F. Yoon, C. Y. Ngo, R. Wang, C. Z. Tong, C. Y. Liu, *et al.*, "Effects of Thermal Annealing on the Dynamic Characteristics of InAs/GaAs Quantum Dot Lasers," *IEEE Photonics Journal*, vol. 2, pp. 630-635, 2010.
- [12] ITU Telecommunications Standardization, "ITU-T G.984.1, Gigabit-capable Passive

- Optical Networks (GPON): Physical Media Dependent (PMD) layer specification ", ed, 2003.
- [13] ITU Telecommunications Standardization, "ITU-T G.987.1, 10-Gigabit-capable passive optical network (XG-PON) systems: General requirements," ed, 2010.
- [14] ITU Telecommunications Standardization, "ITU-T G.989.1, 40-Gigabit-capable passive optical networks (NG-PON2): General requirements," ed, 2013.
- [15] ITU Telecommunications Standardization, "ITU-T G.984.6, Gigabit-capable passive optical networks (GPON): Reach extension," ed, 2008.
- [16] D. Nasset, "NG-PON2 Technology and Standards," *Journal of Lightwave Technology*, vol. 33, pp. 1136-1143, March 2015.
- [17] ITU Telecommunications Standardization, "ITU-T G.984.1, Gigabit-capable Passive Optical Networks (GPON): General characteristics ", ed, 2008.
- [18] ITU Telecommunications Standardization, "ITU-T G.987, 10-Gigabit-capable passive optical network (XG-PON) systems: Definitions, abbreviations and acronyms " in ed, 2012.
- [19] D. Bimberg, N. Kirstaedter, N. N. Ledentsov, Z. I. Alferov, P. S. Kop'ev, and V. M. Ustinov, "InGaAs-GaAs quantum-dot lasers," *IEEE Journal of Selected Topics in Quantum Electronics*, vol. 3, pp. 196-205, 1997.
- [20] K. Akahane, N. Yamamoto, and T. Kawanishi, "High Characteristic Temperature of Highly Stacked Quantum-Dot Laser for 1.55- μm Band," *IEEE Photonics Technology Letters*, vol. 22, pp. 103-105, 2010.
- [21] K. Akahane, A. Matsumoto, T. Umezawa, N. Yamamoto, and T. Kawanishi, "High characteristic temperature for ridge-waveguide laser with a highly stacked InAs quantum dot structure," in *2016 International Semiconductor Laser Conference (ISLC)*, 2016, pp. 1-2.
- [22] K. Stewart, M. Buda, J. Wong-Leung, L. Fu, C. Jagadish, A. Stiff-Roberts, *et al.*, "Strain relaxation in rapid thermally annealed InAs/GaAs quantum dot infrared photodetectors," in *2002 Conference on Optoelectronic and Microelectronic Materials and Devices. COMMAD 2002. Proceedings (Cat. No.02EX601)*, 2002, pp. 475-478.
- [23] L. Fu, P. Kuffner, I. McKerracher, H. H. Tan, and C. Jagadish, "Rapid thermal

- annealing study of InGaAs/GaAs quantum dot infrared photodetectors grown by metal-organic chemical vapor deposition," in *2005 IEEE LEOS Annual Meeting Conference Proceedings*, 2005, pp. 228-229.
- [24] P. M. Lam, J. Wu, S. Hatch, D. Kim, M. Tang, H. Liu, *et al.*, "Effect of rapid thermal annealing on InAs/GaAs quantum dot solar cells," *IET Optoelectronics*, vol. 9, pp. 65-68, 2015.
- [25] A. Nishikawa, Y. G. Hong, and C. W. Tu, "Effects of thermal annealing on GaInNAs QDs grown on GaAs [001]," in *2003 International Symposium on Compound Semiconductors*, 2003, pp. 70-71.
- [26] G. X. Shi, B. Xu, X. L. Ye, P. Jin, Y. H. Chen, Y. L. Wang, *et al.*, "Effect of noncoherent islands on the optical properties of the 1.3 μm InAs/GaAs quantum dots during rapid thermal annealing," in *13th International Conference on Semiconducting and Insulating Materials, 2004. SIMC-XIII-2004.*, 2005, pp. 135-138.
- [27] R. Suzuki, T. Miyamoto, and F. Koyama, "Post-Annealing Effects on Emission Characteristics of InAs Quantum Dots on GaNAs Buffer Layer," in *2007 IEEE 19th International Conference on Indium Phosphide & Related Materials*, 2007, pp. 307-310.
- [28] D. Bhattacharyya, A. S. Helmy, A. C. Bryce, E. A. Avrutin, and J. H. Marsh, "Selective control of $\text{In}_{0.5}\text{Ga}_{0.5}\text{As}/\text{GaAs}$ quantum dot properties by rapid thermal processing: quantum dot intermixing," in *1999 Digest of the LEOS Summer Topical Meetings: Nanostructures and Quantum Dots/WDM Components/VCSELs and Microcavities/RF Photonics for CATV and HFC Systems (Cat. No.99TH8455)*, 1999, pp. I29-I30.
- [29] A. Matsushita, A. Matsumoto, K. Akahane, Y. Matsushima, and K. Utaka, "Intermixing of highly-stacked InAs/InGaAlAs quantum dots grown on InP (311)B substrate by SiO_2 sputtering and annealing technique," in *2013 International Conference on Indium Phosphide and Related Materials (IPRM)*, 2013, pp. 1-2.
- [30] ITU Telecommunications Standardization, "ITU-T G.984.5, Gigabit-capable passive optical networks (GPON): Enhancement band," ed, 2014.
- [31] T. Umezawa, K. Akahane, A. Matsumoto, N. Yamamoto, and T. Kawanishi,

- "Waveguide avalanche photodetector using quantum-dot superlattice for optical fiber communications," in *2017 Conference on Lasers and Electro-Optics Pacific Rim (CLEO-PR)*, 2017, pp. 1-2.
- [32] B. Boriboon, D. Worasuchep, A. Matsumoto, K. Akahane, N. Yamamoto, and N. Wada, "Characteristics-improvement of QD semiconductor optical amplifier using rapid-thermal annealing process," in *SPIE OPTO*, 2018, p. 6.
- [33] K. Akahane, N. Yamamoto, and T. Kawanishi, "The dependence of the characteristic temperature of highly stacked InAs quantum dot laser diodes fabricated using a strain-compensation technique on stacking layer number," in *ISLC 2012 International Semiconductor Laser Conference*, 2012, pp. 82-83.
- [34] R. Wang, S. F. Yoon, H. X. Zhao, and C. Y. Liu, "Self-Heating Effect on Modal Gain of 1.3- μm InAs/GaAs QD Lasers With Different p-Doping Levels," *IEEE Photonics Journal*, vol. 3, pp. 713-717, 2011.
- [35] S. Sygletos, R. Bonk, P. Vorreau, T. Vallaitis, J. Wang, W. Freude, *et al.*, "A wavelength conversion scheme based on a quantum-dot semiconductor optical amplifier and a delay interferometer," in *2008 10th Anniversary International Conference on Transparent Optical Networks*, 2008, pp. 149-152.
- [36] G. Contestabile, Y. Yoshida, A. Maruta, and K. Kitayama, "Coherent Wavelength Conversion in a Quantum Dot SOA," *IEEE Photonics Technology Letters*, vol. 25, pp. 791-794, 2013.
- [37] T. Ohtsuki, T. Yatsu, and M. Matsuura, "Regenerative wavelength conversion of PAM-4 signals using XGM with blue-shift filtering in a QD-SOA," in *2017 Conference on Lasers and Electro-Optics Pacific Rim (CLEO-PR)*, 2017, pp. 1-3.
- [38] T. Ohtsuki and M. Matsuura, "Wavelength Conversion of 25-Gbit/s PAM-4 Signals Using a Quantum-Dot SOA," *IEEE Photonics Technology Letters*, vol. 30, pp. 459-462, 2018.
- [39] E. Dimitriadou and K. Zoiros, "On the feasibility of 320 Gb/s all-optical and gate using quantum-dot semiconductor optical amplifier-based mach-zehnder interferometer," *Progress In Electromagnetics Research B*, vol. 50, pp. 113-140, 01/01 2013.
- [40] E. Dimitriadou, K. E. Zoiros, T. Chattopadhyay, and J. N. Roy, "Design of ultrafast

- all-optical 4-bit parity generator and checker using quantum-dot semiconductor optical amplifier-based Mach-Zehnder interferometer," *Journal of Computational Electronics*, vol. 12, pp. 481-489, 2013/09/01 2013.
- [41] D. Kastritsis, K. E. Zoiros, and E. Dimitriadou, "Design of ultrafast all-optical pulsed-mode 2×2 crossbar switch using quantum-dot semiconductor optical amplifier-based Mach-Zehnder interferometer," *Journal of Computational Electronics*, vol. 15, pp. 1046-1063, 2016/09/01 2016.
- [42] D. K. Gayen, T. Chattopadhyay, and K. E. Zoiros, "All-optical D flip-flop using single quantum-dot semiconductor optical amplifier assisted Mach-Zehnder interferometer," *Journal of Computational Electronics*, vol. 14, pp. 129-138, 2015/03/01 2015.
- [43] S. Lange, Y. Yoshida, G. Contestabile, and K. Kitayama, "Phase transparent amplification of 40 Gbps 16 QAM signals using a QD-SOA," in *2013 18th OptoElectronics and Communications Conference held jointly with 2013 International Conference on Photonics in Switching (OECC/PS)*, 2013, pp. 1-2.
- [44] A. Matsumoto, K. Akahane, T. Umezawa, and N. Yamamoto, "Extreme thermal stability of 1550 nm band highly stacked QD-LDs with p-doped structure," in *2017 Conference on Lasers and Electro-Optics Pacific Rim (CLEO-PR)*, 2017, pp. 1-2.
- [45] D. Bimberg, M. Laemmlin, C. Meuer, G. Fiol, M. Kuntz, A. Schliwa, *et al.*, "Quantum Dot Amplifiers for 100 Gbit Ethernet," in *2006 International Conference on Transparent Optical Networks*, 2006, pp. 237-241.
- [46] H. Schmeckeber, A. Zeghuzi, D. Arsenijević, M. Stubenrauch, C. Meuer, C. Schubert, *et al.*, "40 GBd D(Q)PSK and OOK amplification using o-band quantum-dot semiconductor optical amplifiers," in *2016 18th International Conference on Transparent Optical Networks (ICTON)*, 2016, pp. 1-1.
- [47] A. Matsumoto, Y. Takei, A. Matsushita, K. Akahane, Y. Matsushima, H. Ishikawa, *et al.*, "Gain characteristics and femto-second optical pulse response of 1550 nm-band multi-stacked QD-SOA grown on InP(311)B substrate," *Optics Communications*, vol. 344, 06/01 2015.
- [48] S. Lange, G. Contestabile, Y. Yoshida, and K. Kitayama, "Phase-Transparent

- Amplification of 16 QAM Signals in a QD-SOA," *IEEE Photonics Technology Letters*, vol. 25, pp. 2486-2489, 2013.
- [49] M. Matsuura, H. Ohta, and R. Seki, "Dynamic frequency chirp properties of QD-SOAs," in *2015 Optical Fiber Communications Conference and Exhibition (OFC)*, 2015, pp. 1-3.
- [50] H. Hoshino, N. Ninomiya, and M. Matsuura, "Frequency chirp properties with data pattern dependence in quantum-dot SOAs," in *2016 21st OptoElectronics and Communications Conference (OECC) held jointly with 2016 International Conference on Photonics in Switching (PS)*, 2016, pp. 1-3.
- [51] R. Bonk, R. Brenot, C. Meuer, T. Vallaitis, A. Tussupov, J. C. Rode, *et al.*, "1.3 / 1.5 μm QD-SOAs for WDM/TDM GPON with extended reach and large upstream / downstream dynamic range," in *2009 Conference on Optical Fiber Communication*, San Diego, CA, USA, 2009, pp. 1-3.
- [52] T. Umezawa, K. Akahane, A. Kanno, and T. Kawanishi, "Improvement of photodiode responsivity using the InAs quantum dot family for monolithic integration," in *2014 Conference on Lasers and Electro-Optics (CLEO) - Laser Science to Photonic Applications*, 2014, pp. 1-2.
- [53] A. Matsumoto, T. Umezawa, K. Akahane, A. Kanno, N. Yamamoto, and T. Kawanishi, "90 Gb/s hybrid integrated photoreceiver module with high speed 1.5 μm -band QD-SOA," in *2016 International Semiconductor Laser Conference (ISLC)*, 2016, pp. 1-2.
- [54] J. Tatebayashi, N. Nuntawong, Y. C. Xin, P. S. Wong, S. Huang, C. P. Hains, *et al.*, "Low Threshold Current Operation of Stacked InAs/GaAs Quantum Dot Lasers with GaP Strain-Compensation Layers," in *2006 International Conference on Indium Phosphide and Related Materials Conference Proceedings*, 2006, pp. 108-111.
- [55] K. Akahane, N. Yamamoto, and T. Kawanishi, "High Characteristic Temperature of Highly Stacked Quantum-Dot Laser for 1.55- μm Band," *IEEE Photonics Technology Letters*, vol. 22, pp. 103-105, 2010.
- [56] S. Matsui, Y. Takei, A. Matsumoto, K. Akahane, Y. Matsushima, H. Ishikawa, *et al.*, "Photonic integrated device of highly-stacked quantum dot using quantum dot

- intermixing by ion implantation," in *2016 Compound Semiconductor Week (CSW) [Includes 28th International Conference on Indium Phosphide & Related Materials (IPRM) & 43rd International Symposium on Compound Semiconductors (ISCS)*, 2016, pp. 1-2.
- [57] K. Akahane, N. Yamamoto, S. Gozu, A. Ueta, N. Ohtani, and M. Tsuchiya, "Highly-ordered and highly-stacked (150-layers) quantum dots," in *2006 International Conference on Indium Phosphide and Related Materials Conference Proceedings*, 2006, pp. 192-196.
- [58] A. Matsumoto, Y. Takei, A. Matsushita, K. Akahane, Y. Matsushima, and K. Utaka, "Fundamental characteristics of 1550nm-band 20-layer-stacked QD-SOA grown on InP(311)B substrate for all-optical logic gate device," in *Technical Digest of the Eighteenth Microoptics Conference*, 2013, pp. 1-2.
- [59] N. Yasuoka, H. Ebe, K. Kawaguchi, M. Ekawa, S. Sekiguchi, K. Morito, *et al.*, "Polarization-Insensitive Quantum Dot Semiconductor Optical Amplifiers Using Strain-Controlled Columnar Quantum Dots," *Journal of Lightwave Technology*, vol. 30, pp. 68-75, 2012.
- [60] S. W. C. Larry A. Coldren, Milan L. Mašanović, Diode Lasers and Photonic Integrated Circuits: John Wiley & Sons, Inc., Hoboken, New Jersey, 2012.
- [61] G. Contestabile, A. Maruta, S. Sekiguchi, K. Morito, M. Sugawara, and K. Kitayama, "All-optical signal processing using QD-SOA," in *OECC 2010 Technical Digest*, 2010, pp. 200-201.
- [62] D. Wang, Z. Min, G. Lu, Q. Jun, T. Sakamoto, K. Akahane, *et al.*, "Multifunctional all-optical signal processing scheme for simultaneous multichannel WDM multicast and XOR logic gates based on FWM in QD-SOA," in *2015 Optical Fiber Communications Conference and Exhibition (OFC)*, 2015, pp. 1-3.
- [63] B. Boriboon, D. Worasuchee, A. Matsumoto, K. Akahane, N. Yamamoto, and N. Wada, "Optimized design of QD-LD toward QD-SOA to achieve 35-dB maximum chip gain with 400-mA injected current," *Optics Communications*, vol. 475, p. 126238, 2020/11/15/ 2020.
- [64] R. Bonk, H. Schmuck, W. Poehlmann, and T. Pfeiffer, "Beneficial OLT transmitter and receiver concepts for NG-PON2 using semiconductor optical amplifiers

- [invited], *IEEE/OSA Journal of Optical Communications and Networking*, vol. 7, pp. A467-A473, 2015.
- [65] N. A. Idris, N. Yamamoto, K. Akahane, K. Yoshizawa, Y. Tomomatsu, M. Sudo, *et al.*, "A WDM/TDM Access Network Based on Broad T-Band Wavelength Resource Using Quantum Dot Semiconductor Devices," *IEEE Photonics Journal*, vol. 8, pp. 1-10, 2016.
- [66] R. Bonk, H. Schmuck, B. Deppisch, W. Poehlmann, and T. Pfeiffer, "Wavelength-transparent long-reach-high-split TWsDM-PON utilized by a non-gated parallel cascade of linear SOAs," in *2014 The European Conference on Optical Communication (ECOC)*, 2014, pp. 1-3.
- [67] S. Shimizu and S. Shinada, "1024-way Split, 70-km PAM4 Transmission for PON Uplink Using Cascaded SOAs and Volterra Nonlinear Equalization," in *OSA Advanced Photonics Congress (AP) 2020 (IPR, NP, NOMA, Networks, PVLED, PSC, SPPCom, SOF)*, Washington, DC, 2020, p. PsTh3F.5.
- [68] S. Liu, K. A. Williams, T. Lin, M. G. Thompson, C. K. Yow, A. Wonfor, *et al.*, "Cascaded performance of quantum dot semiconductor optical amplifier in a recirculating loop," in *2006 Conference on Lasers and Electro-Optics and 2006 Quantum Electronics and Laser Science Conference*, 2006, pp. 1-2.
- [69] ITU Telecommunications Standardization, "ITU-T G.989.2, 40-Gigabit-capable passive optical networks 2 (NG PON2): Physical media dependent (PMD) layer specification," ed, 2019.
- [70] S. Liu, Y. Tong, J. Norman, M. Dumont, A. Gossard, H. K. Tsang, *et al.*, "High Efficiency, High Gain and High Saturation Output Power Quantum Dot SOAs Grown on Si and Applications," in *2020 Optical Fiber Communications Conference and Exhibition (OFC)*, 2020, pp. 1-3.
- [71] THORLABS. *C-Band Semiconductor Optical Amplifier SOA1013S* [Online]. Available: <https://www.thorlabs.com/>
- [72] THORLABS. *C-Band Semiconductor Optical Amplifier, Non-linear SOA1117S* [Online]. Available: <https://www.thorlabs.com/>
- [73] D. M. Baney, P. Gallion, and R. S. Tucker, "Theory and Measurement Techniques for the Noise Figure of Optical Amplifiers," *Optical Fiber Technology*, vol. 6, pp.

- 122-154, 2000/04/01/ 2000.
- [74] M. L. N. Jesper Mork, and T.W. Berg, "The Dynamics of Semiconductor Optical Amplifiers: Modeling and Applications," *Optics and Photonics News*, vol. 14, pp. 42-48, 2003/07/01 2003.
- [75] G. Contestabile, A. Maruta, and K. Kitayama, "Gain Dynamics in Quantum-Dot Semiconductor Optical Amplifiers at 1550 nm," *IEEE Photonics Technology Letters*, vol. 22, pp. 987-989, 2010.
- [76] Y. Ben-Ezra, M. Haridim, and B. I. Lembrikov, "Theoretical analysis of gain-recovery time and chirp in QD-SOA," *IEEE Photonics Technology Letters*, vol. 17, pp. 1803-1805, 2005.
- [77] T. Watanabe, N. Sakaida, H. Yasaka, F. Kano, and M. Koga, "Transmission performance of chirp-controlled signal by using semiconductor optical amplifier," *Journal of Lightwave Technology*, vol. 18, pp. 1069-1077, 2000.
- [78] W. Freude, R. Bonk, T. Vallaitis, A. Marculescu, A. Kapoor, E. K. Sharma, *et al.*, "Linear and nonlinear semiconductor optical amplifiers," in *2010 12th International Conference on Transparent Optical Networks*, 2010, pp. 1-4.
- [79] P. N. Goki, M. Imran, F. Fresi, F. Cavaliere, and L. Poti, "Lossless ROADM by Exploiting low gain SOAs in fronthaul network," in *2019 24th OptoElectronics and Communications Conference (OECC) and 2019 International Conference on Photonics in Switching and Computing (PSC)*, 2019, pp. 1-3.
- [80] R. Bonk, T. Vallaitis, J. Guetlein, C. Meuer, H. Schmeckeber, D. Bimberg, *et al.*, "The Input Power Dynamic Range of a Semiconductor Optical Amplifier and Its Relevance for Access Network Applications," *IEEE Photonics Journal*, vol. 3, pp. 1039-1053, 2011.
- [81] M. L. Davenport, S. Skendzic, N. Volet, and J. E. Bowers, "Heterogeneous silicon/InP semiconductor optical amplifiers with high gain and high saturation power," in *2016 Conference on Lasers and Electro-Optics (CLEO)*, 2016, pp. 1-2.
- [82] G. P. Agrawal, *Fiber-Optic Communication Systems*. Canada: Wiley-Interscience, 2002.
- [83] SHF Communication Technologies AG. *SHF 810 Broadband Amplifier* [Online]. Available: <https://www.shf-communication.com/>

- [84] OPTOQUEST. *Tunable Filter Module TFA-D/F with 2 nm* [Online]. Available: <http://www.optoquest.co.jp/en>





จุฬาลงกรณ์มหาวิทยาลัย
CHULALONGKORN UNIVERSITY

VITA

NAME Budsara Boriboon

DATE OF BIRTH 6 June 1991

PLACE OF BIRTH Bangkok

INSTITUTIONS ATTENDED Chulalongkorn University

HOME ADDRESS 800/108 Phahonyothin Raod, Khu Khot, Lam Luk Ka, Pathum Thani
12130 THAILAND

PUBLICATION

[1] Budsara Boriboon, Duang-rudee Worasuchee, Atsushi Matsumoto, Kouichi Akahane, Naokatsu Yamamoto, Naoya Wada, "Optimized design of QD-LD toward QD-SOA to achieve 35-dB maximum chip gain with 400-mA injected current," Optics Communications, vol. 475, p. 126238, 2020/11/15/ 2020.

[2] Budsara Boriboon, Duang-rudee Worasuchee, Atsushi Matsumoto, Kouichi Akahane, Naokatsu Yamamoto, Naoya Wada, "Characteristic-improvement of QD semiconductor optical amplifier using rapid-thermal annealing process", in SPIE Photonics West 2018, San Francisco, USA, January, 2018.

[3] Suchaj Rakkammee, Budsara Boriboon, Duang-rudee Worasuchee, and Naoya Wada "Measurement of characteristic parameters of 10 Gb/s bidirectional optical amplifier for XG-PON", Proc. SPIE 10714, Third International Conference on Photonics Solutions (ICPS), 2017.

[4] Budsara Boriboon, Pattareya Singchand, Duang-rudee Worasuchee, and Naoya Wada, "Interchannel Crosstalk Penalty of Bi-directional Transmission in Passive Optical Network", in The 39th Electrical Engineering Conference (EECON-39), Cha-am, Thailand, November 2016.

[5] Budsara Boriboon, Duang-rudee Worasuchee, Satoshi Shimizu, and Naoya Wada, "Computation and Experiments of 10 Gb/s Optical Access Network with Long Reach and a Large Number of Subscribers", in The 12th International Conference on Electrical Engineering / Electronics, Computer, Telecommunications and Information Technology (ECTI), Thailand, June, 2015.



จุฬาลงกรณ์มหาวิทยาลัย
CHULALONGKORN UNIVERSITY